Hydrate Bearing Sediments - Thermal Conductivity

A Thesis

Presented to

The Academic Faculty

By

Ana I. Martin

In Partial Fulfillment

of the Requirements for the Degree of

Master of Science in Civil and Environmental Engineering

Georgia Institute of Technology

December 28, 2004

Hydrate Bearing Sediments- Thermal Conductivity

Approved:

Dr. J. Carlos Santamarina, Advisor, CEE
School of Civil and Environmental Engineering
Georgia Institute of Technology

Dr. Carolyn Ruppel, EAS
School of Earth and Atmospheric Sciences
Georgia Institute of Technology

Dr. Paul Mayne, CEE
School of Civil and Environmental Engineering
Georgia Institute of Technology

Dr. Glenn Rix, CEE
School of Civil and Environmental Engineering
Georgia Institute of Technology

Date Approved: December 28, 2004

ACKNOWLEDGEMENTS

I got stuck each time I attempted to write this page before. The fears of leaving someone out prevented me from writing. Working on a thesis helps us realize the friends we have. I can only say that I am a very fortunate person. I would not be here if it were not for the people who gave me a hand, advice or support when I needed it the most.

First of all I want to thanks to my advisor Dr. Carlos Santamarina for the opportunity he gave me to join the hydrate research team and conduct this study, despite the fact that my academic background was different than the others in the group. This has been a great opportunity that definitely will impact my professional future. I also want to thank to Dr. Carolyn Ruppel who has provided support and guidance since the project started and Dr. Franco Francisca, who provided me guidance during the time we worked together.

I also thank Patricia Johnston, an expert librarian, who spent countless hours during her last months of work at the Georgia Tech Library to assist me in the literature review. She ended up fascinated with the topic and put a lot of enthusiasm and effort in the search. From our work grew a friendship that will last for many years. Martha Saghini, another librarian with years of expertise, has been giving me support on a daily basis, encouraging me to keep working and making me laugh with her unpredicted phrases. The friendships derived from my interaction with Marta and Patricia are among the most valuables treasures I will carry with me after I leave Georgia Tech.

I want to express my deepest appreciation to Dr. Carlos Ortiz, who helped me in the first editorial review of this document. His support was significant, because his corrections made me realize the magnitude of the work done and the end of the long process. I absolutely enjoyed his original phrases. His help is a demonstration of appreciation for what others did for him when he worked on his Master and Doctorate degrees.

My gratitude also goes to the amazing team at the Georgia Tech Library. These librarians became a family to me. Although I had the opportunity to choose another place to work, I kept going to the Library on a daily basis to meet them. I want to especially

mention the people at the multimedia station. They always have a smile on their faces and are eager to help. They enjoy solving problems, teaching you something new and seeing you happy. Although it is a long list I feel that this is my opportunity and I do not want to miss it. Thanks to all of you: Joel Linderman, Candace Chandler, James Lee, Sergio Gill, Chinh Ngo and Maya Pichkhadze. They received me every day with a beautiful smile, Candace never forgot to say: you will cheer up!

Thanks to Gisselle Martin. She believed in me from the moment we met and gave me all the orientation that I needed taking my first steps at Georgia Tech. I admire her hard work for recruiting great students around the country to enroll in this school.

Thanks to my friend Dominie Garcia. She gave me all the support and advice that I needed all this time. Her suggestions and advice are always extremely wise and right to the point. I absolutely respect and listen to her opinions. Her friendship is one of the blessings of my life.

I want to thanks my parents and relatives, still in Cuba. Although they were very strict, for which I complained so many times during my younger years, today I cannot say anything else but thanks. I always remember their message that respect, education, sincerity, and honesty never ends. I got from them the uncanny perception of people that I have today. I would not be the insightful person I am today without them.

I also want to express my gratitude to my adoptive parents in Puerto Rico Manuela Pernas and Manolo Areses. I do not think that I would be at Georgia Tech if I had had their guidance and support when I first move to this country. Two years later, they gave me all the help and encouragement that I needed to quit my job, pack and follow my dream. Their advice and guidance were and still are all that one needs to choose a path in life through education, dedication, honesty and faith. The love I got daily from this couple is one of the greatest gifts that I have received.

I want to extend my gratitude to Marta and George Garcia for their continuous support and guidance. They started giving me love since the day we met and they keep doing that. They enjoy helping and making people happy, while expecting nothing in return. For them I have the deepest appreciation, love and gratitude.

Finally, thanks to Chevron-JIP who believed in this research and allocated the resources to make it possible.

TABLE OF CONTENTS

ACKNOWLEDGEMENTS iii

LIST OF TABLES vii

LIST OF FIGURES viii

LIST OF SYMBOLS xii

SUMMARY xvi

CHAPTER 1 INTRODUCTION TO GAS HYDRATES 1
- 1.1 Gas Hydrates 2
- 1.2 Gas Hydrates in Sediments 7
- 1.3 Relevance of Gas Hydrates 11
  - 1.3.1 Gas Hydrates as a Potential Resource 11
  - 1.3.2 Methane Hydrates and Global Climate Change 13
  - 1.3.3 Gas Hydrates as Geological Hazard 13
- 1.4 Trends in Gas Hydrate Research - This Thesis 14
- 1.5 Summary 15

CHAPTER 2 THERMAL PROPERTIES OF SOILS AND HYDRATES 17
- 2.1 Heat Transfer 17
- 2.2 Thermal Conductivity of Soils 22
  - 2.2.1 Thermal Conductivity of Dry Soils 23
  - 2.2.2 Effect of Moisture Content 25
  - 2.2.3 Other Effects 26
  - 2.2.4 Data and Correlations 27
  - 2.2.5 Johansen's Model for Calculating the Thermal Conductivity of Soils 40
- 2.3 Thermal Conductivity of Clathrate Hydrates 49
  - 2.3.1 Origin of the Anomalous Thermal Conductivity of Clathrate Hydrates 53
  - 2.3.2 Thermal Conductivity of Hydrates in Sediments 55
- 2.4 Other Thermal Properties 56
  - 2.4.1 Heat Capacity 56
  - 2.4.2 Thermal Diffusivity 58
  - 2.4.3 Latent Heat of Fusion 59
  - 2.4.4 Thermal Expansion (or Contraction) 60
- 2.5 Conclusions 61

CHAPTER 3 THERMAL CONDUCTIVITY OF SOILS – MEASUREMENTS 62
3.1 Introduction 62
3.2 Theory: Mathematical Model for Data Reduction 63
3.3 Needle Probe and Electronics 65
3.4 Specimen Size – Calibration 67
3.5 Specimen Preparation - Data Collection and Reduction 68
3.6 Errors in Measurements of Thermal Conductivity by Needle Probe Method 75
3.7 Conclusions 75

CHAPTER 4 EXPERIMENTAL STUDY AND RESULTS 77
4.1 Physical Properties of Selected Soils 77
4.2 Tetrahydrofuran Solution 84
4.3 Specimen Preparation 86
4.4 Devices and Test Procedure 86
4.5 Experimental Results – Discussions 89
4.5.1 Sand 89
4.5.2 Kaolinite 95
4.5.3 Precipitated Silica Flour 101
4.5.4 Crushed Silica Flour 107
4.6 Summary Observations 112

CHAPTER 5 INTERPRETATION OF RESULTS – CONCLUSIONS 113
5.1 Deviations from the Natural Process 113
5.2 Unfrozen Specimens 114
5.3 Frozen Specimens 116
5.4 Conclusions 119
5.5 Recommendations for Future Research 119

APPENDIX A: FROZEN SOIL 122
A.1 Formation of Ice in Soils 122
A.2 Frozen Soils as Complex Systems 124
A.3 Effect of Unfrozen Water in Frozen Soils 125
A.4 Effect of Solutes in Frozen Soils 125
A.5 Effect of Pressure 126
A.6 Effect of Pore-Size in Frozen Soils 126

REFERENCES 128

LIST OF TABLES

Table 1.1	Geometric characteristics of three hydrate crystal structures I, II and H	4
Table 1.2	Comparison of properties of Ice and sI and sII hydrates	6
Table 2.1	Characteristic void ratio and porosity values for various soils	20
Table 2.2	Characteristic density values for dense soils	21
Table 2.3	Characteristic water content values of water-saturated soils	21
Table 2.4	Thermal conductivity of selected materials	31
Table 2.5	Summary of different methods to calculate thermal conductivity according to soil type	37
Table 2.6	Recommended quartz content and maximum expected variation in thermal conductivity from Johansen's method by soil type	49
Table 2.7	Thermal diffusivity of several materials	59
Table 4.1	Principal characteristics of tested materials	83
Table 4.2	Fluids nomenclature by weight	86
Table 4.3	Thermal conductivity - Sand	92
Table 4.4	Thermal conductivity – Kaolinite	98
Table 4.5	Thermal Conductivity - Precipitated silica flour	104
Table 4.6	Thermal conductivity - Crushed silica flour	110

LIST OF FIGURES

Figure 1.1 Gas hydrate structure. In this structure I methane hydrate the cages are composed of hydrogen-bonded water molecules and each contains a methane molecule 2

Figure 1.2 Three hydrate structures 3

Figure 1.3 Hydrate formation in sediments. a) Cementation. b) In pores 8

Figure 1.4 Worldwide locations of known and inferred gas hydrates deposits in oceanic aquatic sediments of outer continental margins (solid circles) and in polar permafrost regions (solid squares) 12

Figure 2.1 Heat flow through a soil element 19

Figure 2.2 Number of contacts/particle vs. dry density for mixed shaped particles (square) and round shaped particles (cross) 24

Figure 2.3 Thermal conductivity vs. dry density for unfrozen sand at two saturation levels: S≤1% (square) and S≥50% (cross) 25

Figure 2.4 Thermal conductivity k vs. saturation S for gravel: (a) Unfrozen (b) Frozen 28

Figure 2.5 Thermal conductivity k vs. saturation S for sand: (a) Unfrozen (b) Frozen 28

Figure 2.6 Thermal conductivity k vs. saturation S for silt: (a) Unfrozen b) Frozen 29

Figure 2.7 Thermal conductivity k vs. saturation S for clay: (a) Unfrozen (b) Frozen 29

Figure 2.8 Thermal conductivity k vs. saturation S for peat: (a) Unfrozen (b) Frozen 30

Figure 2.9 Thermal conductivity for sand and gravel: (a) Unfrozen (b) Frozen 33

Figure 2.10 Thermal conductivity for silt and clay: (a) Unfrozen (b) Frozen 34

Figure 2.11 Thermal conductivity for peat: (a) Unfrozen (b) Frozen 35

Figure 2.12 Johansen's method for calculating thermal conductivity of soils 41

Figure 2.13a Thermal conductivity of unfrozen soils-Johansen's method 44

Figure 2.13b Thermal conductivity of unfrozen soils-Johansen's method Two examples: Example 1: coarse soil. Example 2: fine soil 45

Figure 2.14a Thermal conductivity of frozen soils-Johansen's method 46

Figure 2.14b Thermal conductivity of frozen soils. Two examples: Example 1: coarse soil. Example 2: fine soil 47

Figure 2.15 Thermal conductivity of pure ice (Ih) and THF hydrate 52

Figure 3.1 Needle probe and electronics: (a) Cell and peripheral electronics (b) Connections schematics 66

Figure 3.2 Calibration of thermocouple built-in the needle probe 68

Figure 3.3 A representative curve- Temperature rise in response to probe heating and interpretation of different heating stages 70

Figure 3.4 Thermal conductivity measurements- Typical curve for Sand 71

Figure 3.5 Thermal conductivity measurements- Typical curve for kaolinite 72

Figure 3.6 Thermal conductivity measurements- Typical curve for precipitated silica flour 73

Figure 3.7 Thermal conductivity measurements- Typical curve for crushed silica flour 74

Figure 4.1 SEM picture of sand (F-110) 79

Figure 4.2 SEM picture of kaolinite (Wilklay SA-1) 80

Figure 4.3 SEM picture of precipitated silica flour (Zeofree 5161) 81

Figure 4.4 SEM picture of the crushed silica flour (Sil-Co-Sil 106) 82

Figure 4.5 General ambient temperature THF-water phase diagram. The dash line represent a molar composition of water-THF on which 50 % of the fluid hydrate (50 % water and 50 % THF) The solid line represent a molar composition of water-THF water-THF on which100 % of the fluid hydrate (80 % water and 20 % THF) 85

Figure 4.6 Modified isotropic confining pressure cell. Vacuum is applied to strengthen the specimen 87

Figure 4.7 Sketch of the modified isotropic confining pressure cell: (1) and (3) cell pressure, (2) specimen port, (4) soil specimen, (5) anti-freeze liquid, (6) mineral oil, (7) electrical connections 88

Figure 4.8 Sand- Thermal conductivity versus effective confining pressure: (a) Thermal conductivity values correspond with an average of six measurements (b) Average minimum and maximum are presented 90

Figure 4.9 Sand- Thermal conductivity versus porosity Thermal conductivity values correspond with an average of six measurements 91

Figure 4.10 Kaolinite- Thermal conductivity versus effective confining pressure: (a) Thermal conductivity values correspond with an average of six measurements (b) Average minimum and maximum are presented 96

Figure 4.11 Kaolinite- Thermal conductivity versus porosity Thermal conductivity values correspond with an average of six measurements 97

Figure 4.12 Precipitated silica flour- Thermal conductivity versus effective confining pressure: (a) Thermal conductivity values correspond with an average of six measurements (b) Average minimum and maximum are presented 102

Figure 4.13 Precipitated silica flour- Thermal conductivity versus porosity Thermal conductivity values correspond with an average of six measurements 103

Figure 4.14 Crushed silica flour- Thermal conductivity versus effective confining pressure: (a) Thermal conductivity values correspond with an average of six measurements (b) Average minimum

and maximum are presented 108

Figure 4.15 Crushed silica flour- Thermal conductivity versus porosity Thermal conductivity values correspond with an average of six measurements 109

Figure 5.1 Thermal conductivity versus porosity for all the soils tested at: 100:0, 50:50 and 80:20-frozen and unfrozen stages 115

Figure 5.2 Thermal conductivity versus effective confining pressure for all soil tested at: 100:0, 50:50 and 80:20 - unfrozen stage 117

Figure 5.3 Sand, kaolinite and precipitated silica flour Thermal conductivity versus effective confining pressure at 50:50 frozen 118

Figure 5.4 Sand, kaolinite, precipitated silica flour and crushed silica flour Thermal conductivity versus effective confining pressure at 80:20 frozen 120

Figure A.1 Cooling curve for soil water and ice 123

LIST OF SYMBOLS

Symbol	Physical meaning	Units
°C	Centdegrees	
K	Kelvin degrees	
MPa	Mega Pascal	
CH_4	Methane	
C_2H_6	Ethane	
C_3H_8	Propane	
C_4H_8	Isobutene	
C_4H_{10}	Normal butane	
N_7	Nitrogen	
CO_2	Carbon dioxide	
H_2S	Hydrogen sulfide	
sI	Structure I hydrate	
sII	Structure II hydrate	
sH	Structure H hydrate	
ηm	Nanometers	
M	Guest molecule	
I_h	Hexagonal ice	
L_H	Liquid water	
H	Hydrate	
G	Gas	
ΔH	Heat of dissociation	
μ	Microns	
m	Meters	
STP	Standard Temperature and Pressure	
k	Thermal conductivity	W/mK, W/m°C
C	Heat capacity	J/Km^3, $J/°Cm^3$
α	Thermal diffusivity	m^2/s
β	Coefficient of thermal expansion or contraction	

List of symbols (cont'd)

Symbol	Physical meaning	Units
E_T	Total energy	J
A	Area	m^2
q	Heat flow per unit area	J/m^2s
Q	Heat transfer	Watts
T	Temperature	K, °C
x	Spatial coordinate	m
i	Thermal gradient	K/m, °C/m
TCR	Thermal Contact Resistance	
k_{eff}	Effective thermal conductivity	W/mK, W/m°C
ω	Water content	
n	Porosity	
k_s	Thermal conductivity of the solid fraction	W/mK, W/m°C
k_{dry}	Thermal conductivity of dry soil	W/mK, W/m°C
k_{sat}	Thermal conductivity of saturated soil	W/mK, W/m°C
K_e	Kersten number	
k_u	Thermal conductivity of unfrozen soil	W/mK, W/m°C
S	Degree of saturation	
ρ_d	Dry density	Kg/m^3
k_w	Thermal conductivity of water	W/mK, W/m°C
ω_u	Unfrozen water content	
k_i	Thermal conductivity of ice	W/mK, W/m°C
$_q$	Quartz fraction of the total solid content	
k_q	Thermal conductivity of quartz	W/mK, W/m°C
k_o	Thermal conductivity of minerals other than quartz	W/mK, W/m°C
v	Phonon mean velocity	
l_m	Phonon mean free path	
THF	Tetrahydrofuran	
H_2O	Water	
Å	Angtroms	

List of symbols (cont'd)

Symbol	Physical meaning	Units
HT	High temperature	
LT	Low temperature	
ρ	Density	Kg/m^3
C_p	Specific heat capacity	J/Kkg, J/°Ckg
m_s	Mass fraction of solid	gr
m_w	Mass fraction of water	gr
m_i	Mass fraction of ice	gr
m_{air}	Mass fraction of air	gr
C_s	Heat capacity of solids	J/Kkg, J/°Ckg
C_w	Heat capacity of water	J/Kkg, J/°Ckg
C_i	Heat capacity of ice	J/Kkg, J/°Ckg
C_{air}	Heat capacity of air	J/Kkg, J/°Ckg
C_v	Volumetric heat capacity	$MJ/m^3.°C$
V	Volume	m^3
ρ_f	Bulk density of a frozen soil	Kg/m^3
ρ_{df}	Dry density of the frozen soil	Kg/m^3
ω_u	Unfrozen water content	
ω_i	Frozen water content	
C_m	Mass heat capacities	J/Kkg, J/°Ckg
C_{vu}	Volumetric heat capacity for unfrozen materials	$MJ/m^3°C$
C_{vf}	Volumetric heat capacity for frozen materials	$MJ/m^3°C$
ρ_w	Density of water	Kg/m^3
L	Body size	m
L'	Mass latent heat for water	KJ/Kg
l_o	Initial length at some reference temperature	m
ε	Strain	
β_v	Volume coefficient of thermal expansion	
ΔT	Temperature change	°C or K
T_o	Initial temperature	°C or K

Symbol	Physical meaning	Units
p	Power consumption of heater wire	W/m
t_o	Time correction factor	seconds
I	Heating current	mA
R_m	Specific resistance of the wire per unit length	Ω/m
s	Slope	
τ	Fourier number	
r_o	Radius of the thermal probe	mm
h	Thermal contact resistance between the probe and the soil	
R	Radius of the soil specimen	cm
D_{cap}	Diameter of the thermal needle cap	cm
e_{min}	Void ratio minimum	
e_{max}	Void ratio maximum	
$Al_2Si_2O_5(OH)_4$	Kaolinite	
SiO_2	Silicon dioxide	
I-H	Ice-Hydrate region in the THF-water phase diagram	
L-H	Liquid-Hydrate region in the THF-water diagram	

SUMMARY

Water mixed with natural gas (e.g., methane) or volatile liquids (e.g., tetrahydrofuran) can form crystalline clathrate compounds known as hydrates. Water (the host) molecules form the framework containing relatively large cavities through hydrogen bonding; cavities are occupied by gas (the guest) molecules, whose diameter is less than the size of the cavity. This hydrate structure is thermodynamically stabilized through non-bonded interactions between the encaged gas and the water lattice. These hydrates crystallize in three prominent structures, structure I, II and H depending on the nature and the size of the guest molecule.

Sediments containing natural gas hydrate are found in permafrost areas onshore and in marine sediments, where pressure and temperature conditions are inside the hydrate stability region and where natural gas is available. Offshore hydrate bearing sediments have generally been found in waters deeper than 300 m and their zone of existence is from the seafloor to a few hundred meters depth, depending upon the local thermal gradient. Enormous amounts of methane are believed to be trapped by hydrates, both in the hydrate crystal structure itself and also in sediments beneath hydrate deposits.

In order to appraise the natural gas hydrate reservoir on regional and global scales, it is important to understand the mechanisms controlling hydrate growth on the pore scale and its physical properties. Methane hydrate physical properties (e.g., thermal conductivity) depend not only on how much hydrate is present, but also how it is distributed in the pore space. Seabed stability is important for planning offshore installations and drilling, for understanding the relation between climate change, continental margin slope failure, and catastrophic hydrate dissociation. The physical properties and surface chemistry of the host sediments affect the thermodynamic state, growth kinetics, spatial distribution and growth forms of clathrates. Finally, scenarios for exploiting gas hydrate reservoirs must take into account the thermodynamic and physical influences that the host sediments play in controlling hydrate stability, growth form, small scale distribution of hydrates within the reservoir and permeability of the formation.

The thermal properties of gas hydrate have not yet been extensively measured. Most measurements and models have been of bulk hydrate specimens, which is important

in pipelines. Previous studies have focused on the thermal conductivity of structure II hydrate (e.g., THF hydrate), while a few studies have been performed on the measurement of thermal conductivity of structure I (e.g., methane hydrate). The influence of the sediments has rarely been considered and thermal conductivity data on hydrate bearing sediments are scarce.

In this research, the thermal conductivity of hydrate bearing sediments is explored with THF-water hydrate. THF is miscible in water and mass transfer effects are eliminated. Tetrahydrofuran (THF) forms structure II hydrate with water at a composition of 1:17 molar ratio or 19 % by weight. This hydrate melts at a temperature of 4.4 °C (277.4 K) at 1 atm. In contrast, hydrates which form from natural gas require elevated pressure for their formation.

Clathrates have been encountered in coarse sediments, such as sands and sandstones and fine-grained sediments, such as clays; and also occur filling in fractures within indurated sediments. Accordingly, the present thermal conductivity study utilized four different soils: Ottawa sand (F-110), kaolinite (Wilklay SA-1), precipitated silica flour (silt-zeofree 5161) and crushed silica flour (Sil-Co-Sil 106). The sediments chosen represent an ordered progression from grain sizes of 120μm (sand) to ~ 1μm (clay) and specific surface ranging from 10^{-4} m^2/g (sand) to ~ 35 m^2/g (clay).

In addition to water, two different mixtures of water and THF were prepared. The first water-THF mixture corresponds to a 50:50 water:THF molar composition. At this molar composition, 50 % of the mixture turns into hydrates; the excess THF remains unfrozen. The second fluid mixture represents the optimum composition consisting of 80 % water with 20 % THF, and all the THF-water mixture forms hydrates. Thermal conductivity is measured in a pressure range between 0.03 MPa and 1.0 MPa.

The thermal needle probe technique is used to determine thermal conductivity. The single probe methodology is based on a solution of the heat conduction equation for a line heat source in a homogeneous and isotropic medium at a uniform initial temperature. The needle probe contains a heater and a thermocouple. With the thermal probe inserted in the soil, constant power is supplied to the heater element and the temperature rise of the heating wire is measured by the thermocouple and recorded with respect to time during a 256 s heating interval. Finally, the thermal conductivity is

computed as a function of the current in the line source, the specific resistance of the wire and the slope of the straight line portion of the temperature rise vs. the logarithm of time.

Results permit exploring the factors that affect thermal conductivity, including: effective confining pressure, porosity and grain size. The highest thermal conductivity values for all the soils are obtained with the optimum THF-water composition. The thermal conductivity of sediments with 50 % hydrates in the pore space is higher than the thermal conductivity of water-saturated sediments. The increase in thermal conductivity with hydrate fraction suggests that hydrates in pores enhance the inter-granular contact.

Data derived from the experiments on thermal conductivity for all soils tested demonstrate that the thermal properties of frozen soil differ from the thermal properties of hydrate-bearing soils. The thermal properties of hydrate-bearing sediments vary according with the soil type. This appears to be a function of porosity, pore size, specific surface, mineralogy. Laboratory experiments demonstrate that the formation of hydrates in porous materials is affected by factors like capillary effects and permeability. These phenomena significantly affect the presence of gas hydrates in fine-grained sediments, in a similar way as capillary effect and permeability control the hydrate growth observed in marine sediments.

Surface effects are also an important factor in the nucleation processes. The laboratory results corroborate the hypothesis that porous media modify the stability of clathrate hydrate according to the pore size and surface properties of the host material.

Among all the factors affecting hydrate formation, the pore size plays a critical role, as it limited the size of nuclei. Variations in the sediment pore size and mineralogy among the soil tested seemed to produce different contributions to the energy state of the water from surface interactions in a way analogous to marine sediments.

CHAPTER 1

INTRODUCTION TO GAS HYDRATES

Clathrate hydrates of natural gases are crystalline solids formed by water mixed with gases or other liquids. Clathrate hydrates owe their existence to the ability of water molecules to undergo hydrogen bonding and form framework structures with cavities that can serve as host sites to small gas molecules (guest). The hydrogen bonded water lattice is stabilized by these individual guest molecules encaged in the intersticial cavities. Depending on the hydrocarbon guest molecule in the hydrate lattice, different structures can form. As clathrates, gas hydrates defied description for many years, since they did not fit the standard classifications of covalent, ionic, or coordination compounds.

The thermodynamic stability of a gas hydrate is determined by temperature, pressure and the activity of water. Typically, gas hydrates are stable at low temperature (< 10 °C) and high pressures (> 3.5 MPa). Therefore, gas hydrates are primarily located in ocean floor sediments and in the Artic permafrost and may contain more CH_4 (methane) than all other known reserves combined (Mahajan et al., 2000). These ice-like solids also form in pipes; they do not flow, but rapidly grow and agglomerate to sizes that can block flow lines, among some other important consequences.

Interest in gas hydrate began in the early part of the nineteenth century when chemists discovered clathrate hydrates of various gases (Ripmeeter, 2000); this early history is summarized in detail by Sloan (1998-b). Engineers became aware of gas hydrate in the 1930's when hydrate formation was discovered to be the cause of pipeline blockage during the transmission of natural gas. The first observation of naturally occurring gas hydrate in permafrost regions took place on July 21, 1961, but the discovery was officially registered on December 24, 1969 (Kuznetsov, 2000). It soon became clear that these compounds are not just chemical curiosities, or a nuisance for gas transportation in pipelines, but rather, they are significantly related to a natural phenomenon. In the 1970's, naturally occurring gas hydrate was found in the Siberian Messoyakha gas field, confirming that gas hydrate occurs naturally not only in polar continental regions, but also in shallow sediments under deep water of oceanic outer continental margins.

1.1 Gas Hydrates

Gas hydrates of economic interest are composed of water and one or more of the following eight molecules: methane (CH_4), ethane (C_2H_6), propane (C_3H_8), isobutene (C_4H_8), normal butane (C_4H_{10}), nitrogen (N_7), carbon dioxide (CO_2), and hydrogen sulfide (H_2S) (Sloan, 1998-a).

Hydrates normally form in one of three crystal structures, either type I, type II or type H. The observed structures differ from one another in the number and sizes of the cages in the "ice" lattice (size of the guest molecule). Although guest molecules are physically enclosed within the lattice, no actual chemical bond exists between the guest and host molecules (Figure 1.1). These structures are further arranged into well-defined three-dimensional crystalline solids (Sloan, 1998-a).

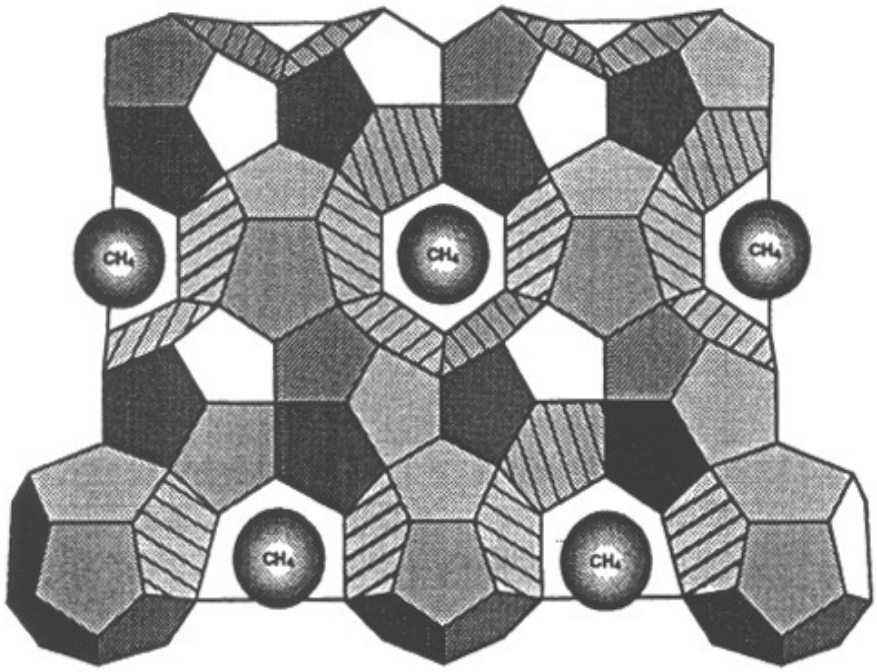

Figure 1.1 Gas hydrate structure. In this structure I methane hydrate the cages are composed of hydrogen bonded water molecules and each contains a methane molecule

Source: Kvenvolden, 1993

The three hydrate unit crystal structures sI, sII and sH are given with reference to the water skeleton, composed of a basic "building block" cavity that has 12 faces with five sides per face, given the abbreviation 5^{12} (Figure 1.2). By linking the vertices of 5^{12} cavities one obtains sI; linking the faces of 5^{12} cavities results in sII; and, in sH, a layer of linked 5^{12} cavities provides connections. An oxygen atom is located at the vertex of each angle in the cavities and connected to a bonded hydrogen on a neighbor water molecule. Inside each cavity resides a maximum of one small guest molecules (Sloan, 1998-a).

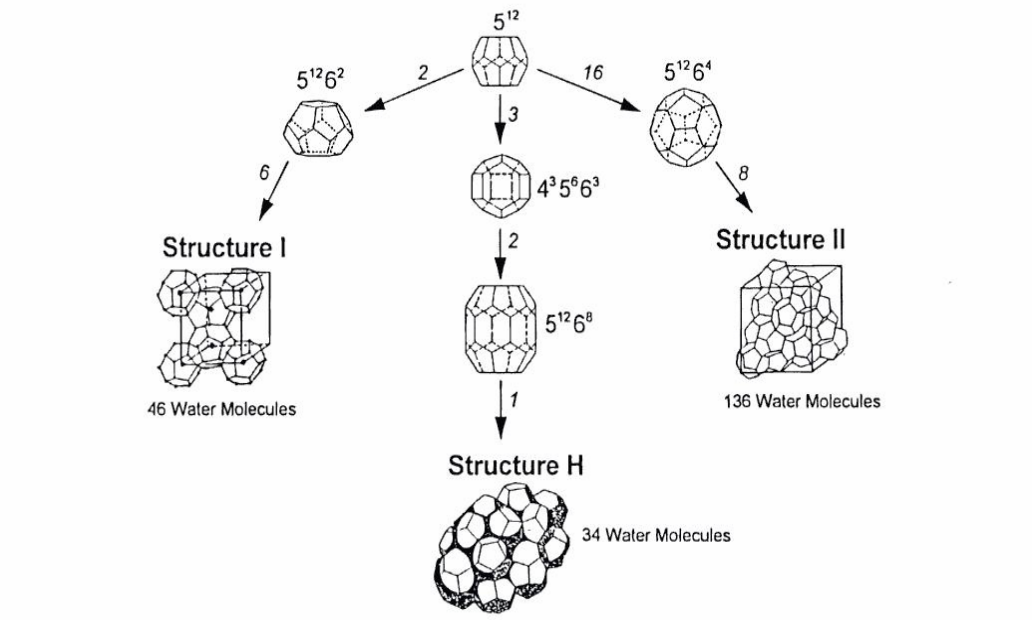

Figure 1.2 Three hydrate structures

Source: Sloan, 1998-a

Table 1.1 summarizes the geometric characteristics of the three hydrate crystal structures I, II and H. A brief description of each structure is presented.

Table 1.1 Geometric characteristics of three hydrate crystal structures I, II and H

CAVITY	STRUCTURE I (SMALL)	STRUCTURE II (SMALL)	STRUCTURE H (SMALL)
No. of cavities per unit cell	2	16	3
Average cavity radius, Å	3.95	3.91	3.91
Coordination number	20	20	20
No. of water per unit cell	46	136	34

Source: Sloan, 1998-a

Structure I gas hydrates. This is a body-centered cubic structure which forms with small natural gas molecules where the guest molecule can be as large as ~ 0.53 ηm in diameter (smaller than propane). It is found in situ in deep oceans with biogenic gases containing mostly methane, carbon dioxide, and hydrogen sulfide. The cubic unit cell has a cell edge of 1.2 ηm and contains 46 water molecules and 8 cavities. There are two small, and six large cavities. The composition in structure I vary from M.(5.75 H_2O) to M.(7.67 H_2O), where M represents the guest molecule (Ashworth et al., 1985).

Structure II gas hydrates. This is a diamond lattice within a cubic framework and forms when natural gases or oils contain molecules larger than ethane but smaller than pentane. Guest molecules are 0.56 to 0.66 ηm. Structure II represents hydrates from thermogenic gases, which commonly occur in hydrocarbon production and processing conditions, as well as in many cases of gas seeps from faults in ocean environments (Ashworth et al., 1985). Again the structure formed has a cubic unit cell, with cell edge ~ 1.73 ηm, contains 136 water molecules and 24 cavities (16 small and 8 large). The composition of structure II can only be in the narrow range near M.(17H_2O). Structures of gas hydrates are different from the ordinary low-pressure hexagonal ice form (designed Ih), and show a more open structure than the latter (Ashworth et al., 1985).

Structure H gas hydrates. This structure is named for its hexagonal framework. Structure H hydrates must have a small occupant, like methane, nitrogen or carbon dioxide for the 5^{12} and $4^3 5^6 6^3$ cages, but the molecules in the $5^{12}6^8$ cage can be as large as 0.9 ηm (e.g. ethylcyclohexane) (Sloan, 1998-a).

Mechanical properties of hydrates. All three hydrate structures (sI, sII, sH) are approximately 85 % (mol) water and 15 % gas, if all cages are filled. The fact that the water content is so high suggests that the mechanical properties of the three hydrate structures should be similar to ice. This conclusion is true as a first approximation, with the exception of thermal conductivity and thermal expansivity, as shown in Table 1.2. For H-structure hydrates, many mechanical properties have not been measured yet (Sloan, 1998-a).

Guest/cavity size ratio. The largest molecules of a gas mixture, usually determines the structure formed. A size ratio (guest molecule/cavity) of approximately 0.9 is necessary for stability of a simple hydrate. When the size ratio exceeds unity, the molecule will not fit within the cavity and the structure will not form. When the ratio is significantly less than 0.9, the molecule cannot lend significant stability to the cavity (Sloan, 1998-a). The sizes of stabilizing guest molecules range between 0.35 and 0.75 ηm for all structure types. Below 0.35 ηm, molecules will not stabilize sI and above 0.75 ηm molecules will not fit in sII.

Phase equilibrium properties. The three-phase system made of [liquid water (L_H) + hydrate (H) + gas (G)] hydrate stability is more sensitive to temperature than to pressure. The pressure and temperature at hydrate formation can be predicted by knowing the gas composition (Sloan, 1998-a). This prediction is possible only for pure water systems. In the presence of seawater or water containing various ions, this prediction is theoretically possible, but much more difficult (Henry et. al., 1999).

Heat of dissociation. The heat of dissociation ΔH for sI and sII is a function of the number of crystal hydrogen bonds, loosely taken as hydration number (Sloan, 1998-a). The value of ΔH is relatively constant for molecules which occupy the same cavity, within a wide range of components sizes.

Table 1.2 Comparison of properties of ice and sI and sII hydrates

PROPERTY	ICE	STRUCTURE I	STRUCTURE II
Spectroscopic crystallographic unit cell			
No. H_2O molecules	4	46	136
H_2O diffusion correlation time (μs)	220	240	25
H_2O diffusion active energy (KJ/m)	58.1	50	50
Dielectric constant at 273 k (-0.15 ºC)	94	~58	58
Mechanical properties			
Isothermal Young's modulus at 268 K (10^9 Pa)	9.5	8.4(est)	8.2 (est)
Poisson's ratio	0.33	~0.33	~0.33
Bulk modulus (272K)	8.8	5.6	N/A
Shear modulus (272K)	3.9	2.4	N/A
Velocity ratio (comp/shear) at 272 K	1.88	1.95	N/A
Thermodynamic property			
Linear thermal expansion: - 73.15 (K^{-1})	56 x 10^{-6}	77 x 10^{-6}	52 x 10^{-6}
Adiab bulk compress: - 0.15 (10^{-11} Pa)	12	14 (est)	14 (est)
Speed sound: -0.15 (Km/s)	3.8	3.3	3.6
Thermal conductivity: -10.15 ºC ($Wm^{-1}K^{-1}$)	2.23	0.49 +/- 0.02	0.51 +/- 0.02

Source: Sloan, 1998-a

1.2 Gas Hydrates in Sediments

Sediment inhibits gas hydrate nucleation and growth, an inference supported by experimental data on gas hydrate formation in porous media. Experiments show that the porous medium modifies the stability of clathrate according to the pore size and surface properties of the host material. The porous medium decreases the stability range of hydrate. A greater pressure or a lower temperature is necessary to form the hydrate (Henry et al., 1999, Clennell et al., 2000).

There are two basic models of hydrate formation in sediments: cementation around grains and formation within pores (Figure 1.3). Cementation affects the mechanical interaction between grains, which become bound together by intergranular hydrate (Dvorkin and Nur, 1993). Only small amounts of cement can significantly increase the stiffness and thus the elastic moduli of granular material. The solidification of methane hydrate in the pore space does not become part of the sediment matrix, and increase in stiffness would result only when hydrate approaches the saturation of the pore space (Dvorkin and Nur, 1993).

Growth initiation on grain surfaces is an appropriate concept because gas hydrate formation requires nuclei to enable the initial growth of a hydrate phase (Matsubayashi and Edwards, 2000). Surfaces of sediment grains act as nuclei (the higher the specific surface, the higher the probability of hydrate nucleation in the pores yet, growth is hindered in small pores) (Matsubayashi and Edwards, 2000).

Most hydrate models are built on the analogy between hydrate in marine sediments and ice in permafrost. Researchers tend to look at hydrates as “ice” filling the pores because gas hydrates share a number of structural and physical similarities with water-ice (Clenell et al., 2000). Although there are no definitive measurements, laboratory experiments show that the thermodynamic properties of hydrates in small pores change in the same way as those for ice. It appears that the interfacial energy between gas hydrate and liquid water is similar to that between ice and water. These facts, and the close resemblance of certain sediment-hosted hydrate occurrences to permafrost ice lenses allow to speculate that gas hydrate might interact with the host

sediments according with the thermodynamic principles that underlie freezing of water in soils pores (Clenell et al., 2000).

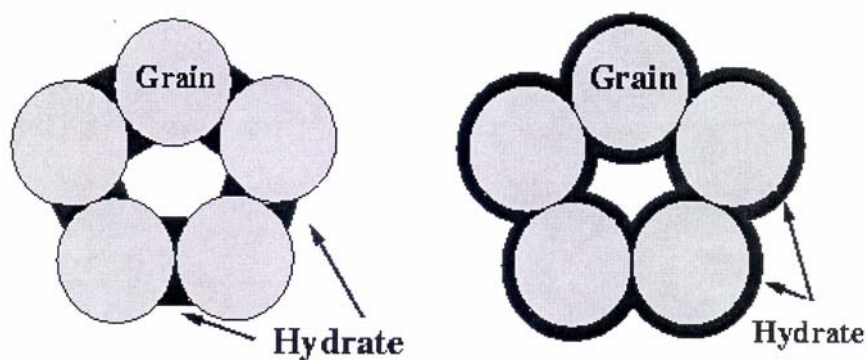

(a)

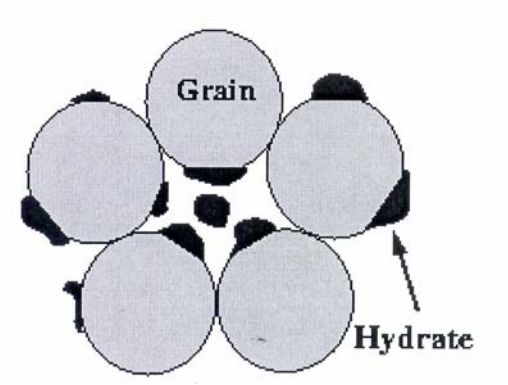

(b)

Figure 1.3 Hydrate formation in sediments. (a) Cementation. (b) In pores

Source: Dvorkin and Nur, 1993

There are two possible mechanisms for the appearance of a new phase (e.g., hydrate): homogeneous nucleation, where a cluster forms in the body of the liquid; and heterogeneous nucleation, where the cluster forms on a third surface such as a gas bubble or a mineral substrate. In marine sediments, the level of supersaturation of a gas supply required for homogeneous nucleation is normally much greater than the required for heterogeneous nucleation, hence, heterogeneous nucleation should be expected. Homogeneous nucleation and efficient growth under diffusion-limited conditions may only occur in larger pores or fractures and then, the maximum degree of inhibition is not set by the pore size of sediments, but by the size of the critical hydrate nuclei (Clennell et al., 2000).

Four basic stages are needed for nucleation, from the perspective of the nucleation theory for the kinetics of hydrate nucleation and growth in porous media (Kvamme, 2000): (1) kinetic transport of hydrate formers towards the particle surface, (2) molecular agglomeration and clustering. The cluster has to be of sufficient size for the free energy change of the reaction to overcome the surface energy of the new interface. The energy excess of the initial cluster just balances the excess chemical potential of the reacting components. This cluster is the nucleus for further growth, which is energetically favorable because the excess chemical potential of the crystal decreases as its radius increases, (3) flux of clusters to hydrates cores, and (4) growth of stable cores according to classical nucleation theory (Kvamme, 2000).

The thermodynamic drive to overcome the energy barrier associated with hydrate nucleation comes from supersaturation of water with methane. Supersaturation may result from increased of methane supply, increased pressure or reduced temperature (Clennell et al., 2000). After hydrate nucleation, crystals will go through a period of rapid growth. If local equilibrium prevails and water and guest molecules are available in the bulk, then hydrate will continue to form, almost uninhibited, and fill any larger pores or fractures already present in the sediments. After this period, the crystals will impinge on the pores walls and necessarily adopt greater surface curvature as intersticies are filled and smaller throats penetrated. In marine sediments, this restricted growth stage requires progressively greater supersaturation, from cooling or an increased methane supply (Clennell et al., 2000).

Coarse textured sandy soils have larger pores than fine-grained soils but fine grained sediments (ranging from silt, silty clay and heavy clay) have a higher pore space per unit than coarse-textured (almost as twice as sandy soils), although individual pores have a smaller diameter and are tortuous. Since capillary forces between the pore spaces and pore throats of fine-grained sediments depress the pressure stability and also the temperature of hydrate formation by as much as 4 °C at a given pressure, gas hydrate formation should be expected to occur first in areas of high porosity, and large pores spaces rather than in more constricted pore spaces within fine sediments (Lorenson, 2000).

Hydrates have been found in all sediments from coarse to fine grained. The critical pore size defines a criterion for segregated growth of hydrates in sediments. The curvature of the clathrate has to be just sufficient to penetrate pores of a certain size. Hydrates growth as an interstitial phase when it can adopt a stable surface curvature that allows it to penetrate pore throats. When this curvature is greater than a certain value (i.e., all pore throats greater than a critical size, which is typical for each soil, have been penetrated), then the hydrate pushes aside the sediments grains and growths displacively, creating segregated masses if this mode of growth is energetically advantageous (Clennell et al., 2000). In sands and coarse sediments, it is more favorable for hydrates to growth wholly within the pores or cement the sediments, whereas in fine grained sediments it is expected that capillary forces will push the sediment grains aside, so that the hydrates form a segregated mass such as lenses, nodule or sheet (Clennell et al., 2000). Therefore massive or segregated hydrate growths forms predominate in fine grained sediments, but sometimes fine sediments can host clathrates that are widely distributed and diffuse within. Diffuse hydrate in sediments might consist of small nodules or inclusions 10 μm to 1 mm across. Although invisible to the naked eye, these small hydrate particles are considerable larger than the pores, therefore they have caused segregation.

A body of hydrate may be considered as a segregated mass if it has evolved into a simple shape, either nodule or lens, that does not include many sediment grains, and if it is large compared to the sediment grain size. In terms of thermodynamics, the mass will effectively assume bulk properties when it is large enough that its surface energy may be

neglected (Henry et al., 1999). With this definition, a spheroid of 100 ηm radius in a clay matrix may actually qualify as a segregated mass. It is expected that hydrates first form in larger pores and segregate only when pores with an access radius of more than 15-30 ηm are no longer available (Klauda and Sandler, 2001).

Capillary effects may affect the large variations of the gas hydrate content observed in natural sediments with lithology and porosity, the hydrate growth forms observed in marine sediments and the distribution of hydrate between interstitial hydrate and segregated masses and the stability conditions of gas hydrates in fine grained sediments.

1.3 Relevance of Gas Hydrates

Interest in naturally occurring gas hydrate has continued to increase during the last 30 years because it can be a potential energy resource, a factor in global climate change, and a submarine geohazard (Kvelvolden, 1993).

1.3.1 Gas Hydrates as a Potential Resource

There is an enormous amount of methane apparently sequestered in gas hydrates at shallow sediment depths within 2000 m of the surface of the Earth, and with a widespread geographic distribution (Figure 1.4). Current estimates are between 1-to-50 x 10^{15} m^3 at standard temperature and pressure STP (Kvenvolden, 1993). Evaluation of these reserves is highly uncertain, yet even the most conservative estimates concur that there is twice as much energy in hydrates as in all other hydrocarbon sources combined.

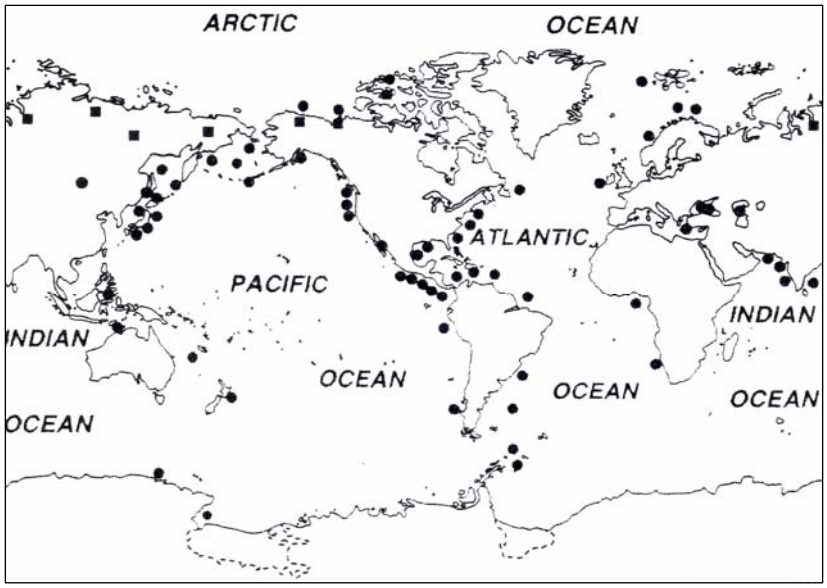

Figure 1.4 Worldwide locations of known and inferred gas hydrate deposits in oceanic aquatic sediments of outer continental margins (solid circles) and in polar permafrost regions (solid squares)

Source: Kvenvolden, 1993

However, there is no consensus that methane can be extracted economically from gas hydrate deposits. Gas hydrate occupy mostly unconsolidated or semiconsolidated sediments. When gas hydrate dissociates, free methane gas and water are produced. Then, the challenge for the production engineer is to move the free methane to collectors through an unconsolidated mix of sediment and water (Kvenvolden, 1993).

Although naturally occurring gas hydrate was recognized in the 1960's, the gas industry has been slow at developing methodologies to recover methane from gas hydrate due in part to a generally abundant conventional gas supply and a lack of economic incentives (Sloan, 1998-b).

1.3.2 Methane Hydrates and Global Climate Change

The Earth's atmosphere has a wide variety of sources and sinks for methane, including methane hydrate, which exists in metastable equilibrium and is affected by changes in pressure and temperature that occur mainly due to factors associated with changes in sea level (Cicerone and Oremland, 1988). Methane is a powerful greenhouse gas. A substantial instantaneous release of methane from gas hydrate could have an important impact on atmospheric composition, and thus, on the radiative properties of the atmosphere that affect global climate (MacDonald, 1990). For example, the release of as little as 0.065 % of the Earth's methane deposits into the atmosphere would be equivalent to doubling the atmospheric CO_2 and would lead to global warming. The temperature increase could cause hydrates to dissociate further, creating a positive feedback loop with potentially catastrophic results. Thus, the detection and evaluation of the extent of subseafloor methane hydrate deposits are of great importance not only to determine the potential for resource recovery but also for natural hazard assessment (Willoughby et al., 2000).

Whether or not methane hydrate gets into the atmosphere depends on the rate of hydrate dissociation, gas migration and trapping in sediments, gas venting into the water column and methane oxidation resulting in carbon dioxide (also a radiatively active gas when in the atmosphere). Then, net effect of all of these processes is not known with certainty but it undoubtedly varies with the geological situation. Thus, the precise role of gas hydrate in global climate change is uncertain. In all cases, the time scales involved in gas-hydrate-induced climate change could be long.

1.3.3 Gas Hydrates as Geological Hazard

Gas hydrate related geohazard issues are likely of immediate importance on both regional and local scales (Kvenvolden, 1999). Regionally, there are many examples of the possible connection between gas hydrate and submarine sediment slides and slumps on the continental slope and rise of West Africa; slumps and collapse features on the U S Atlantic continental slope; large submarine slides on the Norwegian continental margin;

sediment blocks on the sea floor in fjords of British Columbia; and massive bedding-plane slides and rotational slumps on the Alaskan Beaufort Sea continental margin (Kvenvolden, 1993).

These submarine disruptions of the seafloor, probably caused by gas-hydrate dissociation, can affect engineering structures located in regions of potential failure. On the local scale, gas hydrate dissociation in oceanic sediments, caused by heat transfer during petroleum production can lead to sediment failure and collapse of engineering structures (Chaouch and Briaud, 1997). Risk to drilling and production through gas hydrate-bearing sediments include blowouts and casing failures as experienced in Arctic regions (Yakushev and Collett, 1992). These same concerns, such as casing collapse, gas leakage outside of the conductor casing, and gas blowouts, are relevant to gas hydrate in deep oceanic regions as well (Bagirov and Lerche, 1997). Thus, gas hydrate is a significant geohazard of immediate and increasing importance as our industrial society moves to exploit ever-deeper seabed resources. Geohazards provide an additional constraint on exploiting oceanic gas hydrate as a future energy resource.

1.4 Trends in Gas Hydrate Research - This Thesis

The most important directions of the work on hydrates today are: (1) prevention of hydrate formation and removal of large hydrate plugs from production and transportation systems; (2) search, surveying, and mastering of gas deposits in a hydrate state; and (3) development of effective hydrate-based technologies (Kvenvolden, 1993). Neither an effective method for preventing hydrates nor a technology of using hydrates can be developed without revealing the laws of hydrate formation and decomposition kinetics in a free volume (well, pipeline) and in pore space (hydrate-saturated soils) without the knowledge of hydrates properties (Kvelvolden, 1993). Thus, researchers study phase equilibria, the kinetics of hydrate formation, as well as a number of properties, such as, the speed of sound, electromagnetic properties and thermal properties. In particular, understanding the thermal properties of gas hydrates, as well as the thermal properties of hydrate-bearing sediments, is of crucial significance in current and future research.

The purpose of this thesis is to explore the thermal properties of hydrate-bearing sediments. Chapter 2 presents a literature review of thermal properties in soils and tetrahydrofuran hydrates. The thermal properties of soils include unfrozen soils at a different saturation stages as well as frozen soils. Factors affecting the thermal properties of soils in both cases are reviewed.

Chapter 3 explains the devices and methods used to measure the thermal conductivity of soils bearing hydrates.

Chapter 4 presents the tested materials, the specimen preparation, procedures and experimental results.

Chapter 5 analyzes the experimental results and advances possible explanations, providing comparisons with previous investigations.

Appendix A presents considerations on frozen soils.

1.5 Summary

- Clathrate hydrates of natural gases are crystalline solids formed by water mixed with gases or other liquids.
- In hydrates, the water is the host molecule, which forms structures with cavities that serve as host site to small guest molecules through a hydrogen bonding network. No chemical union exists between the guest and host molecules.
- Gas hydrates are stable at temperatures below 10 ºC and pressure above 3.5 MPa.
- Hydrates form in one of the three crystal structures: S I, S II and S H.
- There are two basic models of hydrate formation in sediments: cementation around grains and formation within the pores.
- Most hydrates models are built on the analogy between hydrate in marine sediments and ice in permafrost, because the thermodynamic properties of hydrates in small pores change in the same way as those for ice.
- Gas hydrates are expected to occur first in areas of high porosity and large pore spaces rather than in more constricted pore spaces within fine sediments.

- In coarse grained sediments, hydrates growth within the pores or cement the sediments, while in fine grained sediments, hydrates form a segregated mass such as lenses, nodules or sheets.
- Clathrate hydrate of natural gases can be a potential energy resource, a factor in global climate change and a submarine geohazard.

CHAPTER 2

THERMAL PROPERTIES OF SOILS AND HYDRATES

The study of heat conduction was advanced by Fourier (1768-1830). Several properties characterize the material's thermal response: thermal conductivity k, heat capacity C, thermal diffusivity α, heat of transformation or latent heat of fusion, thermal expansion or contraction β.

The purpose of this chapter is to review the physical interpretation of thermal properties of soils, including frozen soils.

2.1 Heat Transfer

Heat transfer by conduction involves transfer of energy within a material without any motion of the material as a whole. The rate of heat transfer depends upon the temperature gradient and the thermal conductivity of the material. The thermal conductivity is not a constant, but is dependent on temperature, pressure, and porosity of a conducting material among other factors.

Heat transfer is defined as energy in transit from a high temperature object to a lower temperature object. Materials do not possess heat; materials possess internal kinetic energy in the form of random, disordered molecular motion (Young and Freedman, 2000). Therefore, temperature is a measure of the average translational kinetic energy associated with the disorder microscopic motion of atoms and molecules. Temperature is not directly proportional to internal energy since temperature measures only the kinetic energy part of the internal energy: two objects with the same temperature have the same average translational kinetic energy, but do not in general have the same internal energy (Young and Freedman, 2000).

Heat conduction in solids is the molecular exchange of kinetic energy. Therefore, thermal conduction is the result of collisions between molecules with different thermal energies. Through these collisions, energy is transferred from molecules with high E_T to molecules with low E_T.

In the case of gases, collisions are rarer than in liquids and solids. Therefore, the thermal conductivity of gasses is low compared to most solids or liquids. This does not mean that gases are good insulators: the space filled with gas may be large enough that heat transfer by convection is considerable, or the temperature is so high that heat exchange by radiation plays a remarkable part. In these cases, solids will present a better protection against heat exchange than gases, but only if they contain gases, i.e., if they are composed of loosely packed small particles, like powders, grains, and fibers, or if they are porous (Young and Freedman, 2000).

Non-metallic solids transfer heat by lattice vibrations so that there is no net motion of the medium during energy propagation. Transfer is enhanced by cooperative motion in the form of propagating lattice waves, which in the quantum limit are quantisized by phonons (Young and Freedman, 2000). Metals are much better thermal conductors than non-metals because the same mobile electrons which participate in electrical conduction also take part in the transfer of heat. At a given temperature, the thermal and electrical conductivities of metals are proportional, but at high temperatures, the thermal conductivity increases while the electrical conductivity decreases with increasing temperature.

Considering a prismatic element of a material (e.g., soil) with a cross-sectional area A (Figure 2.1), the steady rate of heat transfer in a material by conduction is:

$$q = \frac{Q}{A} = -k\frac{\Delta T}{\Delta x} = ki \tag{1}$$

where q is the rate of heat transfer Q (W) per unit area A (m^2), k (W/mK or W/m°C) is the thermal conductivity of the medium, A is the area (m^2), T (K or °C) is the temperature, x (m) is the spatial coordinate, and $\Delta T/\Delta x$ (K/m or °C/m) represents the thermal gradient i.

The negative sign in Equation 1 indicates that heat flows in the direction of decreasing temperature. Hence, the direction of heat transfer is opposite to the temperature gradient since the net energy transfer will be from high temperature to low

temperature. This direction of maximum heat transfer is perpendicular to the equal-temperature surfaces surrounding a heat source.

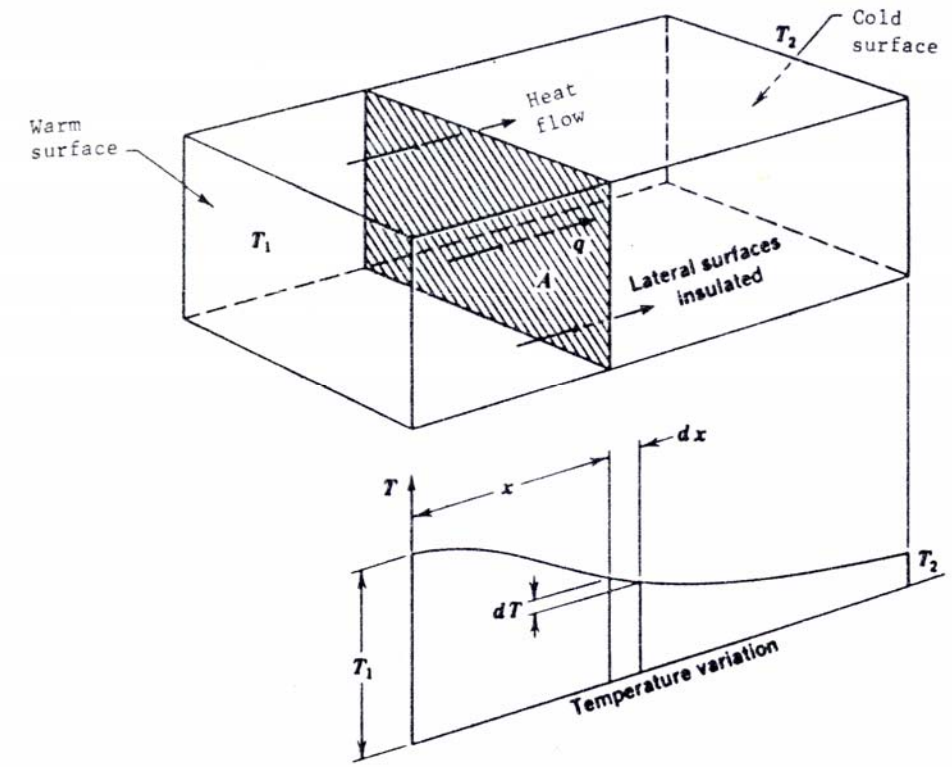

Figure 2.1 Heat flow through a soil element

Source: Andersland and Ladanyi, 1994

The transfer of thermal energy in earth materials can occur by conduction, convection and radiation. Consequently, the response of soils to thermal changes requires an understanding of their thermal properties: thermal conductivity, heat capacity, thermal diffusivity, latent heat, and thermal expansion (or contraction).

The relative importance of conduction and convection in heat-transfer problems depends on a number of factors including the nature of the medium (soil type) and its physical and thermal properties, the temperature of the medium, whether the soil is frozen or unfrozen, its porosity and permeability, water content and soil density.

Density, porosity and void ratio are three properties of special importance in considering the frost susceptibility of soils and their thermal properties. Void ratio and porosity values of typical soils are summarized in Table 2.1; Table 2.2 presents typical density values for dense soils, while Table 2.3 depicts typical water content values of water-saturated soils.

Table 2.1 Characteristic void ratio and porosity values for various soils

Soil	Void ratio, e	Porosity, n (%)
Sand, poorly graded	0.5 – 0.9	35 - 45
Sand, well graded	0.15 – 0.4	15 - 30
Clay, soft	1 - 3	50 - 75
Clay, stiff	0.3 – 0.8	25 - 45
Silt	0.3 – 1.4	25 - 60
Peat	> 5	> 85
Mud	3 - 6	75 - 85
Till	0.1 – 0.3	10 - 25

Source: Andersland and Anderson, 1978

Table 2.2 Characteristic density values for dense soils

Mineral	ρ_s, Kg/m^3
Quartz	2650
Kaolinite	2600 - 2700
Montmorillonite	2400 - 2600
Feldspar	2500 - 2900
Pyrite	5000 - 5100
Pyroxene	3100 - 3600
Illite	2600 - 2700
Chlorite	2600 - 3000
Organic sustance	1400 - 1700
Amphibole	2800 - 3400
Biotite	2700 - 3100
Muscovite	2800 - 3000
Calcite	2700

Source: Andersland and Anderson, 1978

Table 2.3 Characteristic water content values of water-saturated soils

Soil	Water content, ω (%)
Sand, gravel	10 -35
Clay, soft (inorganic)	40 - 100
Clay, stiff	10 -40
Silt	10 - 50
Peat	> 500
Mud	150 - 300
Till	5 - 10

Source: Andersland and Anderson, 1978

Heat conduction in soils takes place from particle-to-particle or through the soil pore fluid. This is the principal mode of heat transfer in soils. If the soil is unfrozen, there may also be convective heat transfer in association with mass transfer.

Heat transfer due to both conduction and convection can also occur in partially frozen soils at temperatures close to 0 °C where both liquid water and ice coexist (see Appendix A for frozen soils details). In this case, water may migrate to the freezing front zone under the potential gradient caused by the thermal gradient. Water migration to the cold side will continue as long as the potential gradient exceeds some critical value (the activation energy) provided that water is available. As a result, the material, at or close to the freezing front, may contain more ice than indicated by the total porosity of the soil at its original unfrozen state (Andersland and Ladanyi, 1994).

2.2 Thermal Conductivity of Soils

Thermal conductivity k characterizes the ability of a material to transmit heat by conduction and is defined as the quantity of heat flow that will occur in unit time through a unit area of a substance under a unit temperature gradient. The thermal conductivity is independent of whether any fluids contained within the interstitial pores are in motion.

The temperature gradient is assumed to be constant: as soon as the temperature starts changing, other parameters must be considered. Therefore, the measurement of thermal conductivity requires steady state conditions. This requires a carefully planned laboratory experiment and time to reach equilibrium.

The thermal conductivity of soils depends on: moisture content, dry density, mineral composition and temperature (Farouki, 1986). These factors can be arranged into two broad groups: those which are inherent to the soil itself and those which can be managed or externally controlled. Factors inherent to the soil include texture, mineralogical composition and organic content. Factors that can be externally altered include water content and soil density (Abu-Hamdeh et al., 2000).

2.2.1 Thermal Conductivity of Dry Soils

Thermal conductivity data for granular materials gathered by the American Society of Testing Materials (A.S.T.M) show that the thermal conductivity of dry soils is related to their unit weight (Thalmann, 1950).

Grain size affects the thermal conductivity of dry soils. Granular materials made of uniform size spherical particles have the same percentage of voids regardless of grain size. Well graded soils have a greater thermal conductivity due to their lower porosity. If particles are large enough to permit convective air currents (D_{50} > 6 mm), then heat can be transferred by convection (Thalmann, 1950).

The shape and arrangement of particles affect the thermal conductivity in dry soils in two ways: first through the packing density, and second through the area of contact between particles. In fact, owing to the increased area of contact between grains, non-spherical particles show a higher thermal conductivity than spherical particles of similar size and packing density (Thalmann, 1950). Thermal conductivity tests conducted on steel roller bearing of the same apparent density as ball bearings of the same material showed a higher thermal conductivity rate through the roller bearings. This is because the roller bearings offered greater contact area (Thalmann, 1950).

The thermal contact resistance TCR in granular media is the ratio of the temperature drop at the contact surface to the average heat flux across the contact (Tarnawski et al., 2002). It has been observed that loose soil packing produces large TCR effects, and higher TCR values are observed for clay than for sand. However, colloidal particles in a coarse soil reduce the TCR. For example, binding (cementation) of quartz particles in sandstone rocks leads to increased k_{eff} of the soil structure by a factor of about five. The thermal contact resistance gradually diminishes as saturation increases. So, the effect of cementation on k_{eff} acts similarly as does increased water content in soils (Tarnawski et al., 2002).

The increase in bulk density causes an increase in the soil thermal conductivity at given moisture content. With the increase in soil dry density, more soil particles are packed into a unit volume and the number of contact points between the particles increases (coordination number) (Figure 2.2). This figure also shows that particle shape

influences how well particles can be packed together. Soils with relatively flat surfaces have a larger number of contact points, thus resulting in greater thermal conductivity as compared to soils composed of round particles which have a smaller number of contact points (Becker et al., 1992).

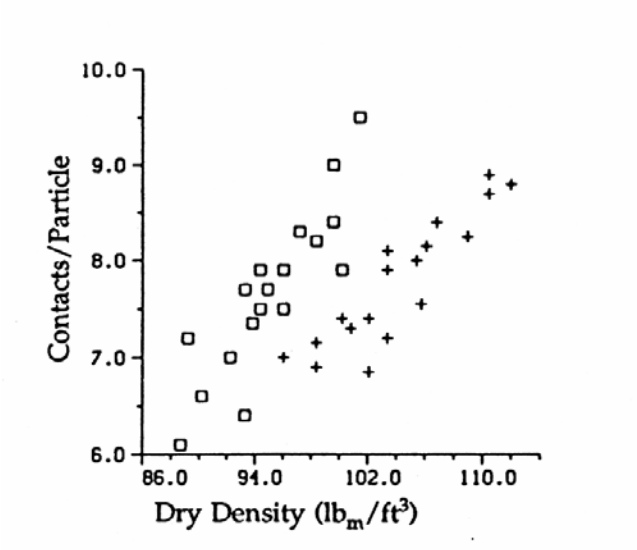

Figure 2.2 Number of contacts/particle vs. dry density for mixed shaped particles (square) and round shaped particles (cross)

Source: Becker et al., 1992

At a constant water content, an increase in dry density results in an increase in thermal conductivity (Figure 2.3) (Abu-Hamdeh et al., 2000).

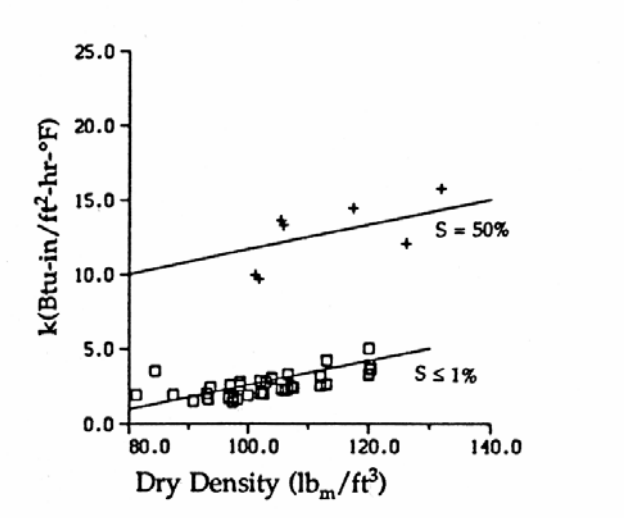

Figure 2.3 Thermal conductivity vs. dry density for unfrozen sand at two saturation levels: S≤1% (square) and S≥50% (cross)

Source: Becker et al., 1992

The mineral composition of the soil affects the soil thermal conductivity. For example, sands with high quartz content generally have a greater thermal conductivity than sands with high plagioclase feldspar and pyroxene content (Peters-Lidard et al., 1998).

Rawls et al., (1982) compile thermal conductivity and soil data from 1323 soils. Data analysis shows that porosity is more significant than quartz content and density (Peters-Lidard et al., 1998).

2.2.2 Effect of Moisture Content

Moisture content has the greatest impact on the thermal conductivity of soils: increasing soil moisture content at a given bulk density increases its thermal conductivity (Abu-Hamdeh et al., 2000). The multi-phase unsaturated granular materials are mixtures

of solids and fluid phases. There is no simple and general relationship between the thermal conductivity of the soil k and its volumetric water content ω because the porosity n and the thermal conductivity of the solid fraction k_s are also important parameters. The relation between thermal conductivity and volumetric water content, though monotonically increasing, can be more complicated, because the mineralogy of the solid fraction and the air content also have a pronounced influence on thermal conductivity (Cosenza et al., 2003).

Thermal conductivity of a soil increases in three stages as the saturation level increases. As moisture is added to a dry soil, a thin water film develops around grains and bridges the gaps between soil particles. These bridges facilitate heat flow and cause higher thermal conductivity.

At low saturation, moisture first coats the soil particles. The gaps between the soil particles are not filled rapidly, and thus, there is a slow increase in thermal conductivity. The liquid replaces the gas in the void space and changes its thermal conductivity. The thermal conductivity of the effective continuous medium also changes, as it strongly depends upon the thermal conductivity of voids. The distribution of fluid around the solid grain is uniform and is proportional to the specific area of the solid grains.

At high water content, liquid bridges the contact between consecutive solid grains, and there is a high increase in conductivity. The liquid surrounds the solid grains and starts to form an effective continuous medium. As the amount of liquid increases, the amount of void gas decreases. At complete liquid saturation, the void is completely free from gas and thermal conductivity reaches its asymptotic value (Pande and Gori, 1986).

2.2.3 Other Effects

Temperature has a small effect on the thermal conductivity of soils at T > 0 °C. Furthermore, there is little change in the thermal conductivity of air-dry soils across 0 °C. However, a dramatic change in the soil thermal conductivity occurs between the frozen and unfrozen states due to the higher thermal conductivity of ice. The thermal conductivity decreases upon freezing at low water content and increases at high (Andersland and Ladanyi, 1994).

Thermally induced moisture migration is a complex phenomenon involving the interaction of several physical mechanisms. Heat conduction, latent heat, heat flow, vapor diffusion and capillary induced liquid flow all take place. For any thermal conductivity measurement a measurable steady state or transient temperature gradient is imposed on the specimen. If the specimen is dry, the imposed gradient can be large so that it can be measured accurately using simple instrumentation. Unfortunately, a temperature gradient causes moisture migration in unsaturated soils. As the soil conductivity typically varies by an order of magnitude between dry and wet states, moisture migration cause large errors in the estimation of the thermal conductivity (Ewen and Thomas, 1987).

2.2.4 Data and Correlations

Data computed by Becker et al., (1992) are presented in Figures 2.4 through Figure 2.8 for both, the frozen and unfrozen state. In each case, the upper curve represents the upper limit of the measured data, the middle curve is the mean and the lower curve represents the lower limit of the measured data. Only a mean correlation is presented for peat, due to the small amount of available data. Measured data collected for gravel includes saturation up to 40 % (Becker et al., 1992).

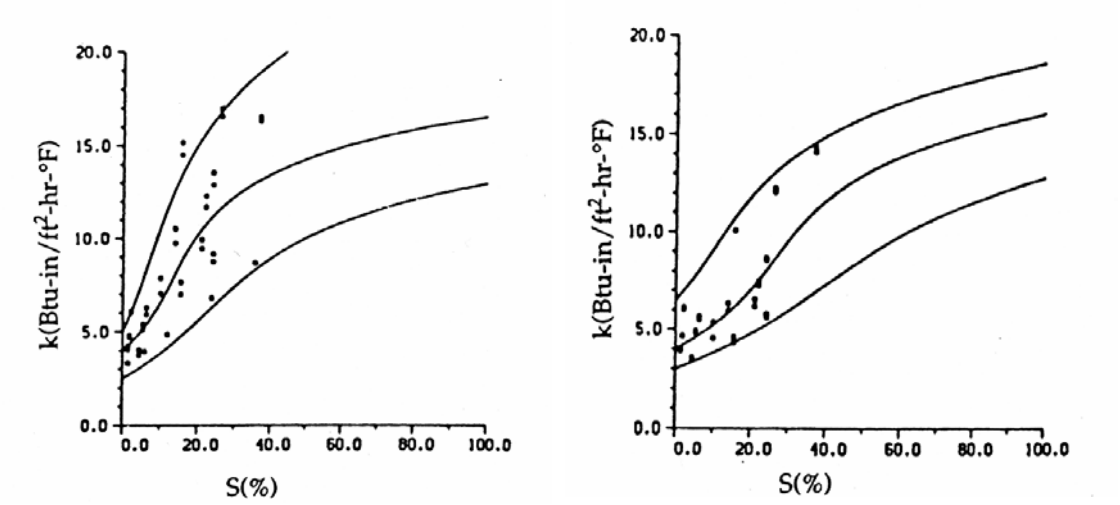

Figure 2.4 Thermal conductivity k vs. saturation S for gravel: (a) Unfrozen; b) Frozen

Source: Becker et al., 1992

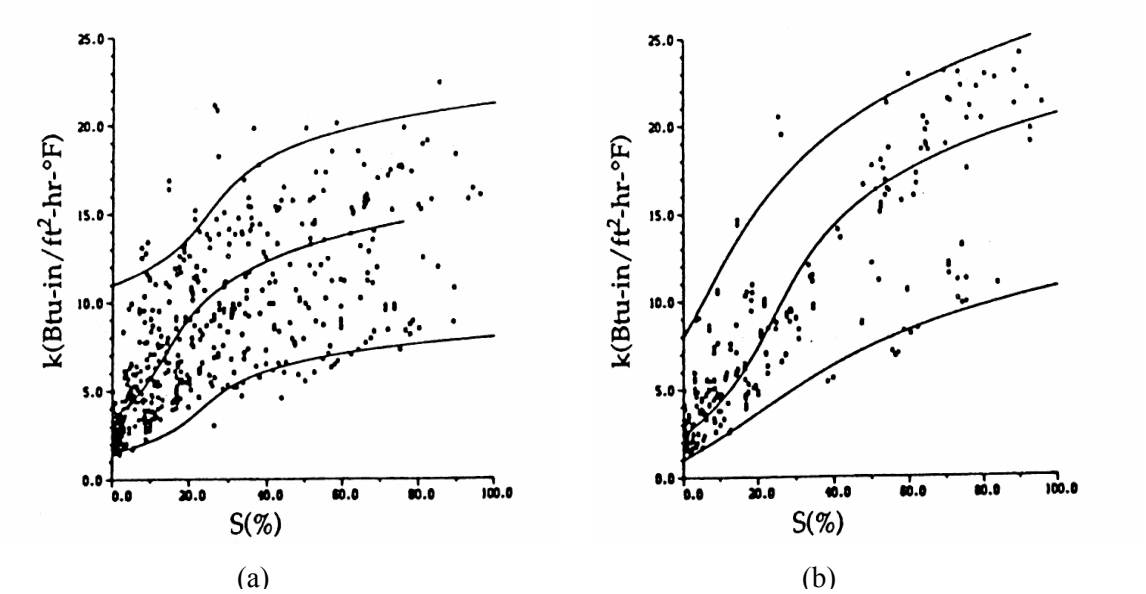

Figure 2.5 Thermal conductivity k vs. saturation S for sand: (a) Unfrozen (b) Frozen

Source: Becker et al., 1992

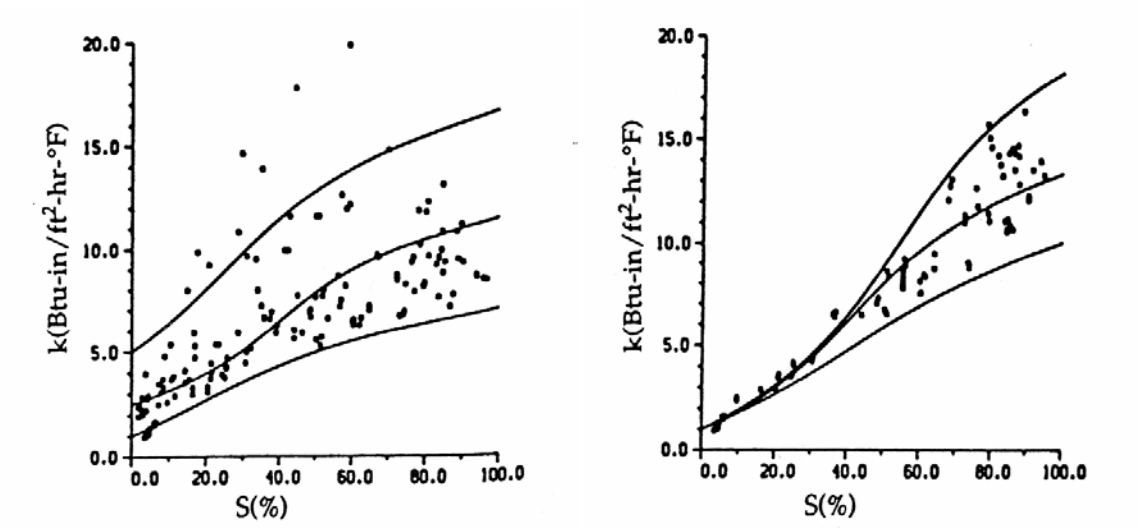

(a) (b)

Figure 2.6 Thermal conductivity k vs. saturation S for silt: (a) Unfrozen (b) Frozen

Source: Becker et al., 1992

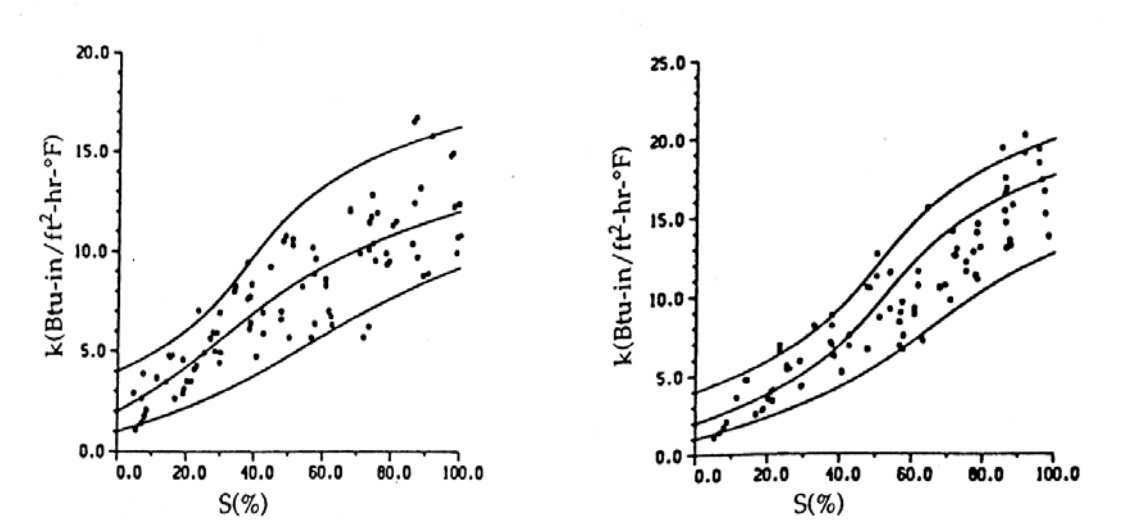

(a) (b)

Figure 2.7 Thermal conductivity k vs. saturation S for clay: (a) Unfrozen (b) Frozen

Source: Becker et al., 1992

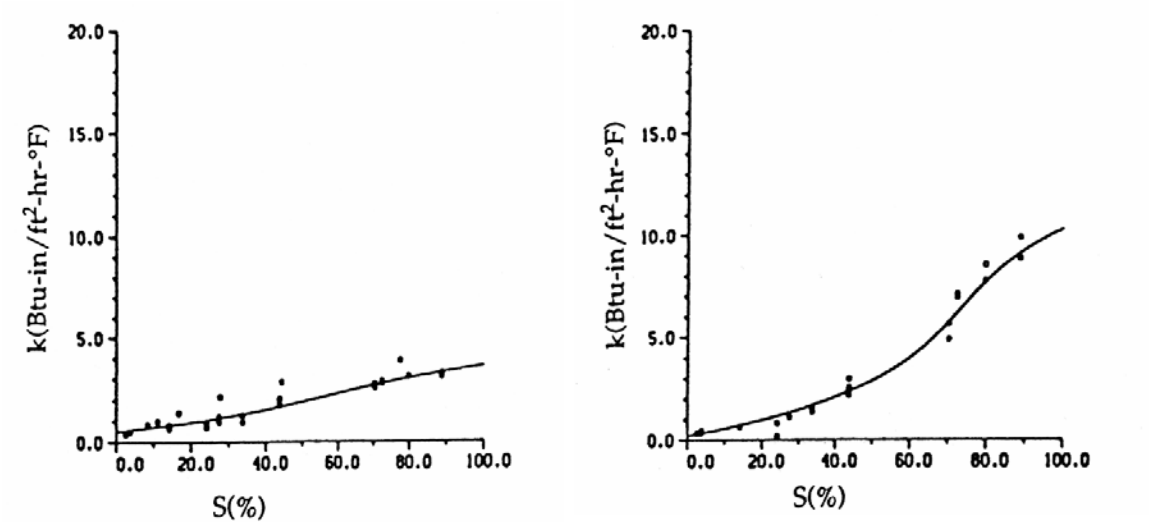

Figure 2.8 Thermal conductivity k vs. saturation S for peat: (a) Unfrozen (b) Frozen

Source: Becker et al., 1992

Thermal conductivity values for soil constituents and selected materials are listed in Table 2.4. Values vary greatly; quartz has the greatest thermal conductivity and air the least. The volumetric proportions of the various soil constituents influence the effective soil thermal conductivity.

Average soil thermal conductivity trends are presented in Figure 2.9 through and Figure 2.11 for coarse, fine and organic soils, both frozen and unfrozen. Values of thermal conductivity are selected on the basis of water content and dry density.

Table 2.4 Thermal conductivity of selected materials

Material	Thermal conductivity, k (W/mK)	Source
Silver	406.0	Andersland and Ladanyi, 1994
Copper	385.0	Andersland and Ladanyi, 1994
Brass	109.0	Andersland and Ladanyi, 1994
Aluminum	205.0	Andersland and Ladanyi, 1994
Iron, ductile	50	Andersland and Ladanyi, 1994
Steel	50.2	Andersland and Ladanyi, 1994
Lead	34.7	Andersland and Ladanyi, 1994
Mercury	8.3	Andersland and Ladanyi, 1994
Air at 0 ºC	0.024	Andersland and Ladanyi, 1994
Air at 10 ºC	0.026	Andersland and Ladanyi, 1994
Oxygen	0.023	Andersland and Ladanyi, 1994
Hydrogen at 0 ºC	0.14	Andersland and Ladanyi, 1994
Helium at 0 ºC	0.14	Andersland and Ladanyi, 1994
Water at 0 ºC	0.56	Andersland and Ladanyi, 1994
Water at 10 ºC	0.58	Andersland and Ladanyi, 1994
Water at 21 ºC	0.72	Andersland and Ladanyi, 1994
Ice at 0 ºC	2.21	Andersland and Ladanyi, 1994
Ice at -40 ºC	2.66	Andersland and Ladanyi, 1994
Snow, loose	0.08	Andersland and Ladanyi, 1994
Snow, compacted	0.7	Andersland and Ladanyi, 1994
Polystyrene foam	0.036	Andersland and Ladanyi, 1994
Rock wool	0.039	Andersland and Ladanyi, 1994
Glass wool	0.042	Andersland and Ladanyi, 1994
Styrofoam	0.01	Andersland and Ladanyi, 1994
Glass, ordinary	0.8	Andersland and Ladanyi, 1994
Asbestos	0.16	Andersland and Ladanyi, 1994
Fiberglass	0.04	Andersland and Ladanyi, 1994
Brick, insulating	0.15	Andersland and Ladanyi, 1994
Brick, red	0.6	Andersland and Ladanyi, 1994
Cork board	0.04	Andersland and Ladanyi, 1994

Table 2.4 (cont'd)

Material	Thermal conductivity, k (W/mK)	Source
Concrete	1.7	Andersland and Ladanyi, 1994
Wood:	1.28	Andersland and Ladanyi, 1994
Plywood, dry	0.17	Andersland and Ladanyi, 1994
Fir or pine, dry	0.12	Andersland and Ladanyi, 1994
Maple or oak, dry	0.17	Andersland and Ladanyi, 1994
Rock, typical	2.2	Andersland and Ladanyi, 1994
Quartz	8.4	Andersland and Ladanyi, 1994
Granite	1.7-4.0	Andersland and Ladanyi, 1994
Soil	0.15 – 1.5 (~ 1.0)	Andersland and Ladanyi, 1994
Soil minerals	2.9	
Soil organics	0.25	
Sand, dry	1.1	Andersland and Ladanyi, 1994
Sand, ω= 18 %, unfrozen	3.14	Andersland and Ladanyi, 1994
Sand, ω= 18 %, frozen	3.84	Andersland and Ladanyi, 1994
Clay, dry	0.9	Andersland and Ladanyi, 1994
Clay, ω= 25 %, unfrozen	1.16	Andersland and Ladanyi, 1994
Clay, ω= 25 %, frozen	1.51	Andersland and Ladanyi, 1994
Peat, dry	0.07	Andersland and Ladanyi, 1994
Rock matrix (marine sediments)	2.0	Matsubayashi and Edwards, 2000
$THF.17H_2O$ (-10.15 ºC)	0.53	Ross et al., 1981
Pure methane hydrate	0.45	Matsubayashi and Edwards, 2000
Pure THF	0.26	Hydrate team at Gatech, 2003
Mixture of 50 % THF and 50% H_2O, unfrozen	0.46	Hydrate team at Gatech, 2003
Mixture of 20 % THF and 80% H_2O, unfrozen	0.60	Hydrate team at Gatech, 2003
Mixture of 20 % THF and 80% H_2O, frozen	0.75	Hydrate team at Gatech, 2003

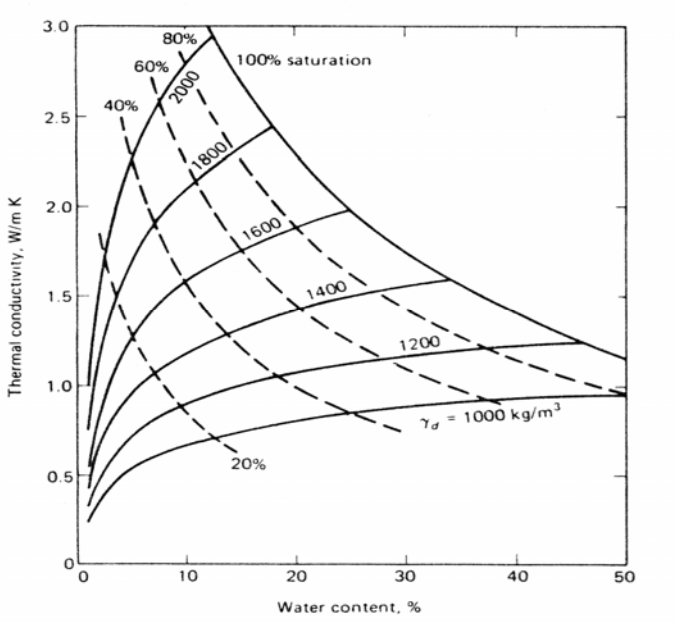

(a)

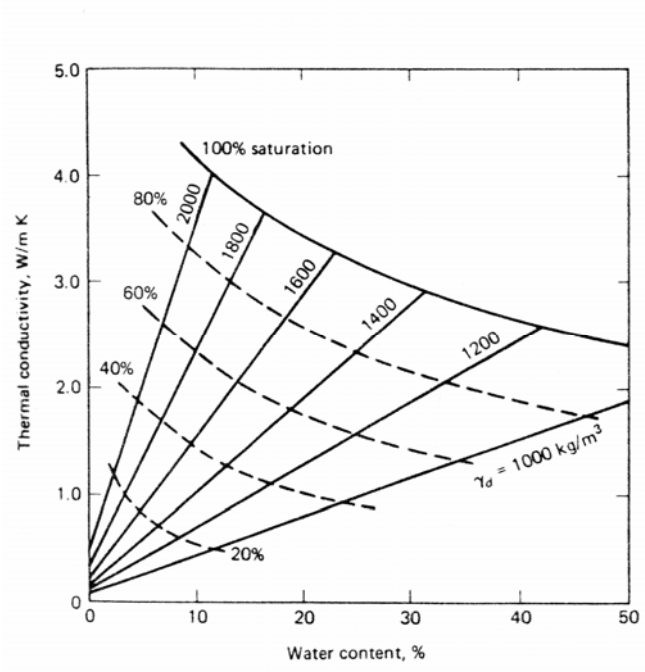

(b)

Figure 2.9 Thermal conductivity for sand and gravel: (a) Unfrozen (b) Frozen

Source: Andersland and Ladanyi, 1994

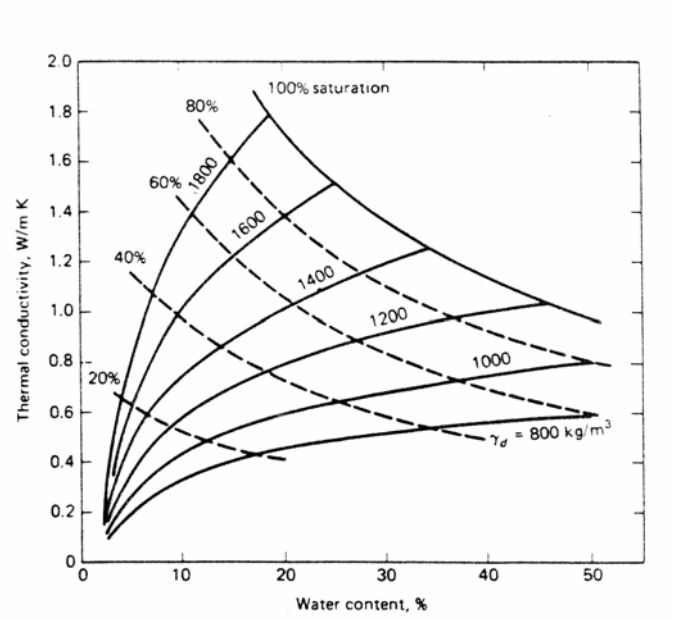

(a)

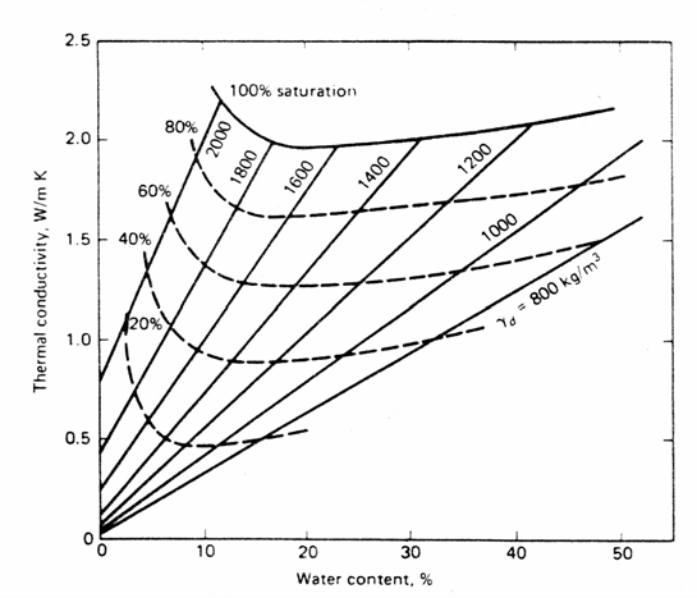

(b)

Figure 2.10 Thermal conductivity for silt and clay: (a) Unfrozen (b) Frozen

Source: Andersland and Ladanyi, 1994

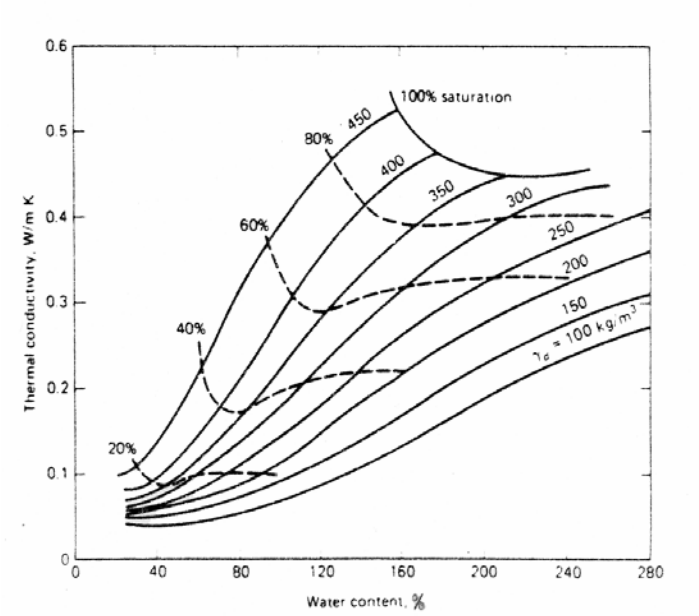

(a)

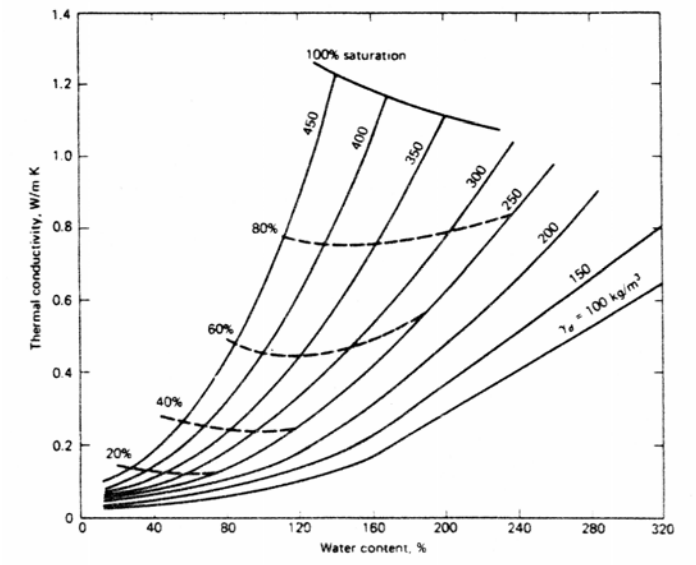

(b)

Figure 2.11 Thermal conductivity for peat: (a) Unfrozen (b) Frozen

Source: Andersland and Ladanyi, 1994

Various empirical or semi-empirical models have been developed for estimating the thermal conductivity of soils. Farouki (1986) presents a comprehensive and detailed review of these models and compares 11 semi-empirical models including those by Kersten (1949) and de Vries (1963), against measured values for a wide range of fine to coarse soils, frozen and unfrozen conditions and a range of soil moistures. The summary of the specific condition to use any of them is presented in Table 2.5, based on Farouki (1986).

Table 2.5 Summary of different methods to calculate k according to soil type

Soil condition	Recommended method
Unfrozen coarse soils $0.015 < S < 0.1$	Van Rooyen for sand and gravels (not for low-quartz crushed rocks)
Unfrozen coarse soils $0.1 < S < 0.2$	De Vries
Unfrozen coarse soils $S > 0.2$	Johansen
Unfrozen coarse soils Sandy silt-clay	Gemant
Unfrozen coarse soils Saturated	Johansen, de Vries, modified resistor, kunii-Smith, Mickley, Gemant, or McGaw
Note: Kersten's method should not be applied to coarse soils with low or high quartz content	
Unfrozen fine soils $0 < S < 0.1$	Johansen (increase prediction by 15 %)
Unfrozen fine soils $0.1 < S < 0.2$	Johansen (increase prediction by 5 %)
Unfrozen fine soils $S > 0.2$	Johansen
Unfrozen fine soils Saturated	Johansen, de Vries, modified resistor, kunii-Smith, Mickley, Gemant, or McGaw
Frozen coarse soils $S > 0.1$	Johansen
Frozen coarse soils Saturated	Johansen, de Vries, Mickley, modified resistor or Kunii-Smith
Note: Kersten's method should not be applied to frozen coarse soils with low or high quartz content	
Frozen fine soils $S < 0.9$	Kersten

Table 2.5 (cont'd)

Soil condition	Recommended method
Frozen fine soils $0.1 < S < 1$	Johansen (with suitable unfrozen water content)
Saturated	Johansen and de Vries (Kersten should not be used where unfrozen water content is appreciable)
Dry coarse soils Natural	Johansen
Dry coarse soils Crushed rocks	Modified resistor, adjusted de Vries
Dry fine soils General	Modified resistor, adjusted de Vries
Dry fine soils Clay	Smith

Source: Farouki, 1986

Kersten (1949) developed empirical equations for thermal conductivity of frozen coarse and fine-grained soils. He tested many soil types and developed equations for the thermal conductivity of frozen and unfrozen silty-clay soils and sandy soils as a function of moisture content and dry density. Kersten's correlations give reasonable results only for frozen soils with saturation up to 90 %. The accuracy of results obtained for coarse-grained soils is ± 25 % but for fine soil the thermal conductivity is overestimated by 25-50 %. Kersten's equations do not account for variations in the quartz content (thermal conductivity of soil solids is 5.0 W/mK and 3.0 W/mK for the sandy soils and the silty-clayey soils, respectively). Therefore, the results for quartz sand are underestimated but for pure clay over estimated. Moreover, these equations are developed for soil temperatures between - 4 °C and + 4 °C and gravimetric moisture content above 7 % and 1 % for fine soils and coarse soils respectively, and they do not give any provision for the presence of unfrozen water (Farouki, 1986).

The model proposed by de Vries (1963) assumes that a soil is a two-phase material composed of uniform ellipsoidal particles dispersed in a fluid phase. The model is based on an analogy to the electrical conductivity of uniform spheres dispersed in a continuous fluid as proposed by Maxwell (1904). De Vries' model, which gives the soil thermal conductivity as a function of the solid volume fraction and the thermal conductivities of the solid and fluid phases, is applicable to unfrozen coarse soils with saturation between 10 to 20 %. It is the most generally accepted model for saturated two-phase media (Tarnawski and Wagner, 1993). The model has been successfully applied to frozen soils having high moisture content (degree of saturation above 0.8). The use of this model requires numerous parameters such as grain shape and unfrozen water content as a function of temperature; these data are generally not available (Tarnawski and Wagner, 1993). On the other hand the model provides valuable insight such as the ratio of the average temperature gradient in air filled pores to the overall temperature gradient, which is used to evaluate the thermal vapor diffusivity of soil (Tarnawski and Wagner, 1993).

Mickley's model lumps all soil grains and assumes perfect thermal contact between grains. Its application to frozen soil is limited to a degree of saturation above 0.6 (Farouki, 1986).

Van Rooyen's and Winterkorn's correlation based on data collected from sand and gravels. It gives soils thermal conductivity as a function of the degree of saturation, dry density, mineral type, and granulometry. The Van Rooyen model is limited to unfrozen sands and gravels with saturation levels between 1.5 to 10 % (Becker et al., 1992).

Gemant's model is based on an idealized geometrical arrangement of soil particles with point contacts. It gives soil thermal conductivity as a function of soil dry density, moisture content, apex water (water collected around the contact points), water absorbed as a film around the soil particles, thermal conductivity of the solids, and thermal conductivity of water. Gemant's method gives reasonable values for unfrozen sandy soils (Becker et al., 1992).

Farouki (1986) indicates that the method developed by Johansen (1975) appears to be the most general method and to be superior to all other methods, except for dry fine soils, where an adjusted de Vries (1963) model is somewhat superior. Johansen (1975)

correlations, gives the thermal conductivity of soils as a function of soil saturation. It provides the best results for unfrozen and frozen soils, coarse or fine, at a degree of saturation above 0.1 (Andersland,1994). However, this method is limited to saturation greater than 20 % (Becker et al., 1992).

Farouki (1986) recommends the use of three separate relationships to determine the thermal conductivity-moisture content relationship of an unsaturated coarse soil, depending on the degree of saturation of the soil: Van-Rooyan and Winterkorn's model when the degree of saturation is less than 0.1, de Vries' model at degrees of saturation between 0.1 and 0.2, and Johansen's model at degrees of saturation greater than 0.2. Unfortunately his proposal produces discontinuities in the form of the relationship when $S< 0.2$. It also leaves large differences between estimated values and measured values in the range $S> 0.2$ (Ewen and Thomas, 1987). Johansen model is reviewed in detail next.

2.2.5 Johansen's Model for Calculating the Thermal Conductivity of Soils

The method developed by Johansen (1975), and summarized in Figure 2.12, is applicable to unfrozen and frozen soils (Andersland and Ladanyi, 1994).

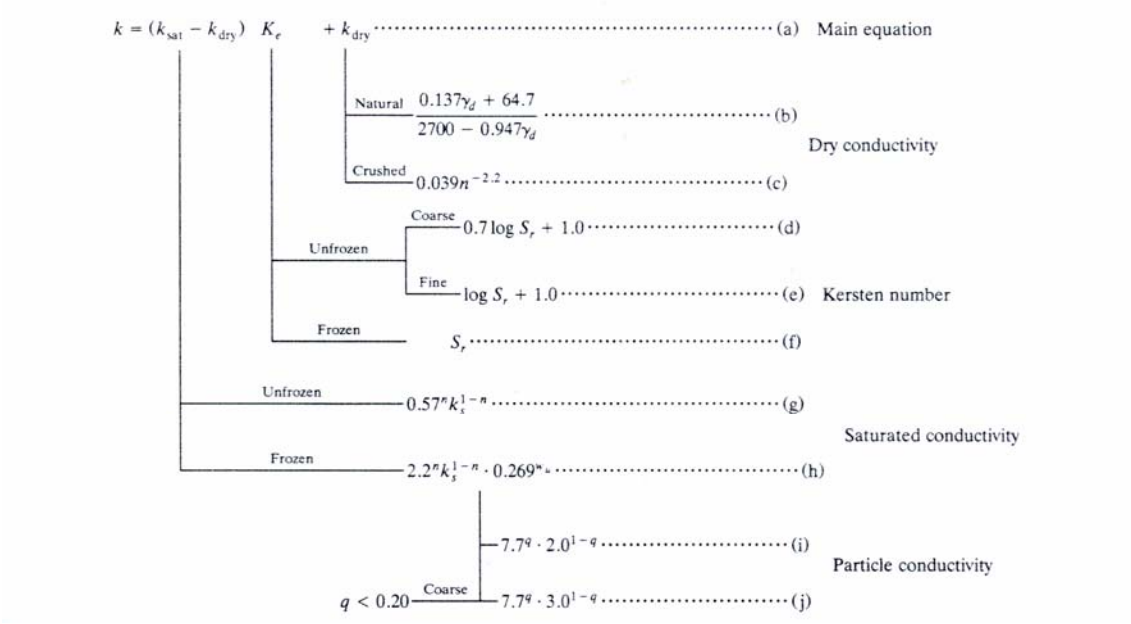

Figure 2.12 Johansen's method for calculating thermal conductivity of soils

Source: Andersland and Ladanyi, 1994

In this method, the thermal conductivity is a function of soil saturation, porosity, quartz content, dry density and phase of the water (frozen or unfrozen). The thermal conductivity k is interpolated between the dry (k_{dry}) and the saturated (k_{sat}) thermal conductivities, weighted by a normalized thermal conductivity (K_e) known as Kersten's number (Andersland and Ladanyi, 1994):

$$k_u = (k_{sat} - k_{dry})K_e + k_{dry} \quad (2)$$

Kersten's number K_e is a function of the degree of saturation S and the phase of the water. For coarse-grained unfrozen soil with the degree of saturation S > 0.05,

$$K_e = 0.7 \log S + 1.0 \quad (3)$$

and for fine-grained unfrozen soil with S> 0.1,

$$K_e = \log S + 1.0 \tag{4}$$

For all frozen soils, K_e = S (with a variation less than $\pm K_e$ = 0.1). This relationship underestimates the value of the thermal conductivity of the soil at low moisture contents (Andersland and Ladanyi, 1994). Johansen's original proposal that the thermal conductivity of an unsaturated soil should be estimated by interpolation between dry and saturated values remains attractive because of the simplicity of this approach (Ewen and Thomas, 1987).

For dry natural soils, Johansen (1975) develops the following semi-empirical equation for k_{dry}.

$$k_{dry} = \frac{0.137\rho_d + 64.7}{2700 - 0.947\rho_d} \pm 20\% \tag{5}$$

where ρ_d is the dry density (Kg/m^3) and the solids unit weight is taken as 2700 Kg/m^3. Johansen (1975) observes that crushed rock materials gave higher thermal conductivity values:

$$k_{dry} = 0.039n^{-2.2} \pm 25\% \tag{6}$$

where n is the soil porosity. For saturated soils, Johansen (1975) observes that variations in microstructure had little effect on thermal conductivity. He proposed the use of a geometric mean equation based on thermal conductivities of the soil constituents and their respective volume fractions. For saturated unfrozen soils, this gives:

$$k_{sat} = k_s^{1-n} k_w^{\ n} \tag{7}$$

where k_s is the thermal conductivity of the soil and k_w is the thermal conductivity of water. For saturated frozen soils containing some unfrozen water ω_u,

$$k_{sat} = k_s^{1-n} k_i^{n-wu} k_w^{wu} \tag{8}$$

taking the thermal conductivity of ice, k_i = 2.2 W/mK and k_w = 0.57 W/mK this expression reduces to:

$$k_{sat} = k_s^{1-n} (2.2)^n (0.269)^{wu} \tag{9}$$

Johansen (1975) suggests the use of a geometric mean equation to determine the thermal conductivity of the solid fraction of the soil k_s:

$$k_s = k_q^q k_o^{1-q} \tag{10}$$

where k_q and k_o are the thermal conductivity of quartz and other minerals, respectively, and q in exponents is the quartz fraction of the total solids content. A value of k_q = 7.7 W/mK is used and the thermal conductivity of other minerals is k_o = 2.0 W/mK for q > 0.2. For coarse-grained soils with a quartz content less than 20 %, Johansen (1975) uses k_o = 3.0 W/mK to account for the probable mineral composition of such soil.

Two examples (crushed gravel and silty clay) illustrate the determination of the thermal conductivity for unfrozen and frozen soils in Figure 2.13 and Figure 2.14, respectively (Andersland and Ladanyi, 1994).

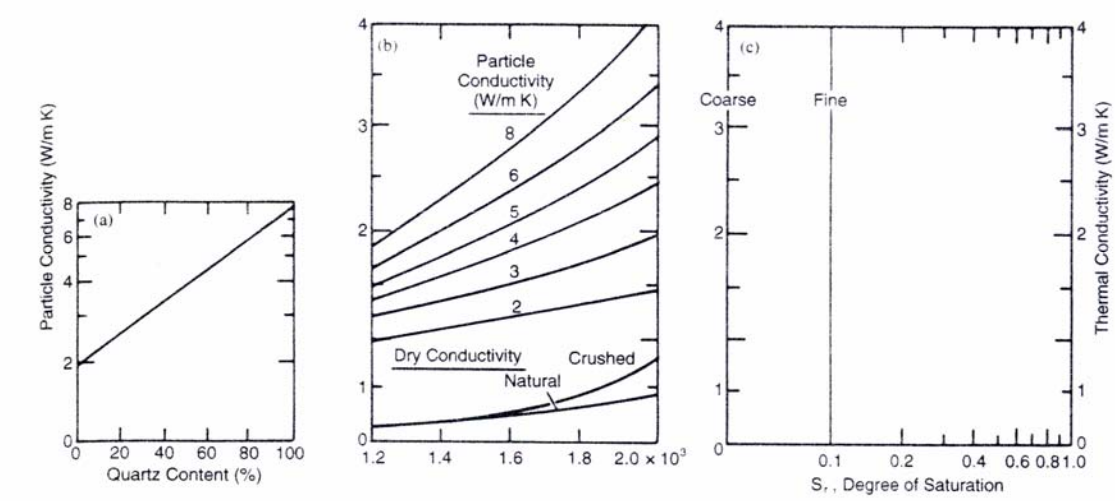

Figure 2.13a Thermal conductivity of unfrozen soils-Johansen's method.
Input variables:
1- quartz content,
2- crushed or natural,
3- coarse or fine (a soil with more than 5% of material having grain size less fine,
4- dry density,
5- degree of saturation.

Source: Andersland and Ladanyi, 1994

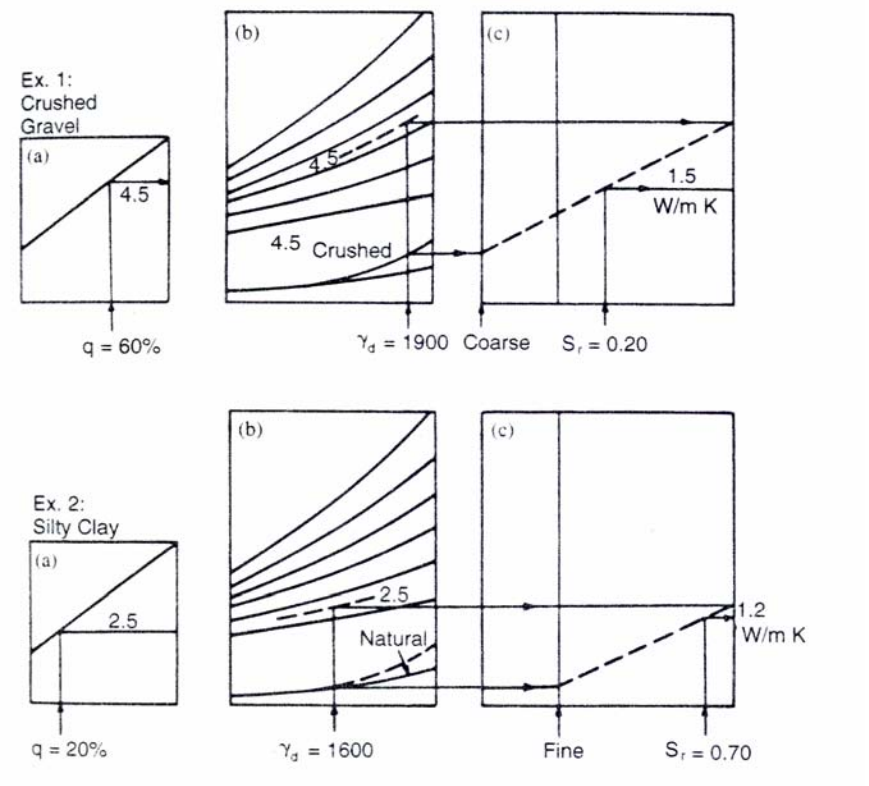

Figure 2.13b Thermal conductivity of unfrozen soils-Johansen's method
Two examples: Example 1: coarse soil. Example 2: fine soil
1- the particle thermal conductivity is estimated from the quartz content,
2- the value obtained is used together with the given dry density, to determine the thermal conductivity in the saturated condition,
3- the conductivity of the dry materials at the same dry density is found from the curves marked dry conductivity in part b (discriminate between crushed and natural soils),
4- from these extremes, the thermal conductivity at the actual degree of saturation is found by interpolation in part c (discriminate between coarse and fine soils.

Source: Andersland and Ladanyi, 1994

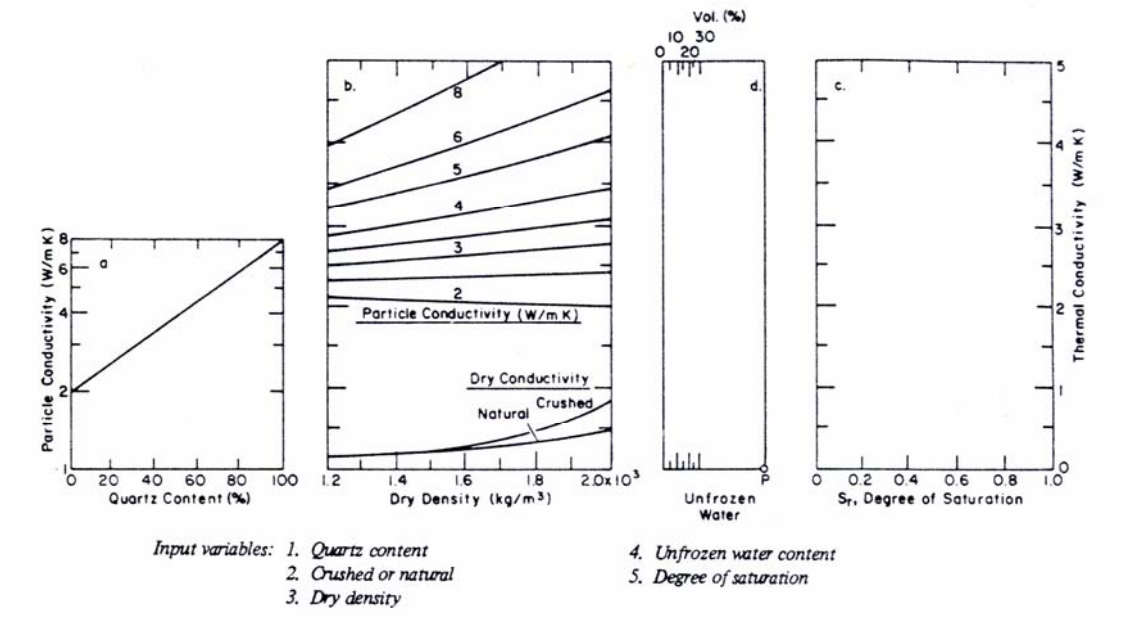

Figure 2.14a Thermal conductivity of frozen soils-Johansen's method
Input variables:
1- quartz content,
2- crushed or natural,
3- coarse or fine (a soil with more than 5% of material having grain size less fine,
4- dry density,
5- degree of saturation.

Source: Andersland and Ladanyi, 1994

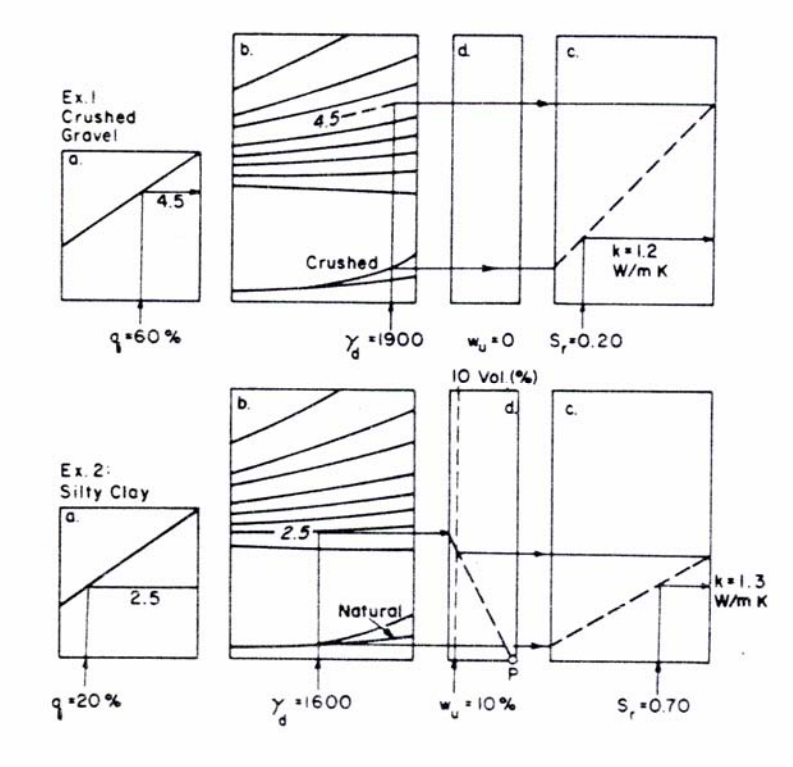

Figure 2.14 b Thermal conductivity of frozen soils.
Two examples: Example 1: coarse soil. Example 2: fine soil
1- the particle thermal conductivity is estimated from the quartz content,
2- the value obtained is used together with the given dry density, to determine the thermal conductivity in the saturated condition,
3- the conductivity of the dry materials at the same dry density is found from the curves marked dry conductivity in part b
4- if a certain percentage of the water is unfrozen, then the saturated thermal conductivity must be reduced in the manner shown by the graphical construction in part d,
5- the thermal conductivity at the actual degree of saturation is then found by linear interpolation as in part c.

Source: Andersland and Ladanyi, 1994

Although Johansen's (1975) method is simple, and the parameters it requires such as porosity, density, and saturation are readily available (e.g., Cosby et al., 1984 or Rawls et al., 1982), the implementation of Johansen's method is hampered by requiring the quartz content. Sand usually contains a very high percentage of quartz in crystalline form (Peters-Lidard et al., 1998). Silts and clays may also contain silicates, but these are not generally in the form of crystals. It is only quartz crystals that have a very high thermal conductivity, whereas the conductivity of quartz or silicate material bound inside clay or silt particles is similar to that of other similar materials (Farouki, 1986). A good approximation is to assume that the quartz content for each soil type is related to the percentage of sand in the soil. The quartz content in the sand varies widely from 0 to 100 %, and the quartz fraction of the soil, therefore, range from zero to the maximum sand content of the soil (Peters-Lidard et al., 1998). Recommended quartz content for various soil types is presented in Table 2.6, as well as a maximum percentage deviation in thermal conductivity due to uncertainties in all other parameters like particle size, porosity and dry density.

Table 2.6 Recommended quartz content and maximum expected variation in thermal conductivity from Johansen's method by soil type.

Soil texture	Quartz content	Maximum k variation (%)
Sand	0.92	55.2
Loamy sand	0.82	52.9
Sandy loam	0.60	49.2
Sandy clay loam	0.60	48.4
Sand clay	0.52	46.2
Loam	0.40	35.0
Clay loam	0.35	34.2
Silt loam	0.25	25.1
Clay	0.25	26.8
Silty clay	0.10	17.3
Silty clay loam	0.10	22.9
Silt	0.10	17.3

Source: Peters-Lidard et al., 1998

2.3 Thermal Conductivity of Clathrate Hydrates

Most physical and mechanical properties of clathrate hydrates are found to be very similar to those of ice, as expected from the similarities in the lattice structure. In contrast with most well-defined crystalline structure, in which the thermal conductivity falls with increasing temperature as T^{-1} (> 100 K), the thermal conductivity of clathrate hydrates increases slightly with increasing temperature (Tse and White, 1988). The thermal conductivity of clathrate hydrates is 5 times lower than that of ice near the melting point, and even lower (by a factor > 20) at lower temperatures. The temperature dependence of thermal conductivity in clathrate hydrates is characteristic of an amorphous material (Tse and White, 1988). From measurements of thermal conductivity at relatively high temperatures, it appears that the unusual thermal conductivity is insensitive to the crystal structure.

Thermal conductivity of a few gas hydrates have been published by Cook and Laubitz (1981), Ross et al., (1981), Stoll and Bryan (1979), Ashworth et al., (1985). These values are much smaller than those of ice, I_h, both at the freezing point and well bellow (Tse and White, 1988).

Thermal conductivity measurements by Afanaseva and Groisman (1973) give values for thermal conductivity of methane hydrates that are the same as for ice within the stated accuracy of about 10 %. Stoll and Bryan (1979) find that the formation of methane and propane hydrates cause a decrease in the thermal conductivity of wet sand, in contrast to the increase which occurs when water freezes (Cook and Leaist, 1983).

Cook and Leaist (1983) measure the thermal conductivity of ethylene oxide hydrate (like methane hydrate, it is a structure I type) and obtained k = 0.49 +/- 0.02 W/mK. For both hydrates, dependence on temperature is slight. Thus, the thermal conductivity of at least some gas hydrates of both structural types is less than a quarter lower than ice at relatively high temperatures and this ratio becomes rapidly smaller with decreasing temperature.

As a result of all the measurements of thermal conductivity of clathrate hydrates it can be concluded that these compounds are very poor thermal conductors. The large difference in the thermal conductivity of pure ice and clathrate hydrates provides a criterion for locating regions of shelf ice which contain potential energy reserves in the form of methane or similar gases. Thermal conductivity is also a vital parameter required for modeling the recovery of natural gas from hydrates: knowledge of the variation of the thermal conductivity with pressure and temperature is required for successful methane hydrates exploitation.

In the Debye model of thermal conduction, the phonons are treated as if they were gas molecules (Tse and White, 1988). This gives a thermal conductivity expression:

$$k = \frac{1}{3} C v l_m \tag{11}$$

where C is the specific heat per unit volume, v is the mean phonon velocity and l_m is the phonon mean free path. According to this model, for a structurally perfect crystal at a

temperature above 100 K (-173.15 °C), the total number of excited phonons is proportional to the absolute temperature T, and the collision frequency of a given phonon is proportional to the number of phonons with which it can collide. Thus, the mean free path is proportional to T^{-1}. Both the mean phonon velocity and the heat capacity are approximately temperature independent. Thermal conductivity is therefore proportional to T^{-1} (Ashworth et al., 1985).

Dharma-Wardana (1982) estimate the thermal conductivity of the various ice-polymorphs and of the clathrate hydrates using a kinetic formula and a scaling model based on ordinary ice and find good agreement with experiments. He assumes that guest molecules have no direct effect on thermal conductivity because of the weak guest-host interaction. However, the guest molecules may contribute to the scattering of heat-conducting phonos (Cook and Leaist, 1983).

For glassy solids, the mean free path is structurally determined and almost independent of temperature. The thermal conductivity therefore has the same temperature dependence as the specific heat: it increases slowly with increasing temperature. This appears to be happening in hydrates (Ashworth et al., 1985). Voids and guest molecules must be responsible for scattering phonons. It is somewhat surprising that the binding of guest molecules is the weak Van der Waals type (Ashworth et al., 1985). Some other possible explanations for this behavior will be found in the next sections.

Although tetrahydrofuran (THF) hydrate is icelike in appearance, its thermal properties behave like those of an amorphous substance (Ashworth et al., 1985). The thermal conductivity of THF hydrate has a weak temperature dependence and a much lower value than of ice, and the k(T) curve has a positive slope. These characteristics differ from the properties of most nonmetallic crystals (Figure 2.15).

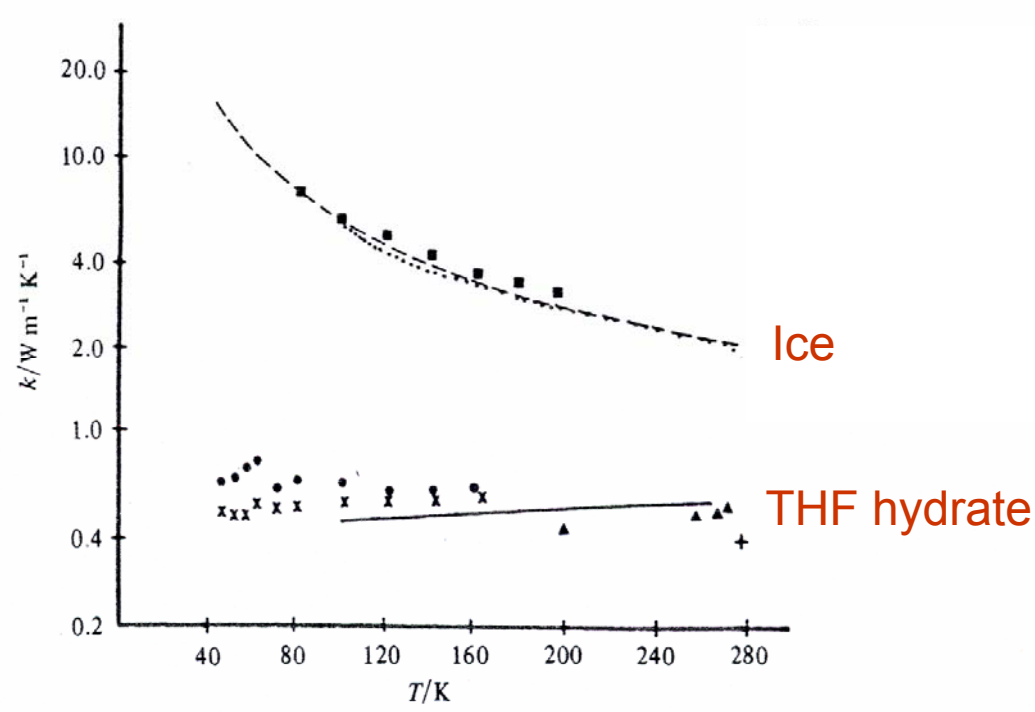

Figure 2.15 Thermal conductivity of pure ice (Ih) and THF hydrate

Source: Ashworth et al., 1985

It is well known that thermal conductivity for ordered crystals decreases with increasing temperature. Ross et al. (1981, 1982) found k = 0.53 +/- 0.02 W/mK at -10 °C for THF hydrate (Cook and Leaist, 1983). Ross et al. (1981), also found that with decreasing temperature, thermal conductivity decreases slightly to 0.49 W/mK at -153.15 °C, in contrast with the behavior of ice, for which k increases with decreasing temperature to a value of 0.53 W/mK at -153.15 °C. With a technique of measurement different from one employed by Ross et al. (1981), Cook and Laubitz (1981) found k = 0.51 +/- W/ mK at – 10 °C for THF hydrate (Cook and Leaist, 1983).

Cook and Leaist (1983) conclude that the thermal conductivity of methane hydrate at - 60 °C is well below that of ice and near that of the hydrates of ethylene and THF. The later, because of their low value and insensitivity to temperature, has been compared to the conductivity of a glass by Ross et al., (1981) and Dharma-Wardana (1982).

2.3.1 Origin of the Anomalous Thermal Conductivity of Clathrate Hydrates

Ordered crystals and glassy liquids are the two extremes in the conception of structural regularity in the solid state. Solid states other than these exhibit a variety of structures which are intermediate or partially disordered. Liquids normally crystallize into this type of mesophase before a subsequent transition to an ordered crystal phase takes place on further cooling (Anderson and Suga, 1996). This partial ordering in discrete steps makes it convenient to study the effect of structural disorder on physical properties such as the thermal conductivity k. The behavior of k in mono-atomic crystals is well understood whereas knowledge of k in glassy liquids and other disordered states can be improved (Anderson and Suga, 1996). Several hypotheses have been proposed to explain the unusual thermal conductivity of the clathrate hydrates with THF hydrate as a model of clathrate hydrate.

The first hypothesis considers that the thermal conductivity seems to be affected by structural disorder in THF clathrate hydrates. At least two different types of structural disorder can occur in THF clathrate hydrate crystals. One is associated with the H_2O molecules and other with the THF molecules (Anderson and Suga, 1996). Structural disorder associated with proton positions can arise. This disorder can also be described in terms of orientational disorder of the H_2O molecules. The degree of freedom for the position of a proton in a clathrate hydrate is essentially the same as that of the proton in ice I_h; therefore, it is reasonable to assume that proton disorder in clathrate hydrates should be present to approximately the same extent as in ice I_h. The other type of structural disorder that can arise in THF clathrate hydrate is associated with the orientation of guest molecules. Since the interaction between the THF and H_2O molecules is considered to be weak and the THF molecules are located inside almost spherical 16-hedral H_2O cages, they exhibit a large degree of orientational disorder, at least at high temperatures (Anderson and Suga, 1996).

Initially the orientational disorder of the THF molecules was considered as a possible source of the glassy behavior (Anderson and Suga, 1996). According to this criterion, the phonon scattering due to point defects and tunneling arising from proton disorder, are the major processes for the dissipation of thermal energy. It is well

established that ordinary orientationally disordered phases like plastic crystal phases commonly exhibit a glass-like thermal conductivity. If THF molecules were alone in the lattice and exhibited reorientational motion among several preferred orientations, then the phase would be regarded as a plastic crystal phase (the ice can be regarded as an orientationally disordered crystal but not a plastic crystal). The case of clathrate hydrates is more complicated, since we must consider both: the host lattice and the guest molecules. One expects that the strongly bonded ice lattice should provide the main path for heat flow, whereas the THF molecules could possibly be regarded as lattice defects that scatter the phonons (Anderson and Suga, 1996). However, since there is only a weak interaction between the ice lattice and a THF molecule, it has been argued that the THF molecules could not provide the strong phonon scattering necessary to obtain the glass-like k. Although this model fits the data at the very low temperature, it fails to account for the rapid rise in thermal conductivity above 10 K (-263.15 °C).

The second hypothesis considers that the vibrational motion of the guest molecule interacts with the host lattice. Due to low-frequency rattling of the guest in the cage, a strong resonance scattering mechanism of the thermal phonons can result from this interaction; which would then explain the glassy behavior and unusually low thermal conductivity. This model can describe the data for k of all clathrate hydrates, but it is in conflict with earlier arguments of weak interactions between the host lattice and the guests (Andersson and Suga, 1996).

Another hypothesis is related to the large unit cell of both type I and type II clathrate hydrates, so that the phonon mean free path is limited by the size of the unit cell. Darma-Wardana (1982) show that k could become glassy as the number of vibrating units in the unit cell becomes large. The limiting free path is assumed to be independent of temperature and chosen arbitrarily to be about 12 Å[13] (Tse and White, 1988). In order to obtain this dependence, however, it was assumed that the atoms in each unit cell have mass or bonds that differ substantially.

The glassy behavior for k is not affected by the high temperature→low temperature HT→ LT phase transition. The slightly increase of k with increasing temperature is observed for both, the LT phase and the HT phase of THF clathrate hydrate, in which the LT phase is believed to be an ordered state (Andersson and Suga,

1996). Since it is unusual for crystals to exhibit glass-like thermal conductivity, a reasonable conclusion is that the same mechanism causes the glassy behavior in both phases. The HT phase exhibits guest molecule (e.g., THF) orientational disorder; whereas the low temperature phase is probably orientationally ordered. Therefore, the orientation of the guest molecules must be insignificant in phonon scattering. The glassy behavior of thermal conductivity can instead be due to resonance scattering against the guest vibration as proposed in one of the earliest models (Andersson and Suga, 1996). However, the scattering cannot be strong enough to yield the minimum possible thermal conductivity for the LT phase, since k decreases at the LT→HT phase transition.

The examination of the low-temperature thermal conductivity of tetrahydrofuran clathrate hydrates allows one to conclude that despite the well defined crystalline structures, clathrates hydrates show glassy behavior attributable to low-frequency guest vibrations, causing the clathrate hydrates to be thermal glasses (Andersson and Suga, 1996).

2.3.2 Thermal Conductivity of Hydrates in Sediments

Regardless the ice-like appearance of hydrates and hydrates growth similarities with ice, thermal properties of ice in soil differ from thermal properties of hydrates in soils. There are several differences between hydrates and permafrost ice. Handa and Stupin (1992) concluded that the enthalpy of formation of gas hydrate is decreased in porous media, and this is in the same proportion as measured between bulk ice and pore ice (Clenell et al., 2000). The induction time for hydrate formation in porous media is reduced with respect to formation in free solution (Clenell et al., 2000). Nevertheless, freezing in porous solids provides a good starting point for the analysis of hydrate formation in sediments.

There are two important assumptions regarding the thermal conductivity of hydrates in porous media: a) either the hydrate is part of the pore fluid and does not affect the thermal conductivity of the dry frame, or b) hydrates become a component of the solid phase, reducing the porosity and modifying the solid phase thermal response.

THF hydrates, as well as natural gas hydrates, characteristically have a low value of thermal conductivity compared with sediment grains. Therefore, if it is assumed that hydrates coats grains, a lower thermal conductivity is obtained (Matsubashi and Edwards, 2000).

2.4 Other Thermal Properties

2.4.1 Heat Capacity

The specific heat (C) or heat capacity (J/K.m^3 or J/°C.m^3) is defined as the amount of energy required to increase the temperature of 1 g of the material by 1°C. The heat capacity C is important in transient conditions.

The heat capacity C is usually linked to the density ρ (kg/m^3) of the material. Thus, the specific heat capacity C_p (J/K.kg or J/°C.kg) is defined as the heat capacity normalized by the mass density:

$$C_p = \frac{C}{\rho} \tag{12}$$

The heat capacity of soils can be computed by adding the heat capacities of the different constituents in a unit mass of soil. If m_s, m_w, m_i, and m_{air} represent the mass fraction and C_s, C_w, C_i, and C_{air} the heat capacity of solids, water, ice, and air, respectively in a soil volume V with total mass m. Then, the specific heat capacity (C_p) of the soil is:

$$C_p\left(\frac{KJ}{Kg}\cdot °C\right) = \frac{1}{m}\left(C_s m_s + C_w m_w + C_i m_i + C_{air} m_{air}\right) \tag{13}$$

The volumetric heat capacity of the soil is obtained by dividing Equation 13 by V and neglecting the very small contribution by the air term (Andersland and Ladanyi, 1994):

$$C_v(\frac{MJ}{m^3}\cdot°C) = C_m\rho_f = \rho_{df}(C_s + C_w\omega_u + C_i\omega_i) \quad (14)$$

where ρ_f and ρ_{df} are the bulk and dry densities of the frozen soil, and ω_u and ω_i are the unfrozen and frozen water contents, respectively. Note that heat capacity C increases linearly with increasing soil moisture content ω_w. The heat capacity of soils is little dependent on temperature.

Mass heat capacity C_m is defined as:

$$C_m = \frac{C_v}{\rho} = \frac{C_v}{\rho_d(1+\omega)} \quad (15)$$

where ρ is mass density.

The specific heat of a material is defined as the ratio of its heat capacity to that of water. Then, the volumetric heat capacities for unfrozen and frozen soils can be calculated as:

$$C_{vu} = \frac{\rho_d}{\rho_w}(0.17 + 1.0\frac{\omega}{100})C_{vw} \quad (16)$$

$$C_{vf} = \frac{\rho_d}{\rho_w}(0.17 + 1.0\frac{\omega_u}{100} + 0.5\frac{\omega - \omega_u}{100})C_{vw} \quad (17)$$

where C_{vw} = 4.187 MJ/m^3°C, and ρ_d and ρ_w are the unit mass of the dry soil and water. Values of specific heat are C_v = 0.17 for mineral, C_v = 1.0 for water and C_v = 0.5 for ice. The specific heat for organic material is C_v = 0.40 (Andersland and Ladanyi, 1994).

2.4.2 Thermal Diffusivity

The thermal diffusivity of a soil determines its temperature response to thermal perturbations. The thermal diffusivity α (m^2/s) combines the thermal conductivity and the specific heat for the analysis of thermal transients,

$$\alpha = \frac{i}{C} \tag{18}$$

where $i=\Delta T/\Delta x$ is the thermal gradient and C is the specific heat. The thermal diffusivity permits estimating the time scale for transient thermal conditions in body size L:

$$t = \frac{L^2}{\alpha} \tag{19}$$

where t is the time (sec) and L is the body size (m).

Typical values listed in Table 2.7 show that the thermal diffusivity of ice is much higher than that of water. For this reason, thermal diffusivity in frozen soils will be much higher than in unfrozen soils. This means that the average temperature frozen soils will increase faster than in an unfrozen soil. The thermal diffusivity of a soil reaches a maximum value at a relatively low value of volumetric water content ω_w (Andersland and Ladanyi, 1994).

Table 2.7 Thermal diffusivity of several materials

Material	Thermal diffusivity (m^2/s) x 10^7
Copper	1133
Iron	173
Dolomite	78
Quartzite	45
Shale	31
Limestone	27
Granite	15
Sandstone	10
Ice	11.2
Dense saturated sand	8
Soft saturated clay	4
Fresh snow	3.3
Dry soil	2.5
Water	1.4
Organic solids	1.0
Air	0.21

Source: Andersland and Ladanyi, 1994

2.4.3 Latent Heat of Fusion

Latent heat is the amount of heat per unit mass involved in phase transformation at constant pressure and temperature. The liquid-solid phase change is characterized by the heat of fusion, while the gas-liquid transformation is characterized by the heat of vaporization.

Latent heat of fusion is the amount of heat absorbed when a unit mass of ice is converted into a liquid at the melting point. The latent heat of fusion for water at 0 °C is 333.7 KJ/Kg. The same amount of heat is liberated when the water is converted into ice with no change in temperature.

The energy involved when pore water changes phase in a soil mass depends on the gravimetric water content that changes phase (Andersland and Ladanyi, 1994):

$$L_v = \rho_d L' \frac{\omega - \omega_u}{100} \tag{20}$$

where L_v (KJ/m^3) is the soil volumetric latent heat of fusion, L' = 333.7 KJ/Kg is the mass latent heat for water, ρ_d (Kg/m^3) the soil dry density, ω the total water content, and ω_u the unfrozen water content (percentage of dry mass) of the frozen soil. For sands and gravels with little or no unfrozen water, the ω_u term will be very small, then, for many practical problems, the assumption that ω_u is zero will give acceptable L_v values for estimation purposes.

2.4.4 Thermal Expansion (or Contraction)

Thermal expansion is the coupling between thermal and mechanical energy. The coefficient of thermal expansion or contraction β is the rate of change of length (l) with respect to temperature, per unit length:

$$\beta = \frac{1}{l_o} \cdot \frac{\Delta l}{\Delta T} = \frac{\varepsilon}{\Delta T} \tag{21}$$

where l_o is length at some reference temperature and $\Delta l/l_o = \varepsilon$ is the strain (Andersland and Ladanyi, 1994). If the material is isotropic (i.e., exhibits the same thermal expansion in every direction), the linear β is related to the volumetric coefficient β_v as:

$$\beta = \frac{\beta_v}{3} \tag{22}$$

For ice, β varies with temperature as:

$$\beta(°C)^{-1} = (54 - 0.18T) \times 10^{-6} \quad (23)$$

An ice cover 1Km long will expand 104 cm for β = 52 x 10^6 $(°C)^{-1}$ and a temperature rise ΔT= 20 °C. The addition of sand (quartz) to ice lowers the β coefficient. At around -60 °C the coefficient β for frozen sand undergoes a significant drop, and subsequently continuous decreasing to the lowest value at around -170 °C. Below -60 °C the coefficient β is more representative of quartz minerals than ice (Andersland and Ladanyi, 1994).

2.5 Conclusions

- The thermal response of a material is characterized by: thermal conductivity, heat capacity, thermal diffusivity, heat of transformation and thermal expansion or contraction.
- The transfer of thermal energy in earth materials can occur by conduction, convection and radiation.
- Heat conduction is the principal mode of heat transfer in soils.
- Heat conduction in soils takes place from particle-to-particle or through the soil pore fluid.
- The rate of heat transfer depends upon the temperature gradient and the thermal conductivity of the material.
- Thermal conductivity characterizes the ability of a material to transmit heat by conduction and is defined as the quantity of heat flow that will occur in unit time through a unit area of a substance under a unit temperature gradient.
- The thermal conductivity of soils depends on: moisture content, dry density, mineral composition and temperature.
- Moisture content has the greatest impact on the thermal conductivity of soils: increasing soil moisture content at a given bulk density increases its thermal conductivity.

CHAPTER 3

THERMAL CONDUCTIVITY OF SOILS - MEASUREMENTS

3.1 Introduction

The methods that are used to determine thermal conductivity can be classified according to the following characteristics (Thalman, 1950):

a) direction of heat flow, whether unidirectional (parallel to the axis of a rod), radially cylindrical, or radially spherical;

b) lateral leakage or no lateral leakage of heat in unidirectional flow;

c) steady-state or time-varying heat supply;

d) heat production throughout the specimen or localized, such as at an end or along an axis.

Steady-state techniques involve a specimen in thermal equilibrium. This approach facilitates data analysis, but it may require a long time to reach equilibrium. Non-steady-state techniques determine thermal properties during a thermal transient. The measurement is fast, but it requires more cumbersome data reduction (Abu-Hamdeh and Randall, 2000).

Three convenient, idealized, steady-state conditions are typically used for the measurement of thermal conductivity k. In the first arrangement, the temperature gradients at all points in the body have the same direction. This corresponds to the uniform, unidirectional heat flow along a rod whose sides are thermally insulated. In the second arrangement, heat flow is radially outward from the axis of a cylindrical rod of circular cross section. Temperature gradients differ from point to point. In the third arrangement, the heat flow is radially out from the center of a sphere.

The transient hot-wire technique is a widely used, accurate non-steady-state, method also known as the needle probe method. The first application of this method to measure the thermal conductivity of unsaturated soils dates from the 1950's by Hooper and Lepper (according to Ewen and Thomas,1987).

The needle probe procedure is applicable for both undisturbed and remolded soil specimens as well as in situ and laboratory soft rock specimens. The length is much greater than the diameter of the needle in order to simulate cylindrical conditions for an infinitely long specimen. Data reduction assumes isotropic materials. Detailed guidelines are provided in the following sections.

3.2 Theory: Mathematical Model for Data Reduction

The single needle probe methodology is based on a solution of the heat conduction equation of a line heat source in a homogeneous and isotropic medium at a uniform initial temperature. The thermal conductivity is determined by a variation of the line source test method. The temperature T at the sensor is related to time t (Abu-Hamdeh and Randall, 2000). For an infinitely long line heat source in an initially isothermal infinite homogeneous medium, the temperature T becomes approximately proportional to the logarithm of time after an early growth stage:

$$T - T_o = \frac{p}{4\pi k} \ln(t - t_o) \tag{24}$$

where T_o (°C) is the initial temperature, p (W/m) is the power consumption of the heater wire and is assumed to be equivalent to the heat output per unit length of wire, k (W/mK) is the thermal conductivity of the material surrounding the line source, t_o (seconds) is a time correction used to account for the finite dimensions of the heat source and the contact resistance between the heat source and the medium outside the source. This analysis assumes that energy transported in the soil by radiation and convection is negligible.

A nonlinear least-squares regression is used to solve for k. An alternative approach is to assume t_o« t so that ln $(t + t_o) \approx$ ln (t). With this assumption, a linear regression can be used considering ln(t) as the independent variable. Furthermore, if the relation between T and ln (t) is linear, then k can be simply estimated from the change in sensor temperature between two times, t_1 and t_2, by:

$$k = \frac{p}{4\pi} \frac{\ln(t_2) - \ln(t_1)}{T(t_2) - T(t_1)} \tag{25}$$

the power input per unit length of the probe is $p= I^2R$, where I is the heating current in the line source (mA), R_m is the specific resistance of the wire per unit length. This equation is linear in ln(t). Regressing T on ln(t) give a slope s of the straight-line portion of the temperature vs. the logarithm of time:

$$k = \frac{I^2 R_m}{4\pi s} \tag{26}$$

Equation (26) shows that the measured value k does not depend on the thermal properties of the probe, the thermal resistance of the contact layer or the radial position of the temperature sensing device within the probe. In the development of Equation (26), it is assumed that the cylindrical heat source is infinitely long, and that it is placed in a specimen with an infinite diameter. Although probes of finite length depart from these assumptions, the errors in the measured values of conductivity are small (less than 1%) if the length-to-diameter ratio of the probe is greater than 25 (Slusarchuk and Watson, 1975).

The thermal response of real cylindrical conductivity probes is affected by the non-negligible heat capacity of the probe, their length, and the contact resistance between the probe surface and the test medium. Nevertheless, within a limited intermediate time span, the form of the equation remains valid and the conductivity can be determined as if the probe were an ideal line heat source.

There are some errors associated with the finite length of the probe, and with the temperature rise of a probe of finite diameter (Ewen and Thomas, 1987). The correction for the temperature rise of the probe is implemented as the Fourier number τ:

$$\tau = \frac{\alpha t}{r_o^2} \tag{27}$$

where r_o being the radius of the thermal probe. For long times ($\tau \gg 1$), the temperature rise at the probe is:

$$T(t) = \frac{p}{4\pi k}(\ln t + \ln(\frac{4\alpha}{r_o^2 \gamma}) + 2H) \tag{28}$$

the value of H can be determined from the expression $H = k/r_o h$ where h is the thermal contact resistance between the probe and the soil. If long time records are gathered, Equation (28) becomes Equation (26) (Ewen and Thomas, 1987).

3.3 Needle Probe and Electronics

The needle probe is a long, thin, straight, stainless steel needle. The needle houses an Evanohm heater (heating element) and a thermocouple embedded within it. The thermocouple is located in the middle of the needle.

The needle probe used in this study was manufactured by Thermal Logic. The circuit diagram and peripheral electronics are sketched in Figure 3.1. The dimensions and electrical resistance of the Thermal Logic sensor are as follow: length 60 mm, diameter 1.27 mm, heater resistance 70 Ω (this corresponds to 1041.5 Ω /m) and cable length 5 ft. (standard).

Peripheral electronics include two digital multimeters (HP 34401 A) and a power supply (E 3630 A 35 W triple output). One multimeter measures the intensity of the applied current (mA) by measuring the voltage drop across a known resistor R_{known}. The second multimeter is a very high input impedance voltmeter that is used to measure the potential generated at the thermocouple.

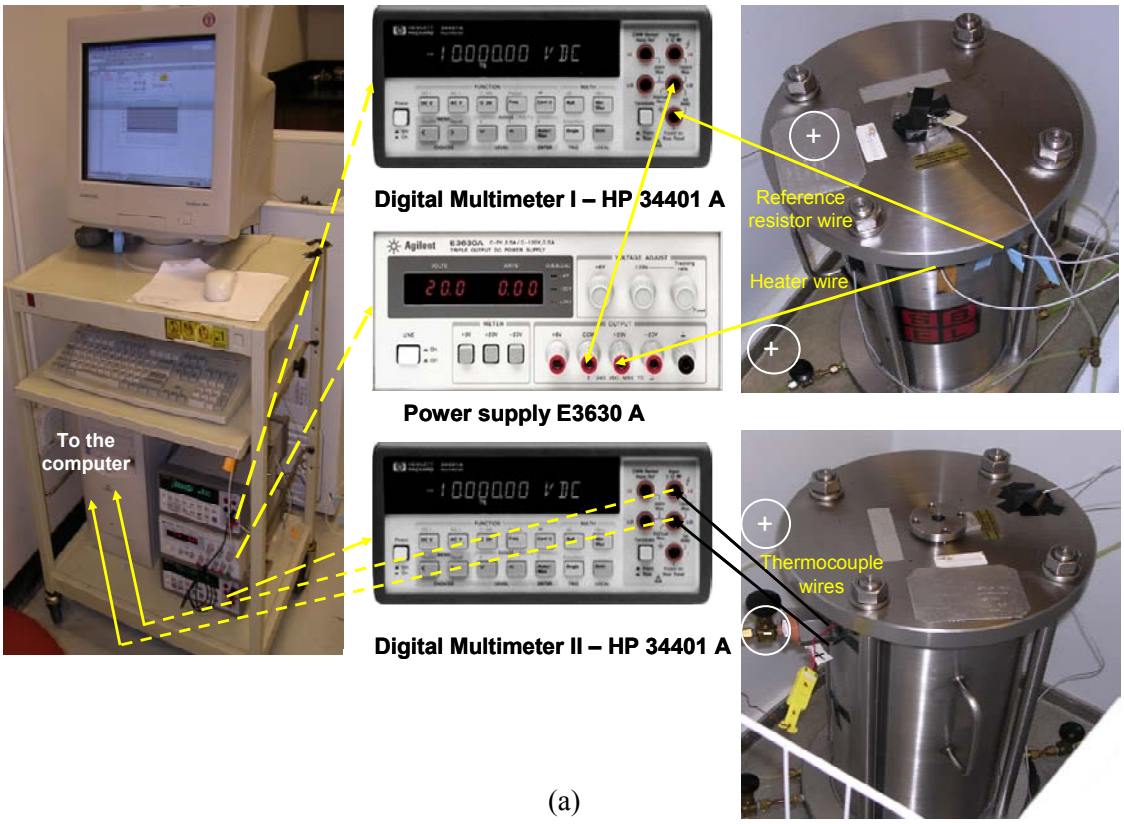

(a)

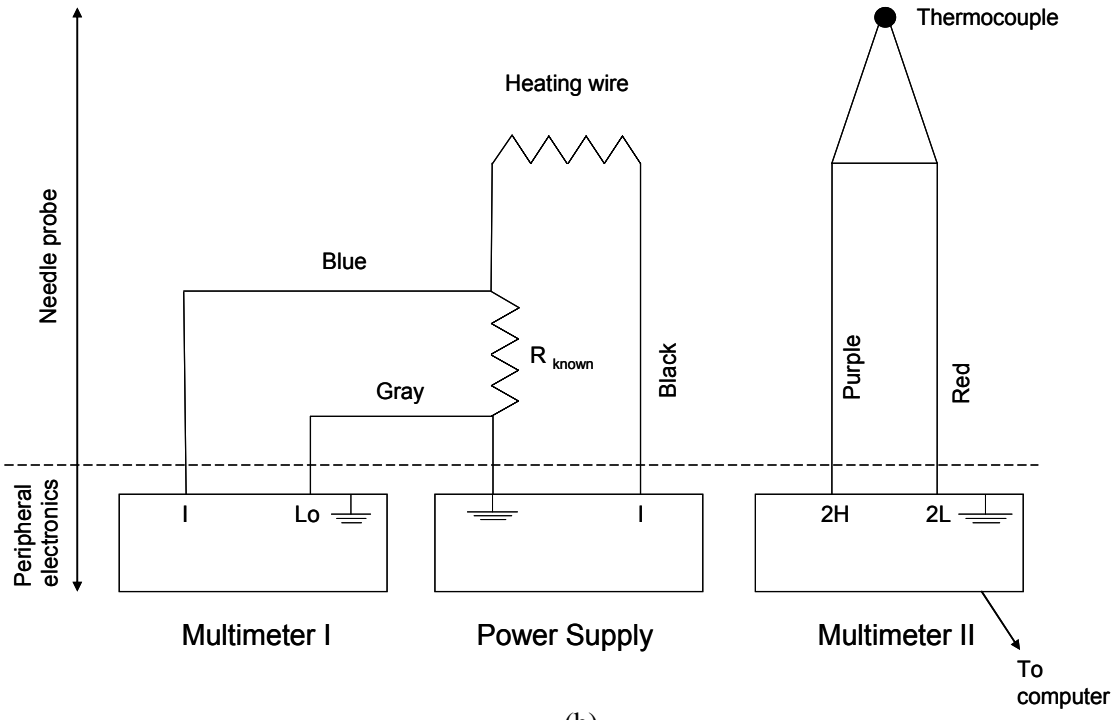

(b)

Figure 3.1 Needle probe and electronics: (a) Cell and peripheral electronics (b) Connections schematics

3.4 Specimen Size - Calibration

Experimental measurements of thermal conductivity with the thermal needle probe require the needle to be inserted vertically into the specimen, avoiding the formation of void spaces between the specimen and the probe. The thermal probe shaft is fully embedded in the specimen without any part exposed.

The diameter of the specimens is established so that the heat flowing through or reflected by the radial boundary is much smaller than the heat supplied by the probe (Slusarchuk and Watson, 1975):

$$\exp\left(-\frac{R^2}{4\alpha t}\right) \leq 0.02 \tag{29}$$

where R is the radius of the specimen, α is the thermal diffusivity of the soil and t is time.

The thermal needle probe and peripheral electronics are then calibrated by comparing the experimental thermal conductivity of a standard material to its known value. Calibrations with different standards help refine the calibration. An adequate calibration standard is a material of known thermal conductivity in the range of the materials being measured (typically $0.2 < k < 5$ W/mK). Suitable materials include dry Ottawa sand, Pyrex 7740, Fused Silica, Pryoceram 9606 and water. If solid materials are used as a calibration standard, the diameter of the hole must be equal to the diameter of the probe so that the probe fits tightly into it. The measured thermal conductivity of the calibration specimen must agree within one standard deviation of the published value of thermal conductivity, or with the value of thermal conductivity determined by an independent method.

The thermocouple built in the needle probe is calibrated over the required temperature range -20 °C to 25 °C (Figure 3.2). Water at laboratory temperature (~ 20 °C) was used as a calibration standard for the measured thermal conductivity. The calibration of the needle probe was conducted in a 40-mm diameter, 10-cm long glass beaker. The measured thermal conductivity has a difference with tabulated values smaller than 1 %.

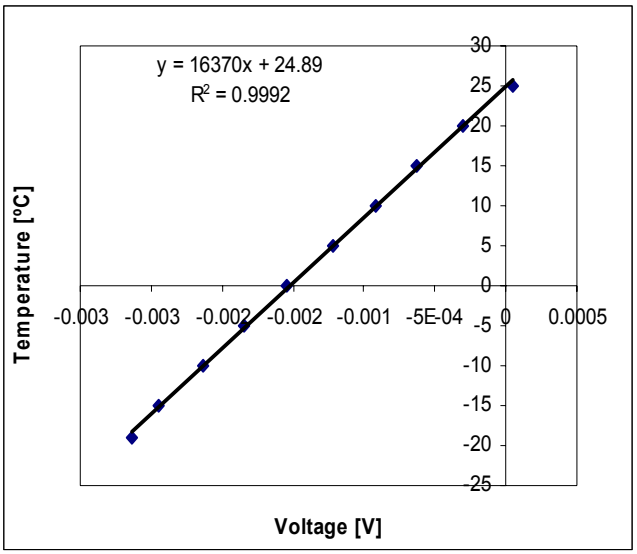

Figure 3.2 Calibration of thermocouple built-in the needle probe

Calibration factors from the graph:

Intercept: at V=0: 24.89 °C
Slope: 16370.28 °C/V

3.5 Specimen Preparation - Data Collection and Reduction

For soil testing, the needle is fixed to a cap of the same diameter as the latex membrane that will contain the soil (D_{cap}= 700 mm). After the soil is poured inside the membrane, the needle probe with the cap is fixed at the top, the membrane is fixed to the cap and the electrical connections through the chamber wall are completed.

Power is supplied to the needle probe once the specimen reaches thermal equilibrium. A measurement begins when the heater in the probe is turned on (time t = 0). The temperature rises as heat is dissipated into the surrounding soil. The rate of dissipation and temperature rise at the needle are functions of the thermal conductivity of the soil. A heating period of ~ 100 seconds normally gives good results. A temperature rise of 2 to 3° C is needed to attain good resolution. The error due to axial heat flow in

the probe is time dependent. For this study, the duration of the test was limited to minimize the impact of time on the probe and the specimens. The power input and temperature rise are measured during a 128 sec heating interval. Readings are taken every half second for a total of 256 readings for each measurement. In some cases, temperatures are monitored after the measurement had been completed and the current to the heater is cut off to obtain a cooling curve. Thermal conductivity measurements with the thermal probe are repeated six times at each equilibrium temperature for a given porosity.

The measured temperature history is plotted as a function of time on a semi-log graph. The linear portion of the curve is selected (pseudo-steady-state portion) and a straight line is drawn through the points. On average, these curves become linear 20 sec after heating was initiated (Figure 3.3). Times t_1 and t_2 are selected at appropriate points on the line and the corresponding temperatures T_1 and T_2 are read (Figure 3.3). Sample plots for each soil tested are presented in Figures 3.4 to 3.7. These values define the slope s used in Equation 28.

The same procedure is repeated for different soils and bulk densities. For high thermal conductivity materials, the temperature rise is lower and the heating voltage has to be increased.

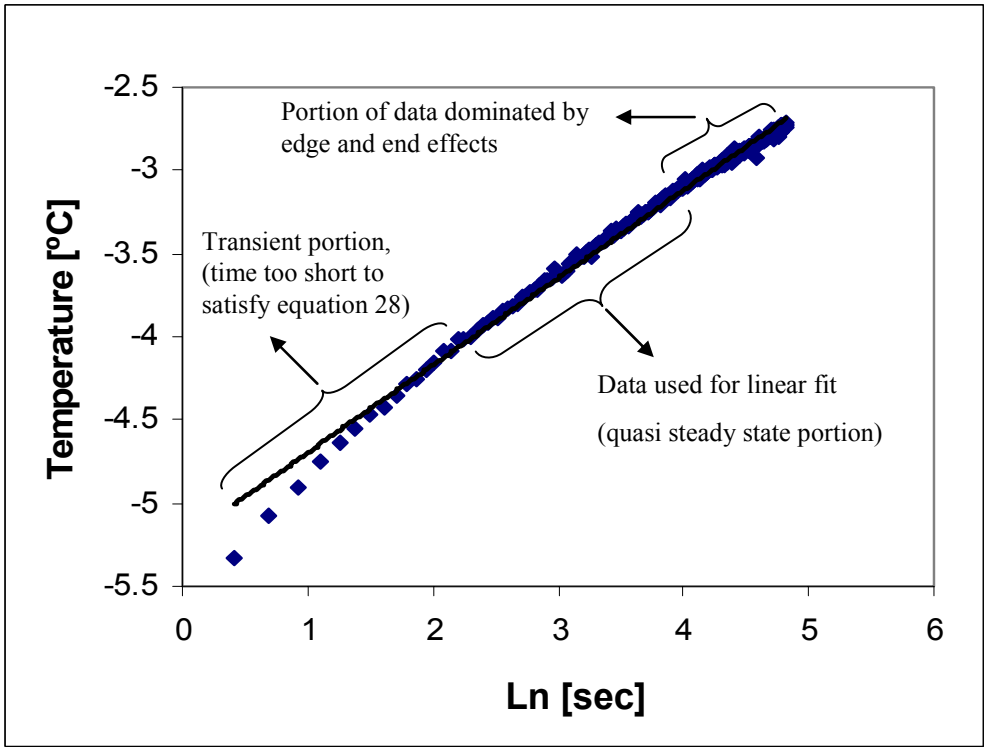

Figure 3.3 A representative curve- Temperature rise in response to probe heating and interpretation of different heating stages

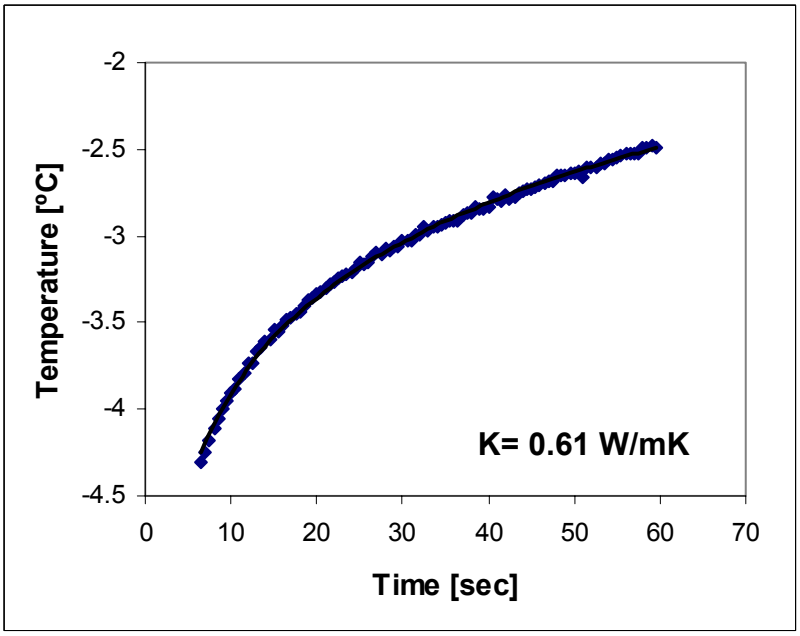

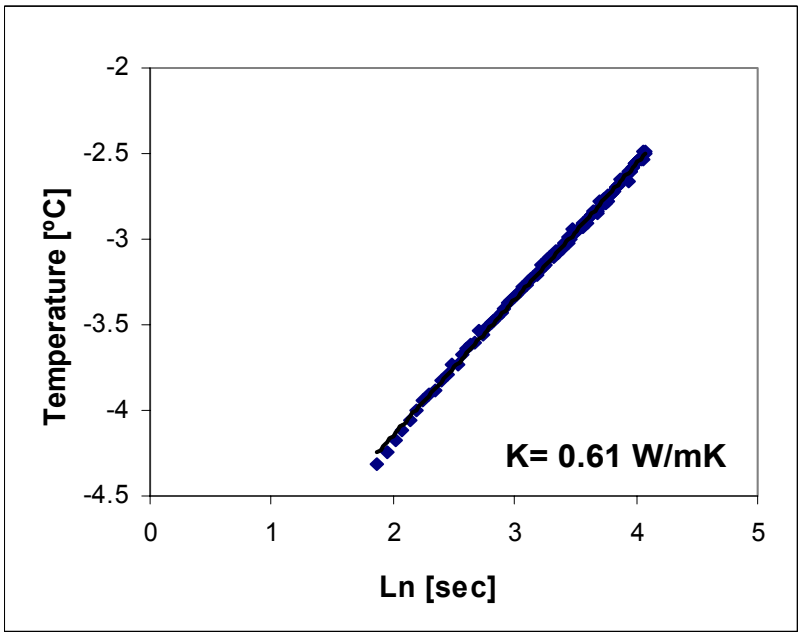

Figure 3.4 Thermal conductivity measurements- Typical curve for sand

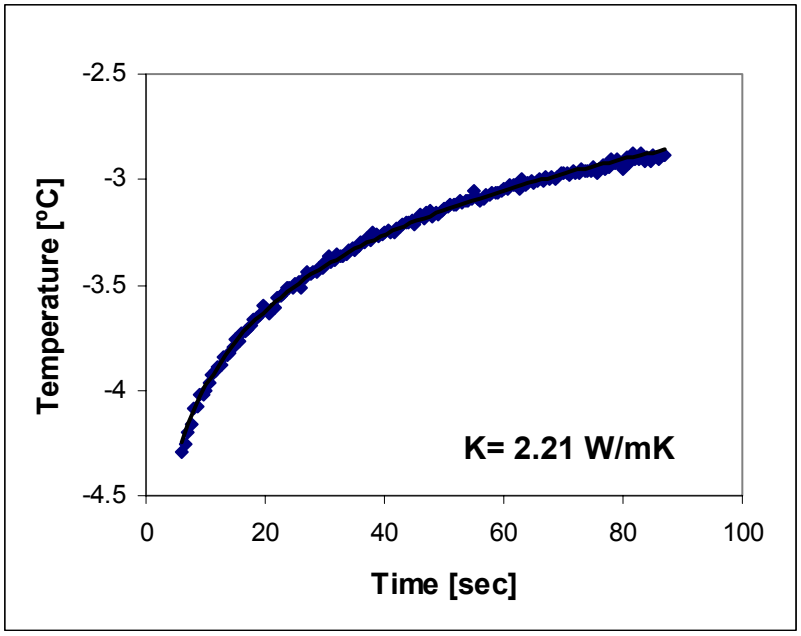

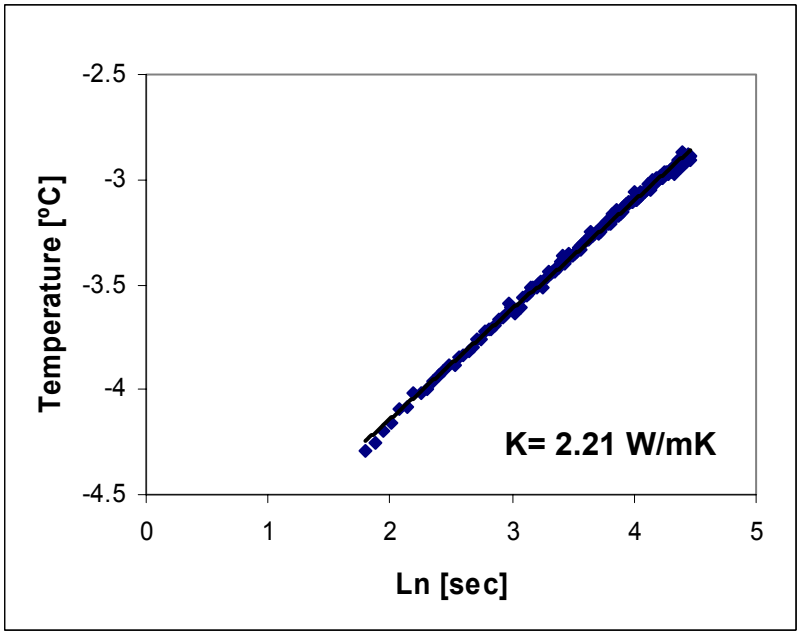

Figure 3.5 Thermal conductivity measurements- Typical curve for kaolinite

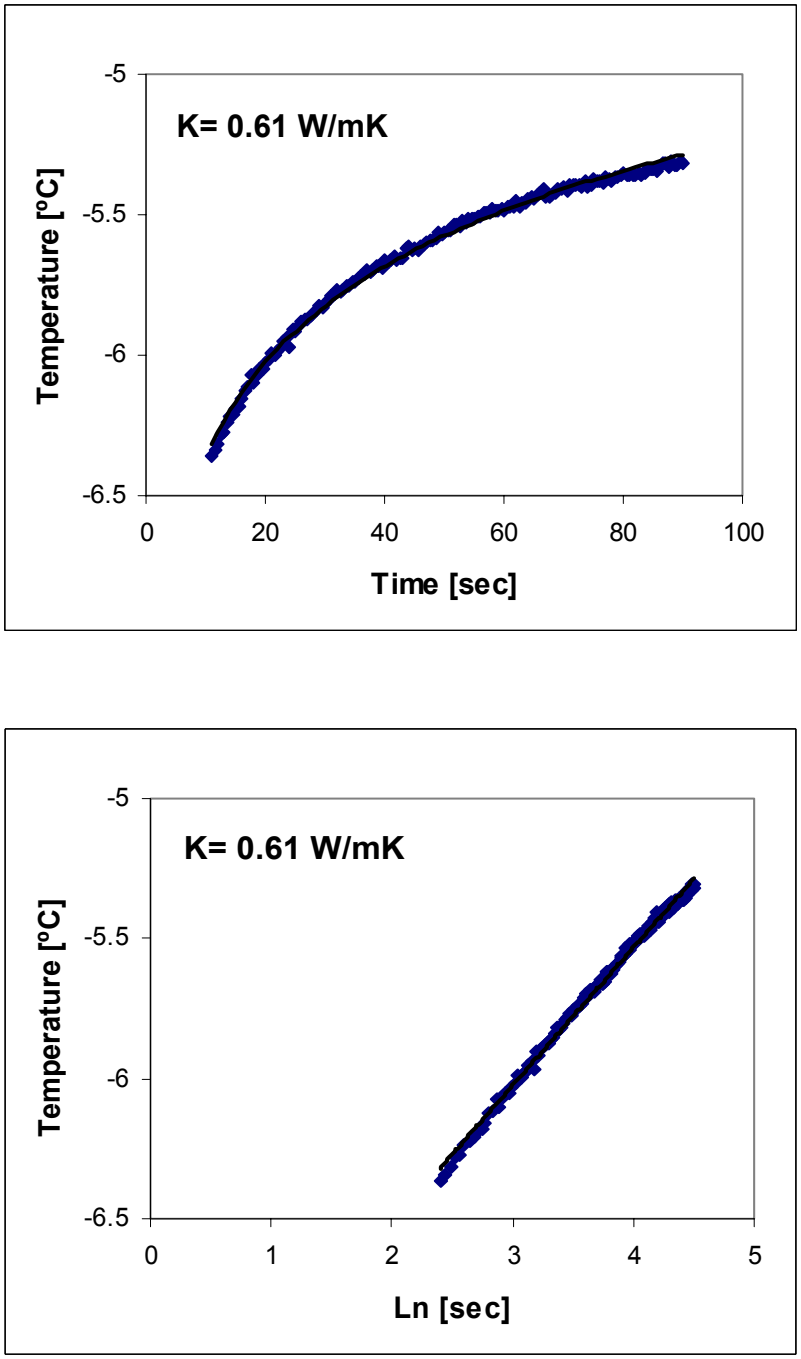

Figure 3.6 Thermal conductivity measurements- Typical curve for precipitated silica flour

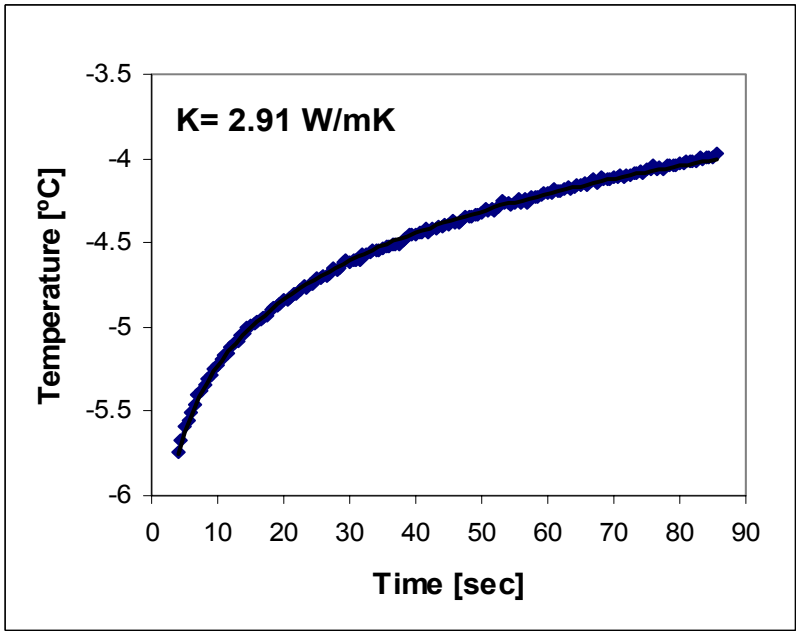

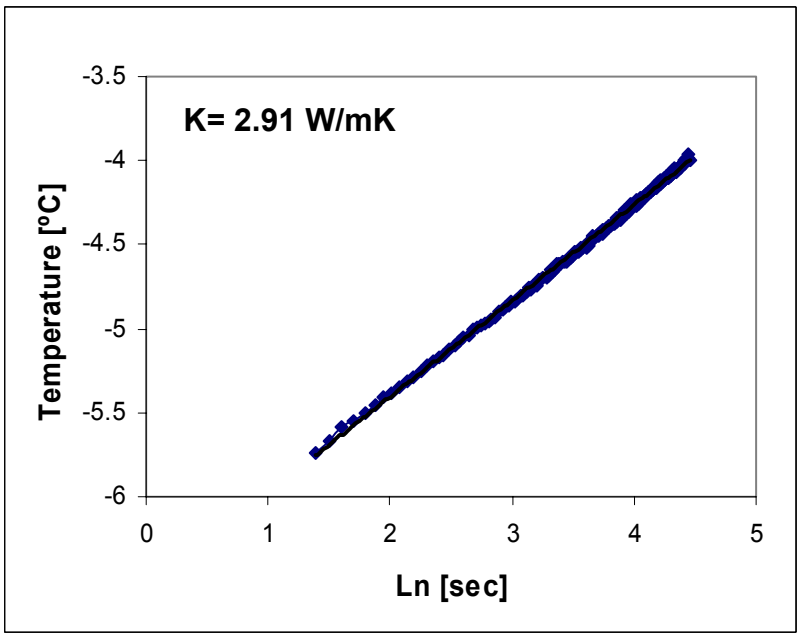

Figure 3.7 Thermal conductivity measurements- Typical curve for crushed silica flour

3.6 Errors in Measurements of Thermal Conductivity by Needle Probe Method

Serious deviations from ideal behavior occur when the apparent thermal properties of the medium are not constant during the measurement period or are not homogeneous over the appropriate spatial scale. This is the case in fine-grained soils at temperatures only slightly below the onset of freezing, where thermal conductivity depends strongly on the composition of the soil-water phase and hence on temperature. For intermediate to coarse grain, unsaturated soils, moisture migration can occur due to the imposed temperature gradient. For gravels, convection may perturb the measurements, and for all soils, a non constant contact resistance will lead to difficulties (Ewen and Thomas, 1987).

There are two competing restrictions on the maximum allowable run time. Moisture migration takes place when the run time is long. On the other hand, an error in the measured slope is introduced if measurements are taken before the straight line region is achieved. Moisture migration due to the imposed thermal gradient is minimazed by lowering the power input and running a shorter test (Ewen and Thomas, 1987). In addition, heating should not cause phase transformation.

3.7 Conclusions

- Steady-state and non-steady-state techniques allow determine the thermal conductivity of a particulate media.
- Steady-state technique involves a specimen in thermal equilibrium, while non-steady-state technique determines thermal properties during a thermal transient.
- The needle probe method or transient hot-wire technique is a non-steady-state technique for thermal conductivity measurements.
- The single needle probe methodology is based on a solution of the heat conduction equation of a line heat source in a homogeneous and isotropic medium at a uniform initial temperature.
- The thermal conductivity is determined by a variation of the line source test method. For an infinitely long line heat source in an initially isothermal infinite

homogeneous medium, the temperature T becomes approximately proportional to the logarithm of time after an early growth stage.

- Data collected is reduced and only the slope of the straight line of the curve of temperature as a function of time in a semi-log graph is used in calculations
- The k value obtained by needle probe method does not depend on the thermal properties of the probe, the thermal resistance of the contact layer or the radial position of the temperature-sensing device within the probe.
- The thermal needle probe and peripheral electronics must be calibrated before any thermal conductivity measurement.
- There are two restrictions on the maximum allowable run time: moisture migration due to long run times and an error in the slope if measurements take place before achieving the straight portion of the curve of T versus t in a semi-log scale.

CHAPTER 4

EXPERIMENTAL STUDY AND RESULTS

The purpose of this chapter is to present the experimentally determined thermal conductivity of hydrate-bearing sediments, for different pore filling values. Selected materials are described first.

4.1 Physical Properties of Selected Soils

Four different soils are used in this study: sand (F-110), kaolinite (Wilklay SA-1), precipitated silica flour (Zeofree 5161) and crushed silica flour (Sil-Co-Sil 106) (Table 4.1). These sediments represent an ordered progression in grain sizes from 120 μm (sand) to ~ 1μm (clay) and in specific surface ranging from 10^{-4} m^2/g (sand) to ~ 35 m^2/g (clay). Details follow.

Sand F-110 (Figure 4.1, Table 4.1) is made of uniform size, semi-angular particles. The maximum and minimum packing densities are $e_{min} = 0.535$ and $e_{max} = 0.848$ (Cho, 2002).

Kaolinite is a hydrous aluminosilicate $Al_2Si_2O_5(OH)_4$ clay mineral of the 1:1 crystal structure group: it consists of one silicon tetrahedral sheet bonded to one aluminum oxide-hydroxide octahedral sheet. It is formed by the weathering of feldspar. Negative or positive surface charge can develop depending on pH and ions in the pore fluid. The Wilklay SA-1 used in these experiments is a high quality, finely pulverized, air-float kaolin (Figure 4.2, Table 4.1).

Two silt-size materials were used. Precipitated silica flour (~ 20 mm size, but high specific surface area due to internal porosity), and crushed silica flour.

The precipitated silica flour (Zeofree 5161) (Figure 4.3, Table 4.1) is a synthetic silicon dioxide manufactured as a spray-dried powder. This compound belongs to the family of several synthetic, amorphous silicas (precipitated silica, silica gel, fumed silica and silica fume).

The crushed silica (Sil-Co-Sil 106) (Figure 4.4, Table 4.1) is produced from high purity silica precision grinding and fine-grinding (micronized). Ground silica is inherently inert, white, bright, has low moisture content and contains at least 99.5 % pure SiO_2.

Silica is composed of silicon and oxygen. Silicon dioxide is composed of one atom of silicon and two atoms of oxygen SiO_2, which is the main constituent of more than 95 % of known rocks. Silica commonly appears in the crystalline state and rarely in an amorphous state in nature. Silica exists in nine different crystalline forms or polymorphs with the three main forms: quartz (which is by far the most common), tridymite and cristobalite (Frondel, 1962). The crystalline structure of quartz is based on four oxygen atoms linked together to form a three dimensional shape called a tetrahedron with one silicon atom at its center. These tetrahedra are joined together by sharing corner oxygen atoms to form quartz crystals. Its high hardness reflects the strength of atomic bonds. Amorphous silica can be transformed into crystalline form by heating to high temperatures (Frondel, 1962). When crystalline quartz silica is powdered, it is called silica flour.

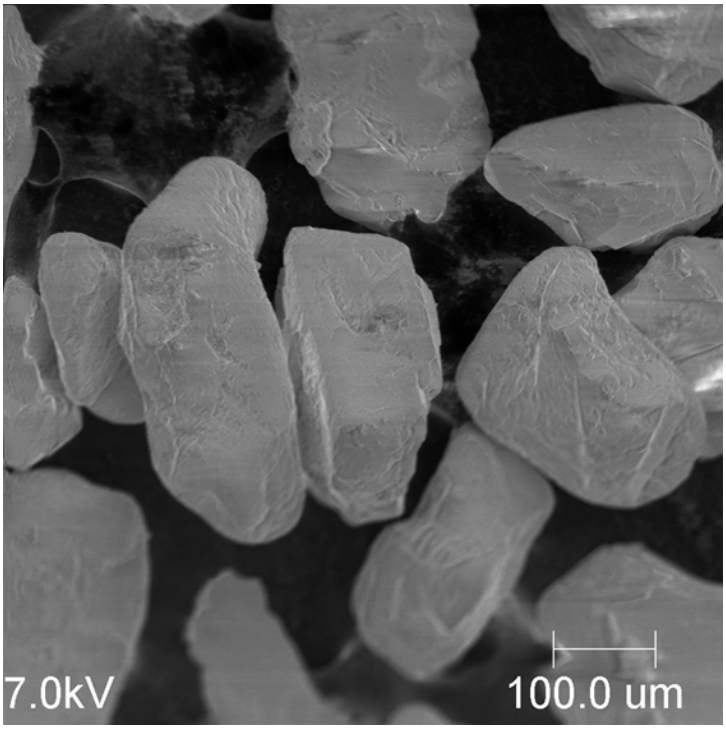

Figure 4.1 SEM picture of sand (F-110)

Source: Courtesy of Angelica Palomino (2003)

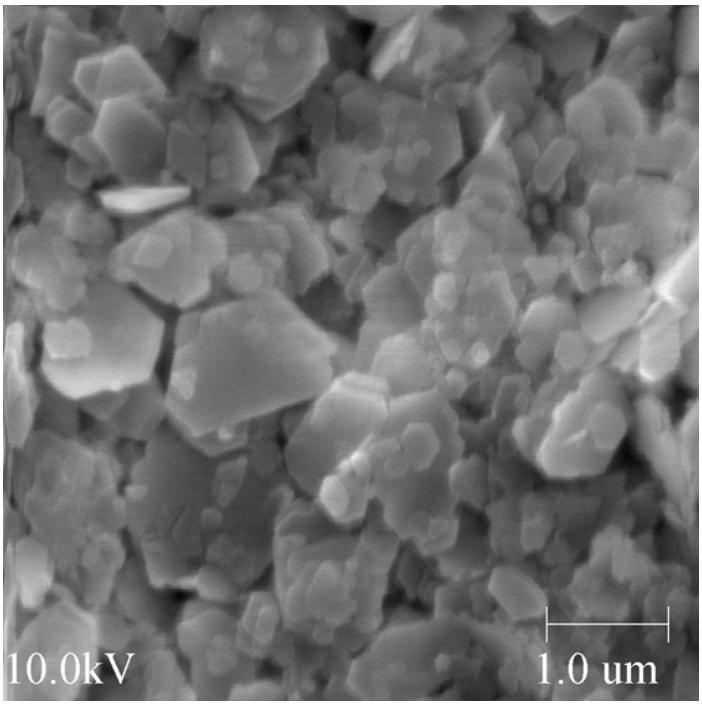

Figure 4.2 SEM picture of kaolinite (Wilklay SA-1)

Source: Courtesy of Angelica Palomino (2003)

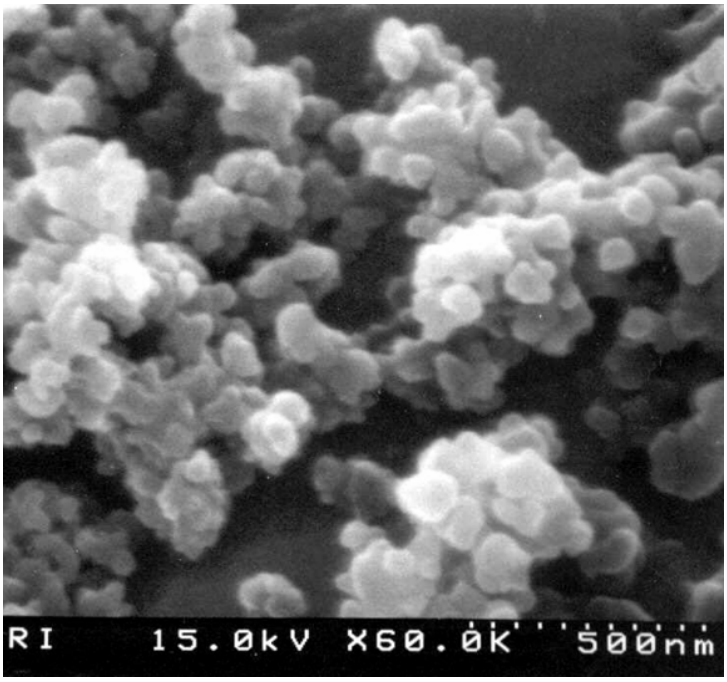

Figure 4.3 SEM picture of precipitated silica flour (Zeofree 5161)

Source: Courtesy of Angelica Palomino (2003)

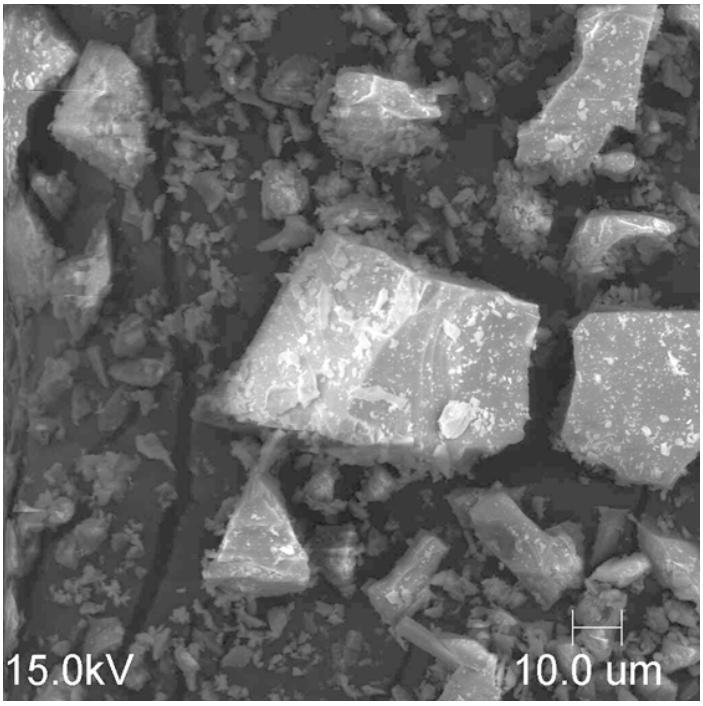

Figure 4.4 SEM picture of crushed silica flour (Sil-Co-Sil 106)

Source: Courtesy of Angelica Palomino (2003)

Table 4.1 Principal characteristics of tested materials

Material	D50 μm	Specific Gravity (Gs)	Specific Surface (Ss) m^2/g	Mineral	Sphericity (Krumbein)	Roudness (Krumbein)	Raw color	Hardness (Moh's scale)	Ph	Typical chemical analysis (Compound)	(Percentage)
Sand (F-110) Source: itcglobal.com	120	2.65	$2^{\wedge}10^{-2}$	Quartz	0.7	0.7	White	7.0	6.8	SiO_2 Fe_2O_3 Al_2O_3 MgO TiO_2 CaO (L.O.I)	99.8 0.026 0.051 0.025 <0.1 <0.1 0.1
Precipitated Silica flour (Silt zeofree 5161) Source: huberemd.com	20	2.65	5-7 (methylene blue method)	Quartz	0.9	0.7	White	7.0	7		
Crushed Silica flour (SIL-CO-SIL 106) Source: u-s-silica.com	20	2.65	≈0.1	Quartz	0.9	0.1	White	7.0	7	SiO_2 Fe_2O_3 Al_2O_3 TiO_2 K_2O CaO MgO Na_2O (L.O.I)	99.8 0.035 0.05 0.02 0.02 0.01 <0.01 <0.01 0.1
Kaolinite (Wilklay SA-1) Source:wilkinsonkaolin.com	1.1	2.65	35-37 (by methylene blue method)	Aluminum (Al) Silicon (Si)	0.7 (flat particles)	0.1	Cream	1.5-2.0	28 % solids aver. 5.4	SiO_2 Al_2O_3 Fe_2O_3 TiO_2 CaO MgO K_2O Na_2O L.O.I	45.60 38.40 0.40 1.50 0.06 Trace 0.18 Trace 13.82

Additional data sources: Santamarina and Cho (2001), Klein (1999), Parks (1990) and Guimaraes (2001)

4.2 Tetrahydrofuran Solution

Two fluids are used in this study: deionized water and tetrahydrofuran (THF purity 99.97%, spectrophometric grade). THF is fully miscible with water and hydrate formation is not diffusion controlled. Furthermore, it is quite easy to control the amount of hydrate formed by controlling the initial mixture. Hydrates form homogeneously through the specimen, and it is possible to form them from aqueous phase THF in fully saturated sediments; which is a closer resemblance to those found in marine sediments.

Hydrogen bonds in the THF hydrate structure are identical with those in normal structure II natural gas hydrates. THF molecules occupy only the larger cages in the structure II hydrate lattice. The hydrate phase behavior of the binary THF and water system at 1 atm is shown in Figure 4.5. The line that separates the region "ice-hydrate I-H" from the region "liquid-hydrate L-H" represents the "ideal" hydrate composition (Sloan and Rueff, 1985). THF clathrate hydrates are easily prepared by freezing at 1 atm an aqueous solution of the appropriate mixture (Tse and White, 1988). Since the hydrogen bonds of the hydrate lattice are the primary targets to be affected by any inhibitors, experiments with THF hydrate yield results that can be extrapolated to normal natural gas hydrates (Tse and White, 1988).

Two different mixtures of water and THF are prepared (see tetrahydrofuran-water phase diagram in Figure 4.5, Table 4.2) The first water-THF mixture is a 50:50 water:THF composition. The designation of 50:50 refers to a mixture of fluids composed of 40.4 % water and 59.6 % tetrahydrofuran by weight. At this composition, 50 % of the mixture turns into hydrate and the excess THF remains unfrozen. The equilibrium temperature is 4.4 °C, the THF freezing point is -108.5 ºC. The second water-THF fluid mixture correspond to a 80:20 water:THF composition and is prepared by mixing by weight 80 % water with 20 % THF, so that all the solution becomes hydrate.

All the solutions were prepared at laboratory temperature around 20 ºC (at 20 ºC, THF is completely miscible with water) and sealed securely to prevent any evaporation of THF.

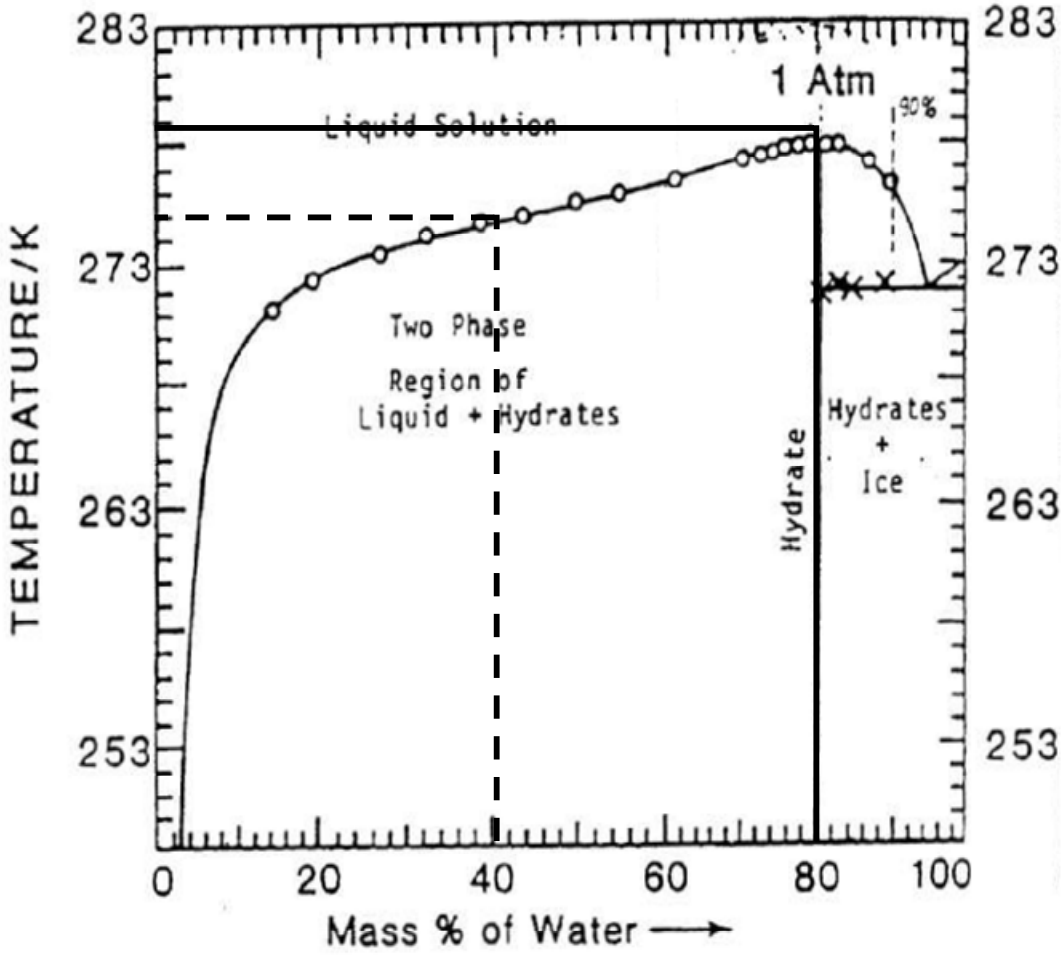

Figure 4.5 General ambient temperature THF-water phase diagram at 1 Atm.
The dash line represent a molar composition of water-THF on which 50 % of the fluid hydrate (40.4 % water and 59.6 % THF)
The solid line represent a molar composition of water-THF on which 100 % of the fluid hydrate (80 % water and 20 % THF)

Source: Bollavaram et al., 2000

Table 4.2 Fluids nomenclature by weight

Designation	Mass of water (%)	Mass of THF (%)
100: 0	100	0
50:50	40.4	59.6
80:20	80	20

4.3 Specimen Preparation

The soil is saturated by adding a known amount of water-THF solution and mixing it thoroughly, until a homogeneous soil specimen is obtained.

Specimens are tested for thermal conductivity in unfrozen and frozen stages. The "unfrozen" condition in this study indicates thermal conductivity measurements taken at around 20 ºC. On the other hand, "frozen" condition indicates measurements conducted at -18 to -20 ºC.

The specimens are tested for thermal conductivity during the unfrozen and frozen stages. Specimens containing water (no ice or THF) are designated as 100:0 unfrozen and are tested exclusively during the unfrozen stage, consequently, specimens are labeled as sand 100:0 unfrozen, kaolinite 100:0 unfrozen, precipitated silica flour 100:0 unfrozen or crushed silica flour 100:0 unfrozen. Specimen designated as 50:50 unfrozen, 50:50 frozen, 80:20 unfrozen and 80:20 frozen indicate the hydrate composition of water and THF plus the stage at which the specimen are tested.

4.4 Devices and Test Procedure

The soil-fluid mixture is weighted before and after the experiment, to calculate the initial and final moisture content. A thin film of vacuum grease seal the membrane to the bottom plate of the cell, and two O rings secure the membrane to the plate. A filter paper is placed at the bottom of the cell to avoid wash out of small particles during

consolidation. Filter paper is also wrapped around the membrane extending from the bottom plate to the lowest part of the needle cap, to facilitate drainage.

The soil mixture is placed by scooping, while the rubber membranes remain supported by the mold. Soil mixtures are carefully placed within the cylinder to ensure a homogeneous, perfectly vertical specimen and to avoid air bubbles inside the specimen.

Once the specimen reaches the desired height, the thermal needle probe is carefully placed in the middle of the specimen. The stainless steel needle probe cap provides the upper seal as the membrane adjusts to it (thin vacuum grease film around the cap and O-rings are used). Because the specimens are tall and the needle-cap assembly is heavy, vacuum is applied to strengthen the specimen until the chamber is pressurized (Figure 4.6). Finally, specimen dimensions are 6.7 to 6.9 cm in diameter and 13.0 to 13.4 cm in height. This specimen size prevents boundary effects during thermal measurements (Chapter 3).

The space between the cell and the specimen is filled with anti-freeze fluid (Figure 4.7). The antifreeze fluid fills the cell to approximately 4 inches above the needle-cap. The remaining space is filled with mineral oil to avoid short-circuiting the exposed wires and connections. The assembled chamber is placed inside a commercial freezer.

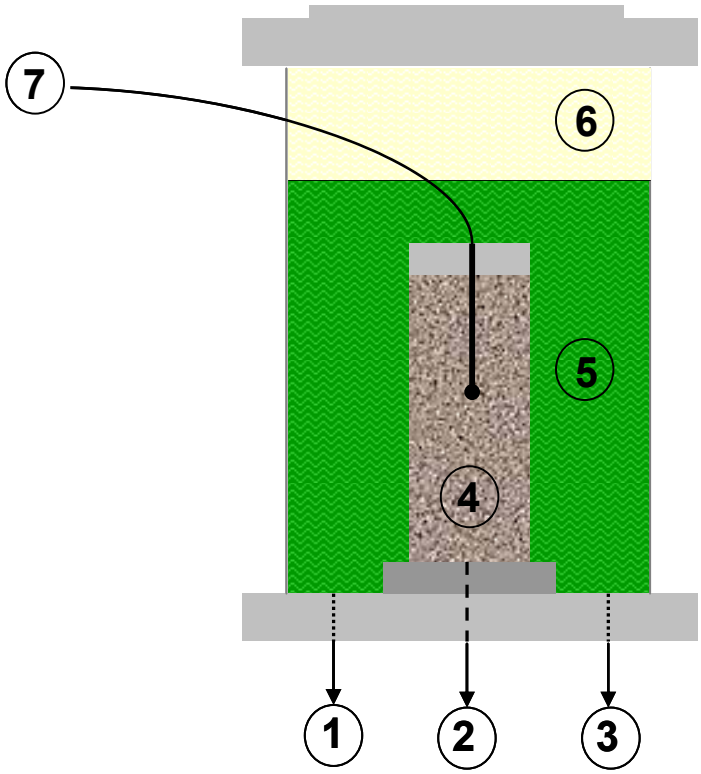

Figure 4.7 Sketch of the modified isotropic confining pressure cell:
(1) and (3) cell pressure, (2) specimen port, (4) soil specimen,
(5) anti-freeze liquid, (6) mineral oil, (7) electrical connections

The plastic tubes connecting the cell to the pressure panel are saturated with the operating water-THF solution to monitor volume changes in the specimen during consolidation. Peripheral electronics are shown in Figure 3.1.

The consolidation process starts by increasing the cell pressure. The preselected confining levels are 0.03 Mpa, 0.10 MPa, 0.25 MPa, 0.50 MPa and 1.0 MPa. Volumetric changes are measured with the pipettes. Thermal conductivity is determined for the consolidated, unfrozen specimens 24 hours after consolidation is completed to ensure equilibrium. Afterwards, specimens are cooled slowly to cause hydrate formation (specimens with THF solution). At equilibrium temperature, the thermal conductivity of the specimen is measured once again. Finally, the specimen is heated to melt the hydrate and the cycle is repeated with a new confinement.

4.5 Experimental Results - Discussions

Experimental thermal conductivity data gathered for all tested soils are summarized in Tables 4.3 to 4.6. The thermal conductivity of sand, kaolinite and precipitated silica flour is determined at 100:0 unfrozen, 50:50 unfrozen, 50:50 frozen, 80:20 unfrozen and 80:20 frozen and at different confining pressure levels (0.0 MPa, 0.03 MPa, 0.10 MPa, 0.25 MPa, 0.50 MPa and 1.0 MPa). In the case of crushed silica flour, only 100:0 unfrozen, 80:20 unfrozen and 80:20 frozen cases are tested.

The following sections present the results and main observations. The thermal conductivity phenomena are interpreted in Chapter 5.

4.5.1 Sand (Table 4.3 - Figures 4.8 to 4.9)

The variation of thermal conductivity with confinement for sand 100:0 unfrozen shows a steady increase (from an initial value of 2.68 W/mK up to 2.77 W/mK) as the porosity decreases from n= 0.42 to n= 0.39.

Thermal conductivity increases up to a maximum and then decreases as porosity decreases for specimens at 50:50 (unfrozen and frozen) as well at 80:20 (unfrozen and frozen).

The higher thermal conductivity values for unfrozen samples with THF mixtures in the pores are observed at 80:20 composition (k= 2.3 W/mK). Thermal conductivity values at 50:50 and 80:20 unfrozen fall bellow the k values observed for 100:0 unfrozen.

The maximum thermal conductivity value was observed at 80:20 frozen (k= 3.36W/mK).

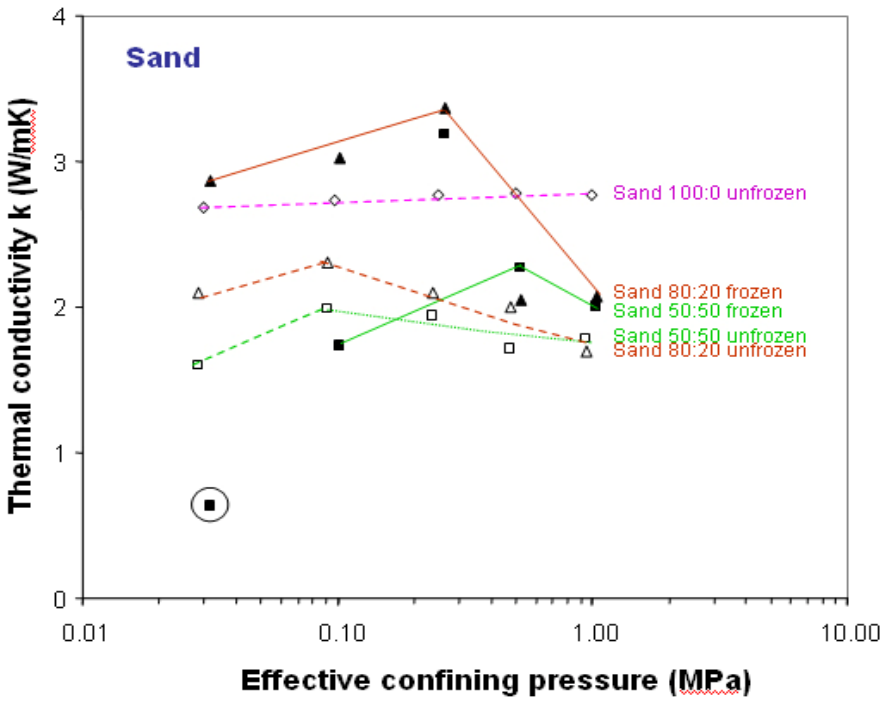

(a)

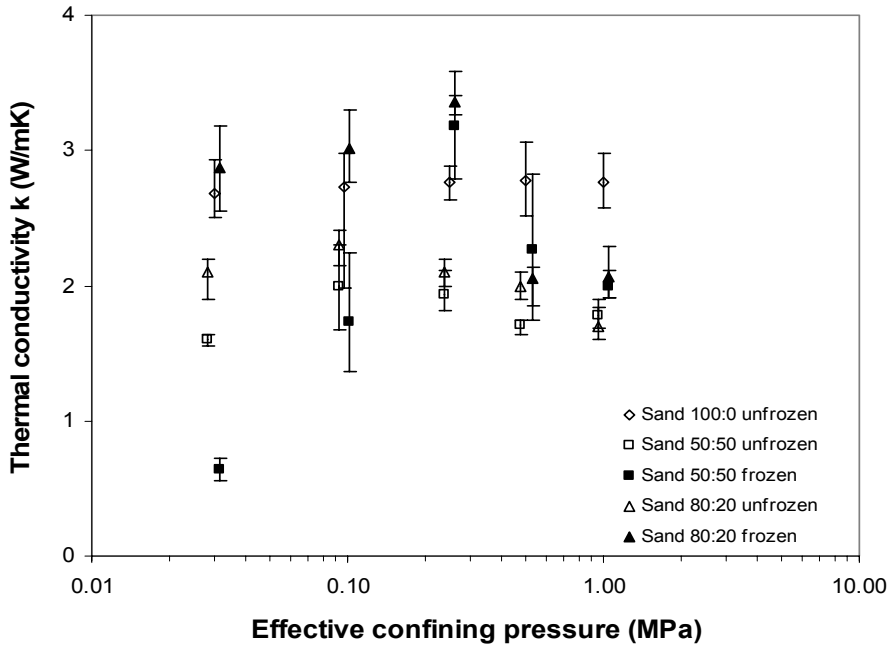

(b)

Figure 4.8 Sand - Thermal conductivity versus effective confining pressure (a) Thermal conductivity values correspond to an average of six measurements. (b) Average minimum and maximum values are presented
Note: To facilitate the data reading, the values of pressure for 50:50 unfrozen and 80:20 unfrozen have been shifted 0.95 to the left. The values of pressure for 50:50 frozen and 80:20 frozen have been shifted 1.05 to the right

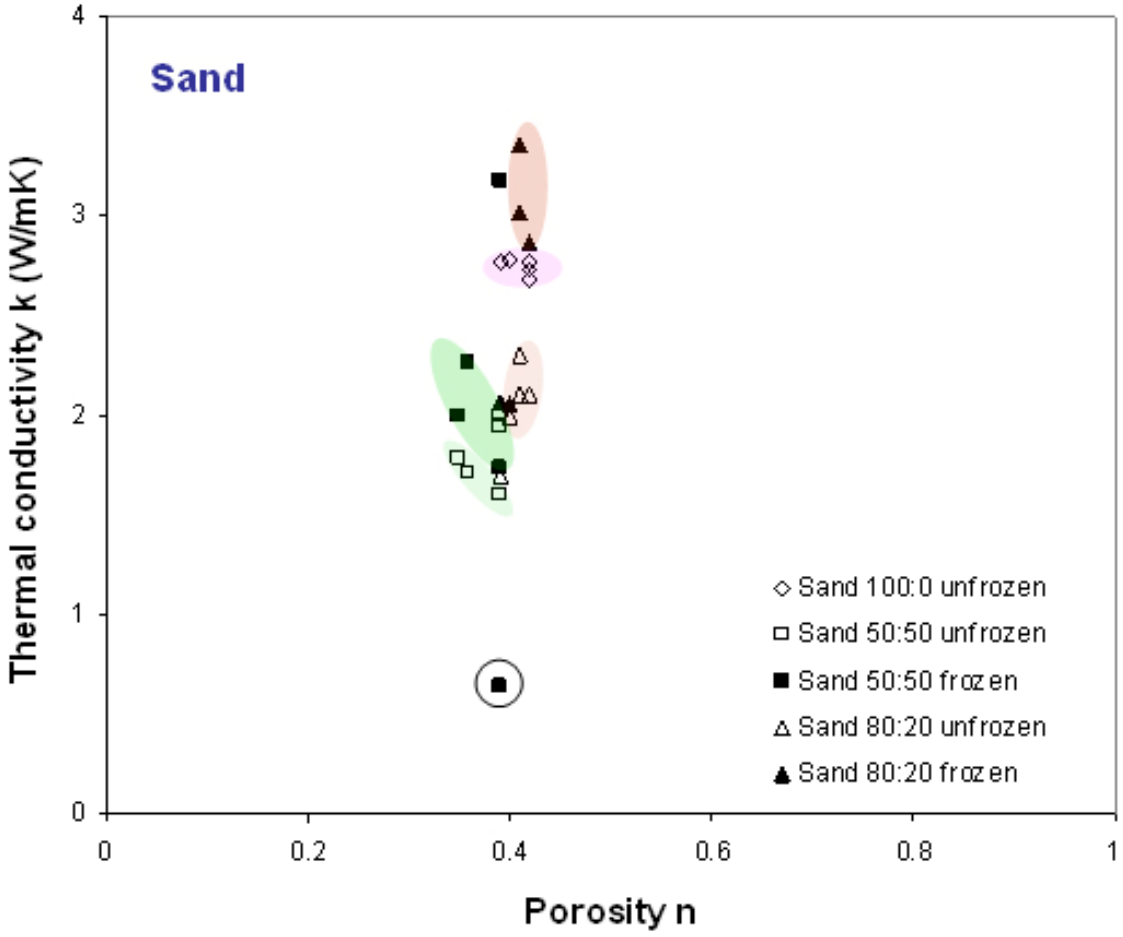

Figure 4.9 Sand - Thermal conductivity versus porosity
Thermal conductivity values correspond to an average of six measurements

Table 4.3 Thermal conductivity - Sand

Hydrate concentration (%) Target value	Grain Size D 50 (microns)	Stage : Unfrozen (~18 °C); Frozen (-10 °C)	Effective confining pressure (MPa)	Moisture content (%)	Dry unit weight (KN/m^3)	Thermal conductivity (W/m/K)	Total change of volume (V-Vo)	Bulk modulus, B= σ/ (ΔV/V) (MPa)	Hydrate distribution (optical/visual-destructive of sample)	Pore filling vs. grain boundaries	Void ratio	Porosity	Sample volume	Change of volume during consolidation	Total change of vol. (V-Vo)/V (%)
100:0	120	Unfrozen	0.00	27.1	15.43	-	0.0	N/A	N/A	N/A	0.72	-	507	0	0.0
100:0	120	Unfrozen	0.03	27.4	15.36	2.68	0.0	-	N/A	N/A	0.73	0.42	509	2.6	0.0
100:0	120	Unfrozen	0.10	27.3	15.38	2.73	0.7	75.4	N/A	N/A	0.72	0.42	509	-0.65	0.1
100:0	120	Unfrozen	0.25	26.8	15.49	2.77	4.4	28.8	N/A	N/A	0.71	0.42	505	-3.75	0.9
100:0	120	Unfrozen	0.50	25.7	15.77	2.78	13.5	18.8	N/A	N/A	0.68	0.40	496	-9.1	2.7
100:0	120	Unfrozen	1.00	23.9	16.23	2.77	27.5	18.4	N/A	N/A	0.63	0.39	482	-14	5.7
50:50	120	Unfrozen	0.00	22.7	17.29	-	0.0		N/A	N/A	0.65	-	529	0	0.0
50:50	120	Unfrozen	0.03	22.7	17.30	1.59	0.1	158.8	N/A	N/A	0.65	0.39	529	-0.1	0.0
50:50	120	Unfrozen	0.10	22.4	17.38	1.99	2.6	19.7	N/A	N/A	0.64	0.39	527	-2.5	0.5
50:50	120	Unfrozen	0.25	22.2	17.45	1.94	4.8	27.6	N/A	N/A	0.63	0.39	525	-2.2	0.9
50:50	120	Unfrozen	0.50	19.8	18.23	1.71	27.2	9.7	N/A	N/A	0.56	0.36	502	-22.4	5.4

Table 4.3 (cont'd)

Hydrate concentration (%) Target value	Grain Size D 50 (microns)	Stage: Unfrozen (~18 °C); Frozen (-10°C)	Effective confining pressure (MPa)	Moisture content (%)	Dry unit weight (KN/m^3)	Thermal conductivity (W/m/K)	Total change of volume (V-Vo)	Bulk modulus, B= σ/ (ΔV/V) (MPa)	Hydrate distribution (optical/visual-destructive of sample)	Pore filling vs. grain boundaries	Void ratio	Porosity	Sample volume	Change of volume during consolidation	Total change of vol. (V-Vo)/V(%)
50:50	120	Unfrozen	1.00	19.0	18.50	1.78	34.5	15.3	N/A	N/A	0.54	0.35	495	-7.3	7.0
50:50	120	Frozen	0.00	N/A	N/A	-	N/A	N/A	H*	M*	N/A	N/A	N/A	N/A	N/A
50:50	120	Frozen	0.03	N/A	N/A	0.64	N/A	N/A	H*	M*	N/A	N/A	N/A	N/A	N/A
50:50	120	Frozen	0.10	N/A	N/A	1.73	N/A	N/A	H*	M*	N/A	N/A	N/A	N/A	N/A
50:50	120	Frozen	0.25	N/A	N/A	3.18	N/A	N/A	H*	M*	N/A	N/A	N/A	N/A	N/A
50:50	120	Frozen	0.50	N/A	N/A	2.27	N/A	N/A	H*	M*	N/A	N/A	N/A	N/A	N/A
50:50	120	Frozen	1.00	N/A	N/A	2.0	N/A	N/A	H*	M*	N/A	N/A	N/A	N/A	N/A
80:20	120	Unfrozen	0.00	28.0	15.38	-	0	N/A	N/A	N/A	0.76	0.43	502	0	0.0
80:20	120	Unfrozen	0.03	27.3	15.57	2.1	6	2.5	N/A	N/A	0.74	0.42	496	-6	1.2
80:20	120	Unfrozen	0.10	26.1	15.85	2.3	14.8	3.3	N/A	N/A	0.71	0.41	487	-8.8	3.0
80:20	120	Unfrozen	0.25	25.7	15.94	2.1	17.6	7.1	N/A	N/A	0.70	0.41	484	-2.8	3.6

Table 4.3 (cont'd)

Hydrate concentration (%) Target value	Grain Size D 50 (microns)	Stage: Unfrozen (~18 °C); Frozen (-10°C)	Effective confining pressure (MPa)	Moisture content (%)	Dry unit weight (KN/m^3)	Thermal conductivity (W/m/K)	Total change of volume (V-Vo)	Bulk modulus, B= σ/ (ΔV/V) (MPa)	Hydrate distribution (optical/visual-destructive of sample)	Pore filling vs. grain boundaries	Void ratio	Porosity	Sample volume	Change of volume during consolidation	Total change of volume, (V-Vo)/V (%)
80:20	120	Unfrozen	0.50	24.8	16.18	2.0	24.8	10.1	N/A	N/A	0.67	0.40	477	-7.2	5.2
80:20	120	Unfrozen	1.00	23.3	16.59	1.7	36.5	13.7	N/A	N/A	0.63	0.39	465	-11.7	7.8
80:20	120	Frozen	0.00	N/A	N/A	-	N/A	N/A	H*	M*	N/A	N/A	N/A	N/A	N/A
80:20	120	Frozen	0.03	N/A	N/A	2.87	N/A	N/A	H*	M*	N/A	N/A	N/A	N/A	N/A
80:20	120	Frozen	0.10	N/A	N/A	3.02	N/A	N/A	H*	M*	N/A	N/A	N/A	N/A	N/A
80:20	120	Frozen	0.25	N/A	N/A	3.36	N/A	N/A	H*	M*	N/A	N/A	N/A	N/A	N/A
80:20	120	Frozen	0.50	N/A	N/A	2.05	N/A	N/A	H*	M*	N/A	N/A	N/A	N/A	N/A
80:20	120	Frozen	1.00	N/A	N/A	2.07	N/A	N/A	H*	M*	N/A	N/A	N/A	N/A	N/A

H* = Homogeneous

M* = Massive

4.5.2 Kaolinite (Table 4.4 - Figures 4.10 to 4.11)

Thermal conductivity increases slightly as porosity decreases for specimens at 100:0 unfrozen. The tendency of thermal conductivity to increase with the reduction in porosity is more noticeable at 50:50 unfrozen and 80:20 unfrozen. The highest k values for unfrozen specimens are observed at 100:0 composition and the lowest k values are observed at 50:50 composition.

Thermal conductivity abruptly decreases after the initial n value decreases for specimens at 50:50 frozen. After the minimum, the thermal conductivity increases slightly as porosity decreases.

Thermal conductivity tends to increase up to a maximum as porosity decreases and then drops for specimens at 80:20 frozen. The thermal conductivity values observed for 50:50 frozen fall below the thermal conductivity values for 80:20 frozen.

The maximum thermal conductivity value is observed at 80:20 frozen (k= 2.81 W/mK).

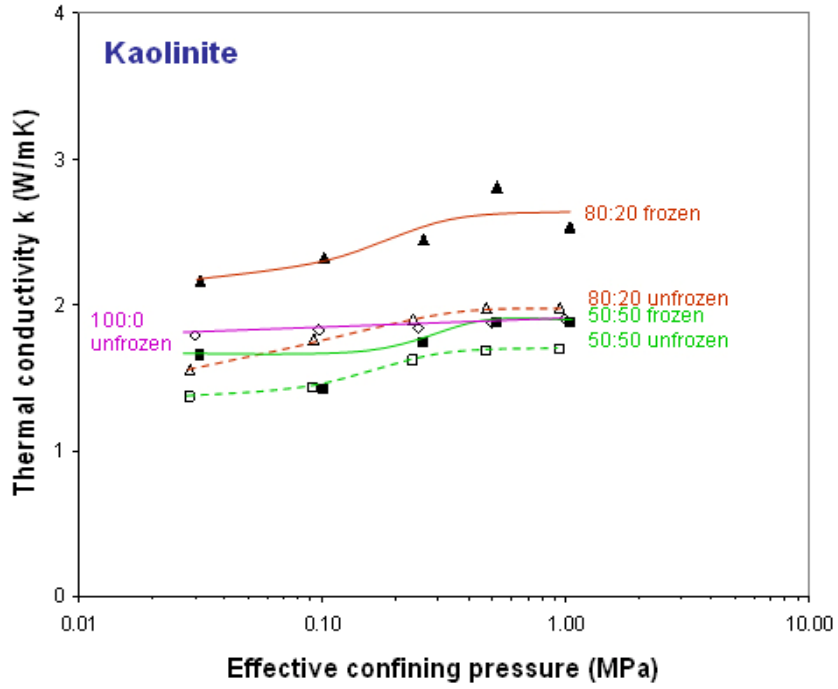

(a)

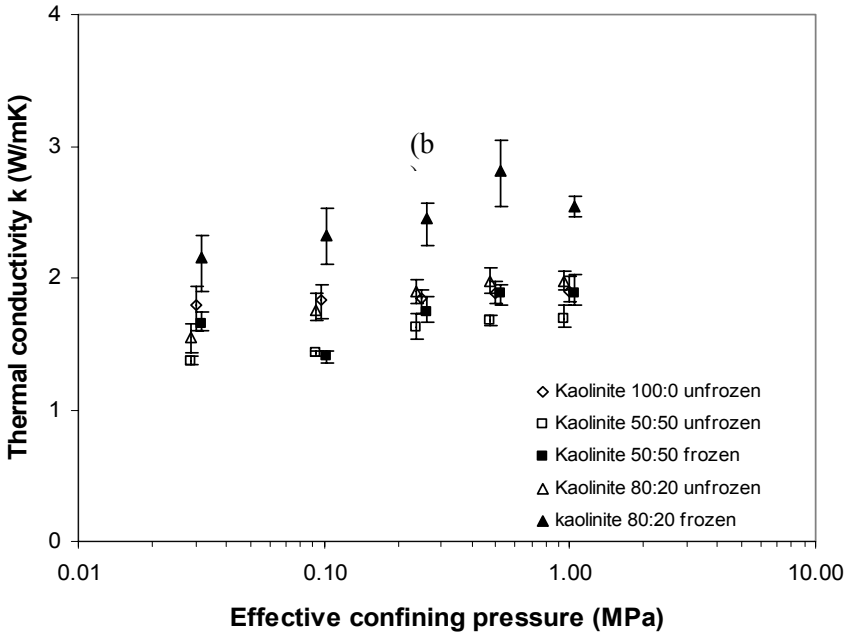

(b)

Figure 4.10 Kaolinite - Thermal conductivity versus effective confining pressure (a) Thermal conductivity values correspond to an average of six measurements. (b) Average minimum and maximum values are presented
Note: To facilitate the data reading, the values of pressure for 50:50 unfrozen and 80:20 unfrozen have been shifted 0.95 to the left. The values of pressure for 50:50 frozen and 80:20 frozen have been shifted 1.05 to the right

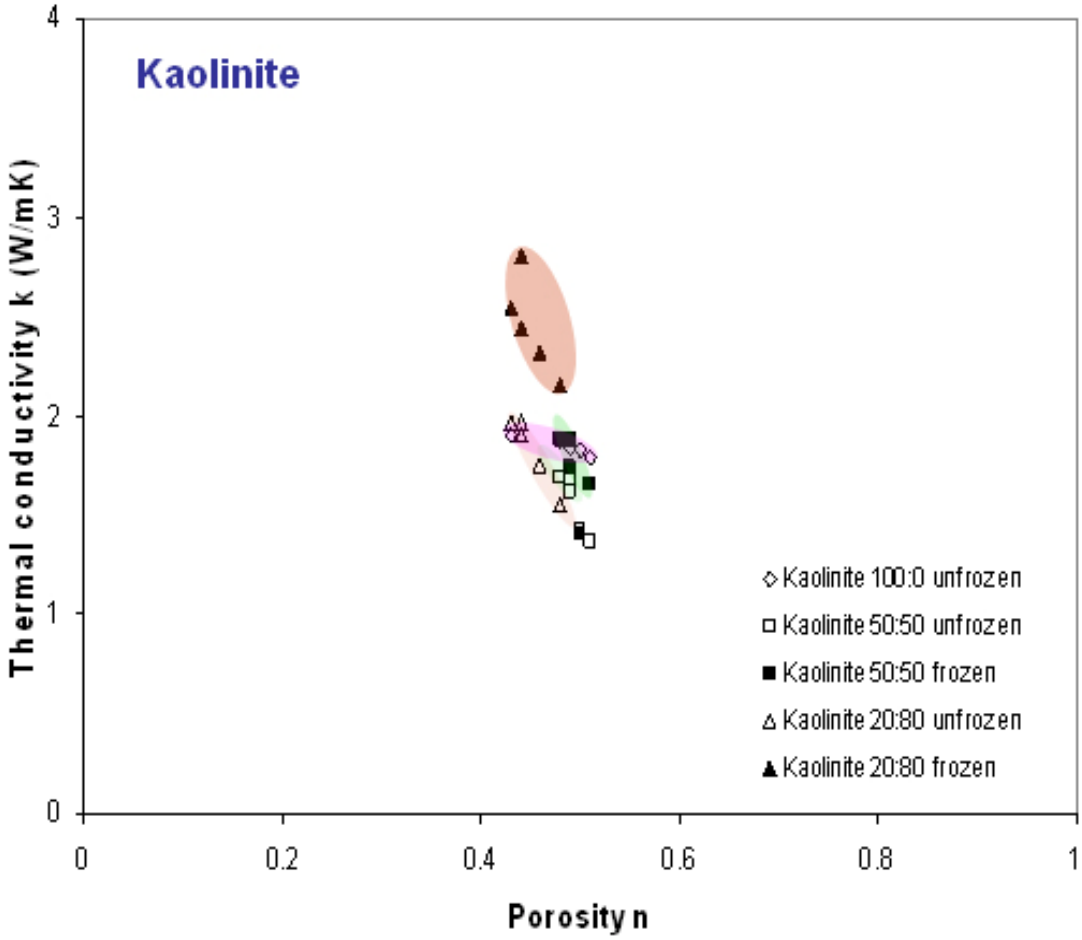

Figure 4.11 Kaolinite - Thermal conductivity versus porosity
Thermal conductivity values correspond to an average of six measurements

Table 4.4 Thermal conductivity - kaolinite

Hydrate concentration (%) Target value	Grain Size D 50 (microns)	Stage: Unfrozen (~18 °C); Frozen (-10°C)	Effective confining pressure (MPa)	Moisture content (%)	Dry unit weight (KN/m^3)	Thermal conductivity (W/m/K)	Total change of volume (V-Vo)	Bulk modulus, B= σ/ (ΔV/V) (MPa)	Hydrate distribution (optical/visual-destructive of sample)	Pore filling vs. grain boundaries	Void ratio	Porosity	Sample volume	Change of volume during consolidation	Total change of vol. (V-Vo)/V (%)
100:0	1.1	Unfrozen	0.00	40.2	12.71	-	0.0	N/A	N/A	N/A	1.05	0.51	530	0	0.0
100:0	1.1	Unfrozen	0.03	40.1	12.73	1.79	1	15.9	N/A	N/A	1.04	0.51	529	-1	0.2
100:0	1.1	Unfrozen	0.10	39.0	12.91	1.83	8.2	6.3	N/A	N/A	1.01	0.50	522	-7.2	1.6
100:0	1.1	Unfrozen	0.25	37.2	13.21	1.84	20.1	6.6	N/A	N/A	0.97	0.49	510	-11.9	3.9
100:0	1.1	Unfrozen	0.50	35.4	13.54	1.90	32.6	8.1	N/A	N/A	0.92	0.48	498	-12.5	6.6
100:0	1.1	Unfrozen	1.00	28.8	14.86	1.90	76.6	6.9	N/A	N/A	0.75	0.43	454	-44	16.9
50:50	1.1	Unfrozen	0.00	41.4	12.95	-	0.0	N/A	N/A	N/A	1.16	0.54	442	0	0.0
50:50	1.1	Unfrozen	0.03	36.8	13.79	1.37	26.8	0.6	N/A	N/A	1.03	0.51	415	-26.8	6.5
50:50	1.1	Unfrozen	0.10	35.2	14.08	1.43	35.5	1.4	N/A	N/A	0.98	0.50	407	-8.7	8.7
50:50	1.1	Unfrozen	0.25	34.5	14.23	1.61	39.6	3.3	N/A	N/A	0.96	0.49	402	-4.1	9.8
50:50	1.1	Unfrozen	0.50	34.0	14.33	1.68	42.6	6.2	N/A	N/A	0.95	0.49	399	-3	10.7

Table 4.4 (cont'd)

Hydrate concentration (%) Target value	Grain Size D 50 (microns)	Stage: Unfrozen (~18 °C); Frozen (10°C)	Effective confining pressure (MPa)	Moisture content (%)	Dry unit weight (KN/m^3)	Thermal conductivity (W/m/K)	Total change of volume (V-Vo)	Bulk modulus, B= σ/ (ΔV/V) (MPa)	Hydrate distribution (optical/visual- destructive of	Pore filling vs. grain boundaries	Void ratio	Porosity	Sample volume	Change of volume during consolidation	Total change of vol.(V-Vo)/V (%)
50:50	1.1	Unfrozen	1.00	33.2	14.51	1.69	47.3	11.2	N/A	N/A	0.93	0.48	395	-4.7	12.0
50:50	1.1	Frozen	0.00	N/A	N/A	-	N/A	N/A	H*	M*	N/A	N/A	N/A	N/A	N/A
50:50	1.1	Frozen	0.03	N/A	N/A	1.65	N/A	N/A	H*	M*	N/A	N/A	N/A	N/A	N/A
50:50	1.1	Frozen	0.10	N/A	N/A	1.40	N/A	N/A	H*	M*	N/A	N/A	N/A	N/A	N/A
50:50	1.1	Frozen	0.25	N/A	N/A	1.74	N/A	N/A	H*	M*	N/A	N/A	N/A	N/A	N/A
50:50	1.1	Frozen	0.50	N/A	N/A	1.88	N/A	N/A	H*	M*	N/A	N/A	N/A	N/A	N/A
50:50	1.1	Frozen	1.00	N/A	N/A	1.88	N/A	N/A	H*	M*	N/A	N/A	N/A	N/A	N/A
80:20	1.1	Unfrozen	0.00	35.2	13.72	-	0	N/A	N/A	N/A	0.93	0.48	483	0	0.0
80:20	1.1	Unfrozen	0.03	35.0	13.77	1.55	1.5	9.7	N/A	N/A	0.93	0.48	482	-1.5	0.3
80:20	1.1	Unfrozen	0.10	32.5	14.24	1.76	17.6	2.7	N/A	N/A	0.86	0.46	466	-16.1	3.8
80:20	1.1	Unfrozen	0.25	30.0	14.78	1.90	34.6	3.5	N/A	N/A	0.79	0.44	449	-17	7.7
80:20	1.1	Unfrozen	0.50	29.0	14.99	1.97	40.8	5.9	N/A	N/A	0.77	0.44	442	-6.2	9.2

Table 4.4 (cont'd)

Hydrate concentration (%) Target value	Grain Size D 50 (microns)	Stage: Unfrozen (~18 °C); Frozen (10°C)	Effective confining pressure (MPa)	Moisture content (%)	Dry unit weight (KN/m^3)	Thermal conductivity (W/m/K)	Total change of volume (V-Vo)	Bulk modulus, B= σ/ (ΔV/V) (MPa)	Hydrate distribution (optical/visual-destructive of sample)	Pore filling vs. grain boundaries	Void ratio	Porosity	Sample volume	Change of volume during consolidation	Total change of vol. (V-Vo)/V (%)
80:20	1.1	Unfrozen	1.00	27.9	15.25	1.97	48.5	10.0	N/A	N/A	0.74	0.43	435	-7.7	11.2
80:20	1.1	Frozen	0.00	N/A	N/A	-	N/A	N/A	H*	M*	N/A	N/A	N/A	N/A	N/A
80:20	1.1	Frozen	0.03	N/A	N/A	2.16	N/A	N/A	H*	M*	N/A	N/A	N/A	N/A	N/A
80:20	1.1	Frozen	0.10	N/A	N/A	2.32	N/A	N/A	H*	M*	N/A	N/A	N/A	N/A	N/A
80:20	1.1	Frozen	0.25	N/A	N/A	2.45	N/A	N/A	H*	M*	N/A	N/A	N/A	N/A	N/A
80:20	1.1	Frozen	0.50	N/A	N/A	2.81	N/A	N/A	H*	M*	N/A	N/A	N/A	N/A	N/A
80:20	1.1	Frozen	1.00	N/A	N/A	2.54	N/A	N/A	H*	M*	N/A	N/A	N/A	N/A	N/A

H* = Homogeneous

M* = Massive

4.5.3 Precipitated Silica Flour (Table 4.5 - Figures 4.12 to 4.13)

Thermal conductivity increases slightly as porosity decreases at 100:0 unfrozen. Same phenomenon is observed for 50:50 unfrozen and 80:20 unfrozen specimens. The highest k values at unfrozen stage are observed for specimens without THF filling the pores. The lowest k values are observed for 50:50 unfrozen specimens.

Thermal conductivity values at 50:50 frozen fall below thermal conductivity values at 80:20 frozen. The same trend is observed in sand frozen and kaolinite frozen.

Thermal conductivity increases as porosity decreases for specimens at 50:50 frozen and 80:20 frozen. A maximum is observed in both cases, which corresponds with the maximum reduction in porosity. A drop in thermal conductivity after the maximum is not observed in frozen specimens.

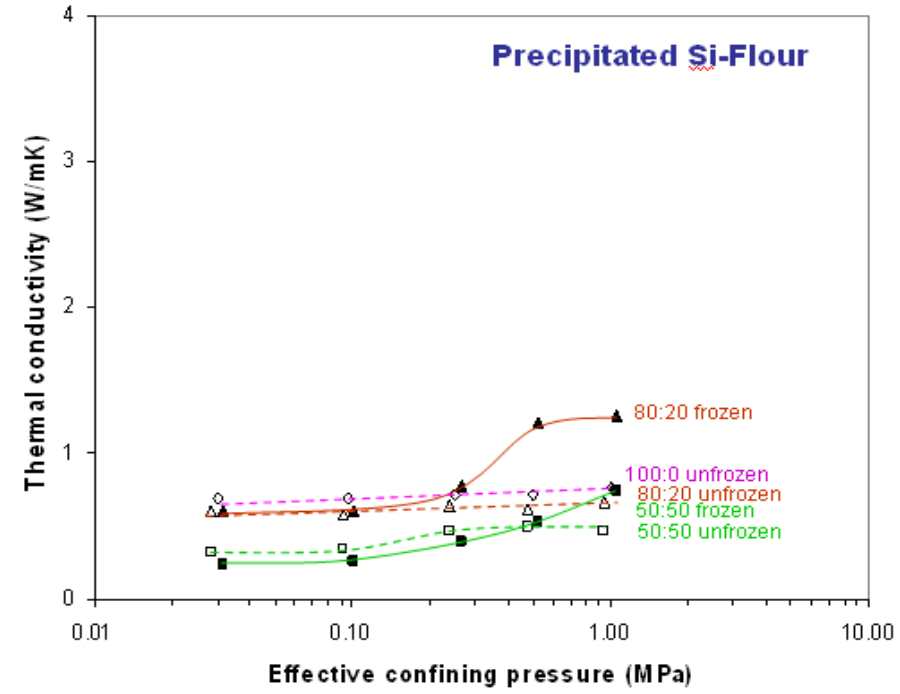

(a)

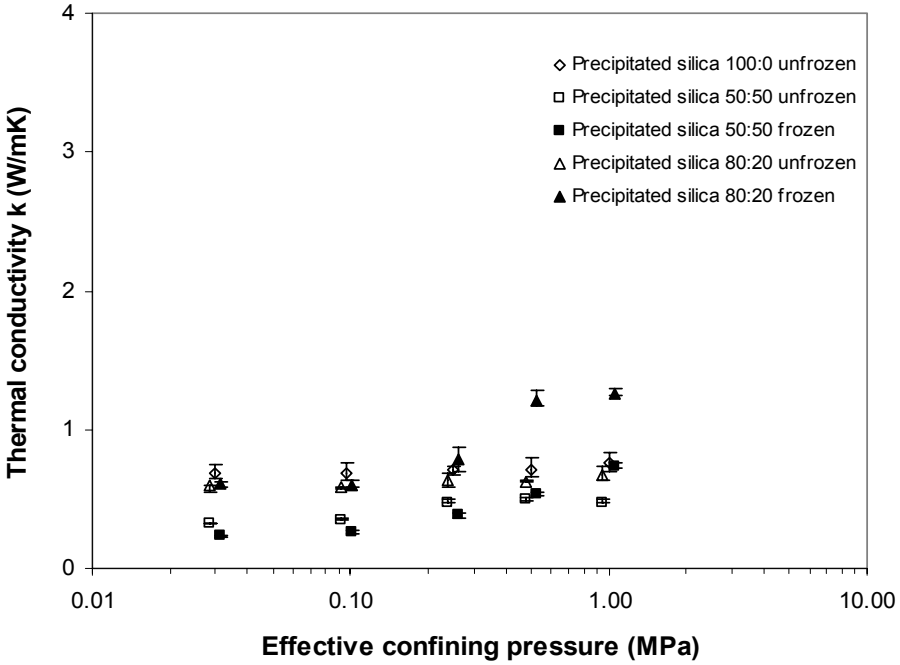

(b)

Figure 4.12 Precipitated silica flour - Thermal conductivity versus effective confining pressure (a) Thermal conductivity values correspond to an average of six measurements. (b) Average minimum and maximum values are presented

Note: To facilitate the data reading, the values of pressure for 50:50 unfrozen and 80:20 unfrozen have been shifted 0.95 to the left. The values of pressure for 50:50 frozen and 80:20 frozen have been shifted 1.05 to the right

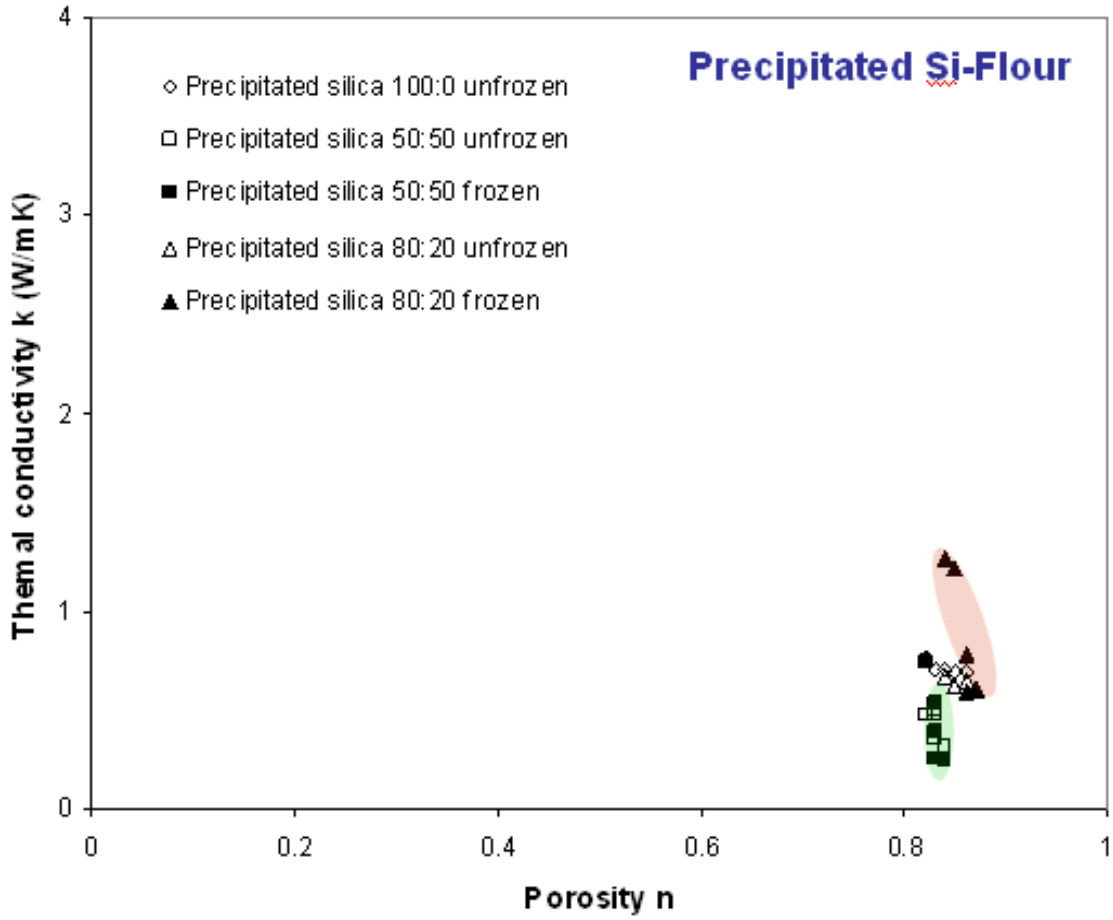

Figure 4.13 Precipitated silica flour - Thermal conductivity versus porosity
Thermal conductivity values correspond to an average
of six measurements

Table 4.5 Thermal conductivity- Precipitated silica flour

Hydrate concentration (%) Target value	Grain Size D 50 (microns)	Stage: Unfrozen (~18 °C); Frozen (-10°C)	Effective confining pressure (MPa)	Moisture content (%)	Dry unit weight (KN/m^3)	Thermal conductivity (W/m/K)	Total change of volume (V-Vo)	Bulk modulus, B= σ/ (ΔV/V) (MPa)	Hydrate distribution (optical/visual-destructive of sample)	Pore filling vs. grain boundaries	Void ratio	Porosity	Sample volume	Change of volume during consolidation	Total change of vol. (V-Vo)/V (%)
100:0	20	Unfrozen	0.00	292.0	2.94	-	0.0	N/A	N/A	N/A	6.07	0.86	443	0.00	0.00
100:0	20	Unfrozen	0.03	287.6	2.98	0.69	5.7	2.3	N/A	N/A	5.98	0.86	437	-5.7	1.3
100:0	20	Unfrozen	0.10	280.1	3.05	0.69	15.5	2.8	N/A	N/A	5.83	0.85	427	-9.8	3.6
100:0	20	Unfrozen	0.25	257.3	3.27	0.71	45.1	2.5	N/A	N/A	5.35	0.84	397	-29.6	11.3
100:0	20	Unfrozen	0.50	239.8	3.47	0.71	67.9	3.3	N/A	N/A	4.99	0.83	375	-22.8	18.1
100:0	20	Unfrozen	1.00	221.4	3.71	0.76	91.9	4.8	N/A	N/A	4.60	0.82	351	-24.0	26.2
50:50	20	Unfrozen	0.00	230.9	3.63	-	0.0	N/A	N/A	N/A	5.17	0.84	413	0.00	0.00
50:50	20	Unfrozen	0.03	226.3	3.69	0.32	6.9	1.9	N/A	N/A	5.06	0.84	406	-6.9	1.7
50:50	20	Unfrozen	0.10	223.2	3.73	0.35	11.6	3.7	N/A	N/A	4.99	0.83	401	-4.7	2.9
50:50	20	Unfrozen	0.25	220.8	3.77	0.47	15.2	7.3	N/A	N/A	4.94	0.83	398	-3.6	3.8

Table 4.5 (cont'd)

Hydrate concentration (%) Target value	Grain Size D 50 (microns)	Stage: Unfrozen (~18 °C); Frozen (-10°C)	Effective confining pressure (MPa)	Moisture content (%)	Dry unit weight (KN/m^3)	Thermal conductivity (W/m/K)	Total change of volume (V-Vo)	Bulk modulus, B= σ/ (ΔV/V) (MPa)	Hydrate distribution (optical/visual- destructive of	Pore filling vs. grain boundaries	Void ratio	Porosity	Sample volume	Change of volume during consolidation	Total change of vol. (V-Vo)V (%)
50:50	20	Unfrozen	0.50	217.1	3.82	0.49	20.7	10.7	N/A	N/A	4.86	0.83	392	-5.5	5.3
50:50	20	Unfrozen	1.00	210.6	3.92	0.47	30.5	14.5	N/A	N/A	4.71	0.82	383	-9.8	8.0
50:50	20	Frozen	0.00	N/A	N/A	-	N/A	N/A	H*	M*	N/A	N/A	N/A	N/A	N/A
50:50	20	Frozen	0.03	N/A	N/A	0.24	N/A	N/A	H*	M*	N/A	N/A	N/A	N/A	N/A
50:50	20	Frozen	0.10	N/A	N/A	0.26	N/A	N/A	H*	M*	N/A	N/A	N/A	N/A	N/A
50:50	20	Frozen	0.25	N/A	N/A	0.39	N/A	N/A	H*	M*	N/A	N/A	N/A	N/A	N/A
50:50	20	Frozen	0.50	N/A	N/A	0.53	N/A	N/A	H*	M*	N/A	N/A	N/A	N/A	N/A
50:50	20	Frozen	1.00	N/A	N/A	0.74	N/A	N/A	H*	M*	N/A	N/A	N/A	N/A	N/A
80:20	20	Unfrozen	0.00	322.7	2.70	-	0.00	N/A	N/A	N/A	6.85	0.87	411	0.00	0.00
80:20	20	Unfrozen	0.03	316.9	2.75	0.57	6.5	1.9	N/A	N/A	6.73	0.87	404	-6.5	1.6
80:20	20	Unfrozen	0.10	292.5	2.94	0.58	33.6	1.2	N/A	N/A	6.21	0.86	377	-27.1	8.9
80:20	20	Unfrozen	0.25	281.0	3.05	0.64	46.3	2.2	N/A	N/A	5.96	0.86	364	-12.7	12.7

Table 4.5 (cont'd)

Hydrate concentration (%) Target value	Grain Size D 50 (microns)	Stage: Unfrozen (~18 °C); Frozen (-10°C)	Effective confining pressure (MPa)	Moisture content (%)	Dry unit weight (KN/m^3)	Thermal conductivity (W/m/K)	Total change of volume (V-Vo)	Bulk modulus, B= σ/ (ΔV/V) (MPa)	Hydrate distribution (optical/visual- destructive of	Pore filling vs. grain boundaries	Void ratio	Porosity	Sample volume	Change of volume during consolidation	Total change of vol. (V-Vo) V (%)
80:20	20	Unfrozen	0.50	271.2	3.14	0.62	57.2	3.6	N/A	N/A	5.76	0.85	353	-10.9	16.2
80:20	20	Unfrozen	1.00	256.8	3.29	0.67	73.2	5.6	N/A	N/A	5.45	0.84	337	-16.0	21.7
80:20	20	Frozen	0.00	N/A	N/A	-	N/A	N/A	H*	M*	N/A	N/A	N/A	N/A	N/A
80:20	20	Frozen	0.03	N/A	N/A	0.61	N/A	N/A	H*	M*	N/A	N/A	N/A	N/A	N/A
80:20	20	Frozen	0.10	N/A	N/A	0.60	N/A	N/A	H*	M*	N/A	N/A	N/A	N/A	N/A
80:20	20	Frozen	0.25	N/A	N/A	0.78	N/A	N/A	H*	M*	N/A	N/A	N/A	N/A	N/A
80:20	20	Frozen	0.50	N/A	N/A	1.21	N/A	N/A	H*	M*	N/A	N/A	N/A	N/A	N/A
80:20	20	Frozen	1.00	N/A	N/A	1.26	N/A	N/A	H*	M*	N/A	N/A	N/A	N/A	N/A

H* = Homogeneous

M* = Massive

4.5.4 Crushed Silica Flour (Table 4.3 - Figures 4.13 to 4.14)

Thermal conductivity tends to increase as porosity decreases at 100:0 unfrozen, while thermal conductivity increases up to a maxima and then decreases as porosity decreases for specimens at 80:20 unfrozen. The highest thermal conductivity value at unfrozen stage corresponds to 100:0 composition (k= 3.13 W/mK).

Thermal conductivity values at 80:20 frozen decreases up to a minimum value as porosity decreases. After that minimum, thermal conductivity increases slightly.

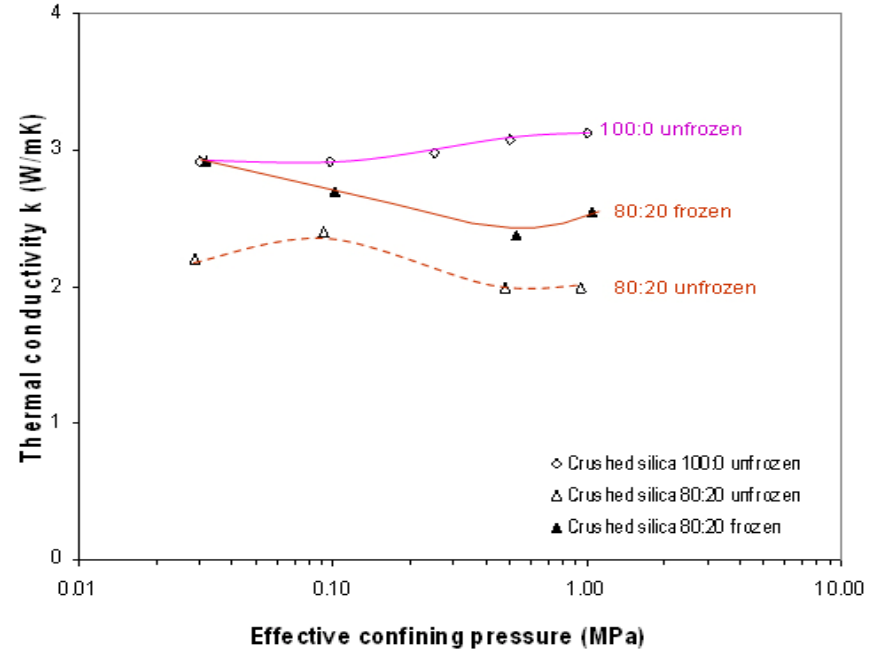

(a)

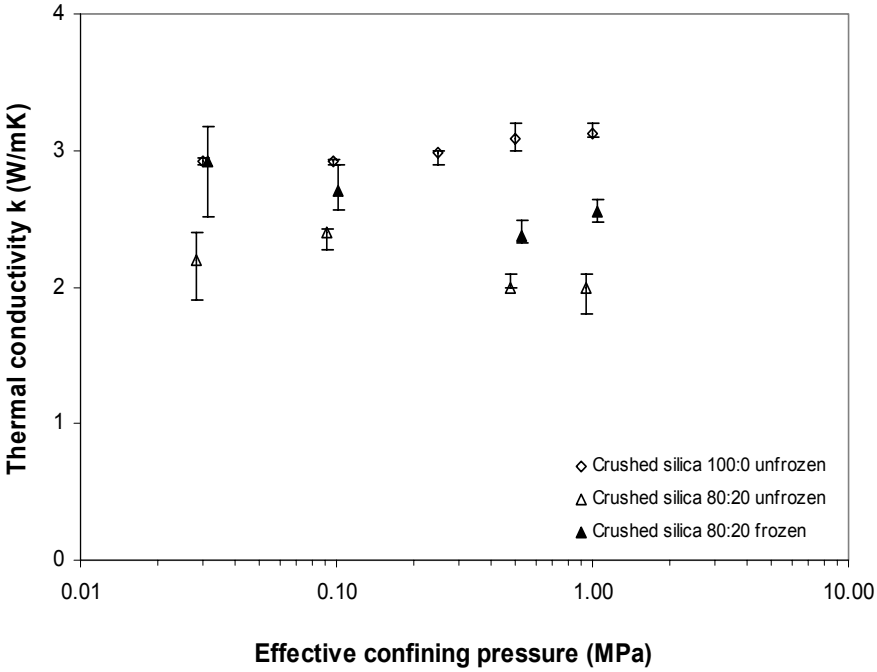

(b)

Figure 4.14 Crushed silica flour - Thermal conductivity versus effective confining pressure. (a) Thermal conductivity values correspond to an average of six measurements. (b) Average minimum and maximum values are presented
Note: To facilitate the data reading, the values of pressure for 50:50 unfrozen and 80:20 unfrozen have been shifted 0.95 to the left. The values of pressure for 50:50 frozen and 80:20 frozen have been shifted 1.05 to the right

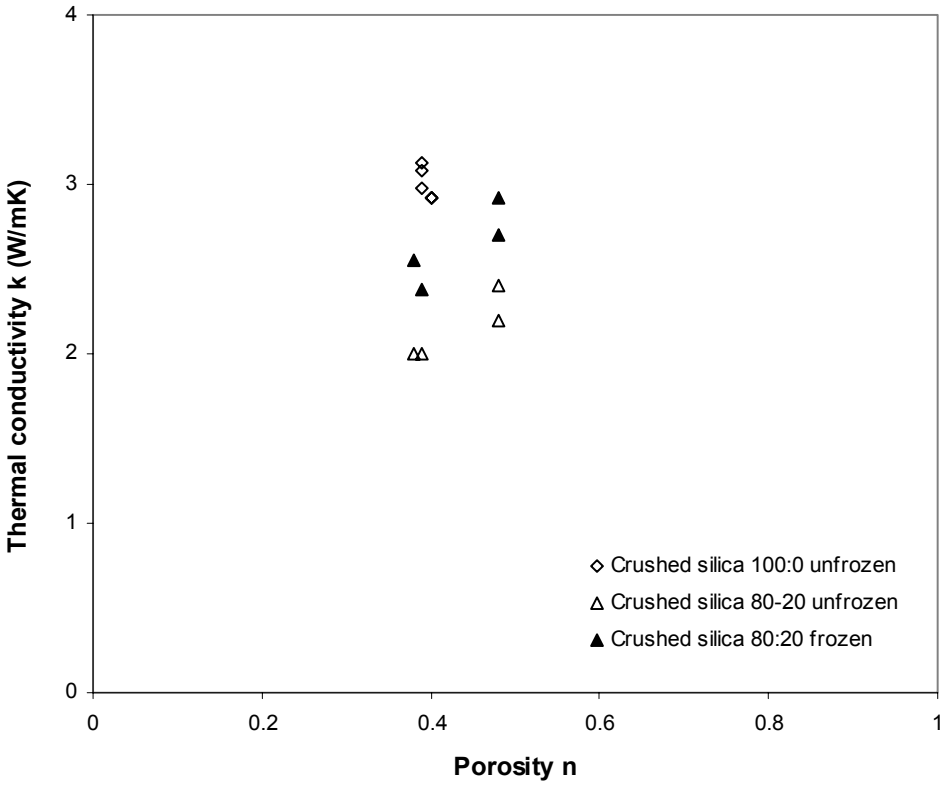

Figure 4.15 Crushed silica flour -Thermal conductivity versus porosity

Thermal conductivity values correspond to an average of six measurements

Table 4.6 Thermal conductivity- Crushed silica flour

Hydrate concentration (%) Target value	Grain Size D 50 (microns)	Stage: Unfrozen (~18 °C); Frozen (-10°C)	Effective confining pressure (MPa)	Moisture content (%)	Dry unit weight (KN/m^3)	Thermal conductivity (W/m/K)	Total change of volume (V-Vo)	Bulk modulus, B= σ/ (ΔV/V) (MPa)	Hydrate distribution (optical/visual-destructive of sample)	Pore filling vs. grain boundaries	Void ratio	Porosity	Sample volume	Change of volume during consolidation	Total change of volume, (V-Vo)/V (%)
100:0	20	Unfrozen	0.00	25.5	15.83	-	0.0	N/A	N/A	N/A	0.67	0.40	455	0.0	0.0
100:0	20	Unfrozen	0.03	25.0	15.95	2.92	0.0	-	N/A	N/A	0.66	0.40	452	-3.6	0.0
100:0	20	Unfrozen	0.10	24.7	16.01	2.92	1.7	25.9	N/A	N/A	0.65	0.40	450	-1.7	0.4
100:0	20	Unfrozen	0.25	24.5	16.06	2.98	3.1	36.7	N/A	N/A	0.65	0.39	449	-1.4	0.7
100:0	20	Unfrozen	0.50	24.1	16.17	3.08	6.2	36.7	N/A	N/A	0.64	0.39	445	-3.1	1.4
100:0	20	Unfrozen	1.00	23.9	16.23	3.13	7.8	58.4	N/A	N/A	0.63	0.39	444	-1.6	1.8
80:20	20	Unfrozen	0.00	35.0	13.89	-	0.0	N/A	N/A	N/A	0.95	0.49	469	0.0	0.0
80:20	20	Unfrozen	0.03	34.7	13.94	2.17	1.9	7.4	N/A	N/A	0.94	0.48	467	-1.9	0.4
80:20	20	Unfrozen	0.10	34.3	14.02	2.35	4.6	9.9	N/A	N/A	0.93	0.48	465	-2.7	1.0
80:20	20	Unfrozen	0.25	29.7	15.00	-	34.8	3.4	N/A	N/A	0.80	0.45	434	-30.2	8.0
80:20	20	Unfrozen	0.50	23.8	16.46	2.04	73.4	3.2	N/A	N/A	0.64	0.39	396	-38.6	18.5

Table 4.6 (cont'd)

Hydrate concentration (%) Target value	Grain Size D 50 (microns)	Stage: Unfrozen (~18 °C); Frozen (-10°C)	Effective confining pressure (MPa)	Moisture content (%)	Dry unit weight (KN/m^3)	Thermal conductivity (W/m/K)	Total change of volume (V-Vo)	Bulk modulus, B= σ/ (ΔV/V) (MPa)	Hydrate distribution (optical/visual-destructive of sample)	Pore filling vs. grain boundaries	Void ratio	Porosity	Sample volume	Change of volume during consolidation	Total change of vol. (V-Vo)/V (%)
80:20	20	Unfrozen	1.00	22.4	16.84	1.95	82.3	5.7	N/A	N/A	0.61	0.38	387	-8.9	21.3
80:20	20	Frozen	0.00	N/A	N/A	-	N/A	N/A	H*	M*	N/A	N/A	N/A	N/A	N/A
80:20	20	Frozen	0.03	N/A	N/A	2.92	N/A	N/A	H*	M*	N/A	N/A	N/A	N/A	N/A
80:20	20	Frozen	0.10	N/A	N/A	2.70	N/A	N/A	H*	M*	N/A	N/A	N/A	N/A	N/A
80:20	20	Frozen	0.25	N/A	N/A	-	N/A	N/A	H*	M*	N/A	N/A	N/A	N/A	N/A
80:20	20	Frozen	0.50	N/A	N/A	2.38	N/A	N/A	H*	M*	N/A	N/A	N/A	N/A	N/A
80:20	20	Frozen	1.00	N/A	N/A	2.55	N/A	N/A	H*	M*	N/A	N/A	N/A	N/A	N/A

H* = Homogeneous

M* = Massive

4.6 Summary Observations

- Hydrate in pore space increases the thermal conductivity of the systems. Hydrates facilitate heat conduction.
- Thermal conductivity of specimens with hydrates in the pores is higher than thermal conductivity of the same soil specimens with fluids (water, THF-water) in pores.
- Overall trend: thermal conductivity increases as porosity decreases (all soils and fluids) as a result of increased coordination.
- Thermal conductivity drops after a maximum in sand and crushed silica flour (50:50 and 80:20). Might be a slightly chance of experimental bias or a physic phenomenon not clear to gauge at the moment.
- Thermal conductivity of specimens with 80:20 frozen compositions is always higher than thermal conductivity of specimens with 50:50 frozen, due to a higher amount of hydrates at 80:20 composition.

CHAPTER 5
INTERPRETATION OF RESULTS – CONCLUSIONS

The understanding of the thermal properties of hydrate-bearing sediments is crucial for the future exploitation of methane gas trapped in sediments. Thermal properties are also needed to assess sea floor stability, global climate change, sedimentation and submarine slide formation. Unfortunately, the state of the art in hydrate research does not permit the determination of hydrate thermal properties inside the hydrate stability envelope.

In order to better understand the thermal properties of hydrate-bearing sediments, this research covered an unprecedented range of soils, which exhibit variations in grain size, pore size, specific surface area and mineralogy. Since natural methane hydrate formation in sediments has not been successfully simulated in the laboratory, this research was based on THF hydrate.

This chapter provides some possible hypotheses to explain experimental results. Porosity is the fundamental soil parameter considered to evaluate the thermal conductivity of the sediments in this study. The influence of grain size, particle shape and specific surface area are evaluated as well.

5.1 Deviations from the Natural Process

The presence of salts depresses the water activity (Klauda and Sandler, 2001). However, experiments in this thesis used fresh water rather than saline pore water. The uniform sediments that were tested have a single pore size because grain size distributions are narrow. Real sediments often have a broad distribution. The non-wetting phases (gas, ice and hydrate) will preferentially occupy the largest pores available, in order to minimize surface energy (Klauda and Sandler, 2001).

The physical properties and surface chemistry of the host sediments affect the thermodynamic state, growth kinetics, spatial distribution and growth forms of clathrates. These physical properties (e.g., thermal conductivity) depend not only on how much

hydrate is present, but also how it is distributed in the pore space. Water and THF are highly miscible, but water and gas are immiscible, and methane hydrate formation is susceptible to interfacial effects. Finally, while THF forms structure II hydrate, pure methane forms structure I (Talley et al., 2000).

5.2 Unfrozen Specimens

The thermal conductivity of saturated water-soil mixtures increases as porosity decreases in all soils (Figure 5.1). This reflects the increase in inter-particle coordination, which favors heat conduction.

The highest k values observed for unfrozen specimens correspond to the crushed silt, followed by the sand (Figure 5.1). Both materials have higher quartz (in crystalline form) content than clay or precipitated silica flour.

The highest k values in unfrozen specimens correspond to water (100:0), while the lowest k values are observed at 50:50 fluid composition (Figure 5.2). Specimens with mixtures in a ratio of 80:20 fall in between. This reflects the lower k value of THF compared to water.

Precipitated silica flour exhibits lower k values than crushed silica flour even though they have the same D_{50}. The higher specific surface area in the precipitated silica flour compared with crushed silica flour explains its higher water content and porosity. Furthermore, results indicate the thermal conductivity is not only dependent on contacts per unit volume, but on the effective transfer of heat across contacts.

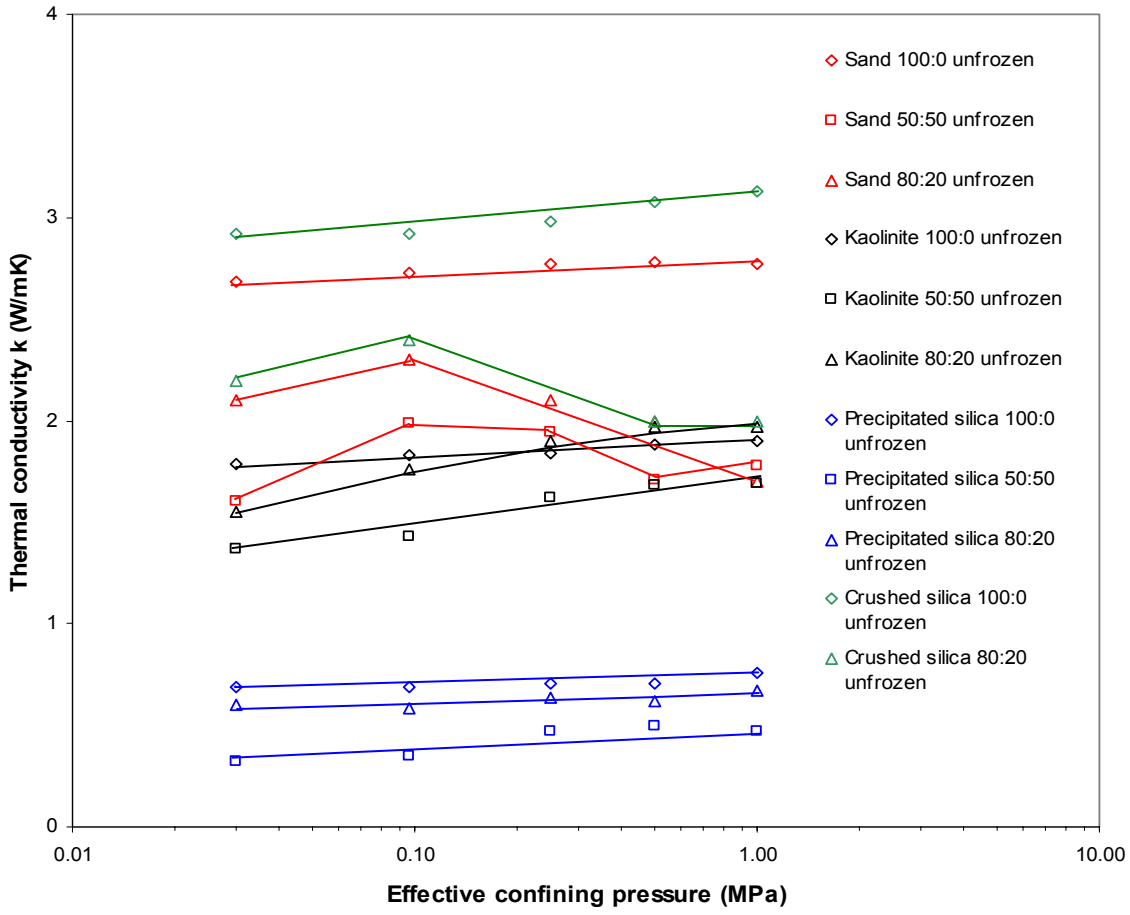

Figure 5.1 Thermal conductivity versus effective confining pressure for all soil tested at: 100:0, 50:50 and 80:20 - unfrozen stage

5.3 Frozen Specimens

Overall, THF hydrate filling the pore space facilitates heat conduction. This is evident in all the tested soils. The highest k values are observed in THF hydrate-filled sand (Figures 5.2 and 5.3). The sand 50:50 and 80:20 frozen specimens show a drop in thermal conductivity after a maximum value is reached. This may reflect volume expansion and inter-granular contact loss, yet, it cannot be assured precisely.

To prevent ice formation, soil mixtures with 50:50 fluid mixtures have liquid THF after hydrate formation. Since THF has the lowest value of thermal conductivity among all the compounds present in the mixtures, the thermal conductivity of 50:50 frozen specimens fall bellow those of 80:20 frozen specimens (Figures 5.2 and 5.3).

Thermal conductivity of sand 50:50 frozen is higher than k for kaolinite 50:50 frozen, which in turn is higher than k for precipitated silica flour 50:50 frozen, due to the presence of quartz in sand, and overall, due to the increase in contact between particles (Figure 5.2)

Thermal conductivity of sand 80:20 frozen is higher than k for kaolinite 80:20 frozen, which in turn, is higher than k for precipitated silica flour 80:20 frozen. Crushed silica flour 80:20 frozen does not follow these trends. The highest quart content in sand explains its k values. Experimental bias might explain the behavior for crushed silica flour 80:20 frozen, but there might be a physic explanation not available at this time

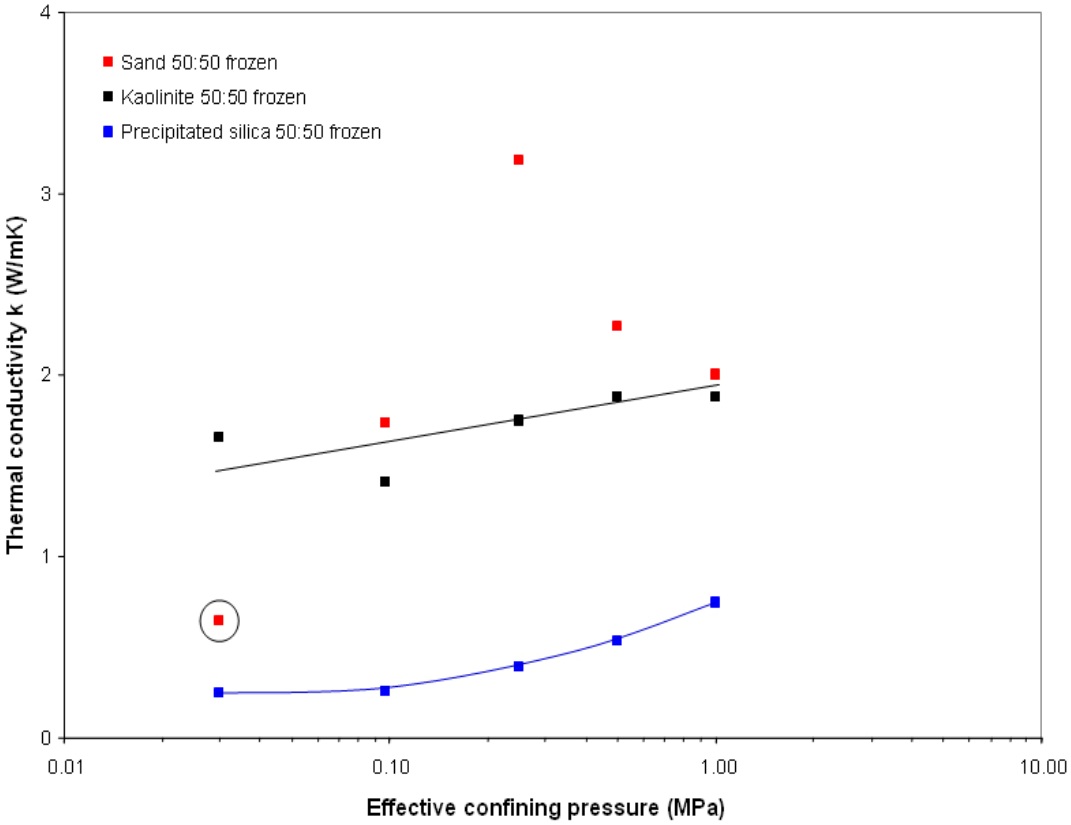

Figure 5.2 Sand, kaolinite and precipitated silica flour
Thermal conductivity versus effective confining pressure at 50:50 frozen

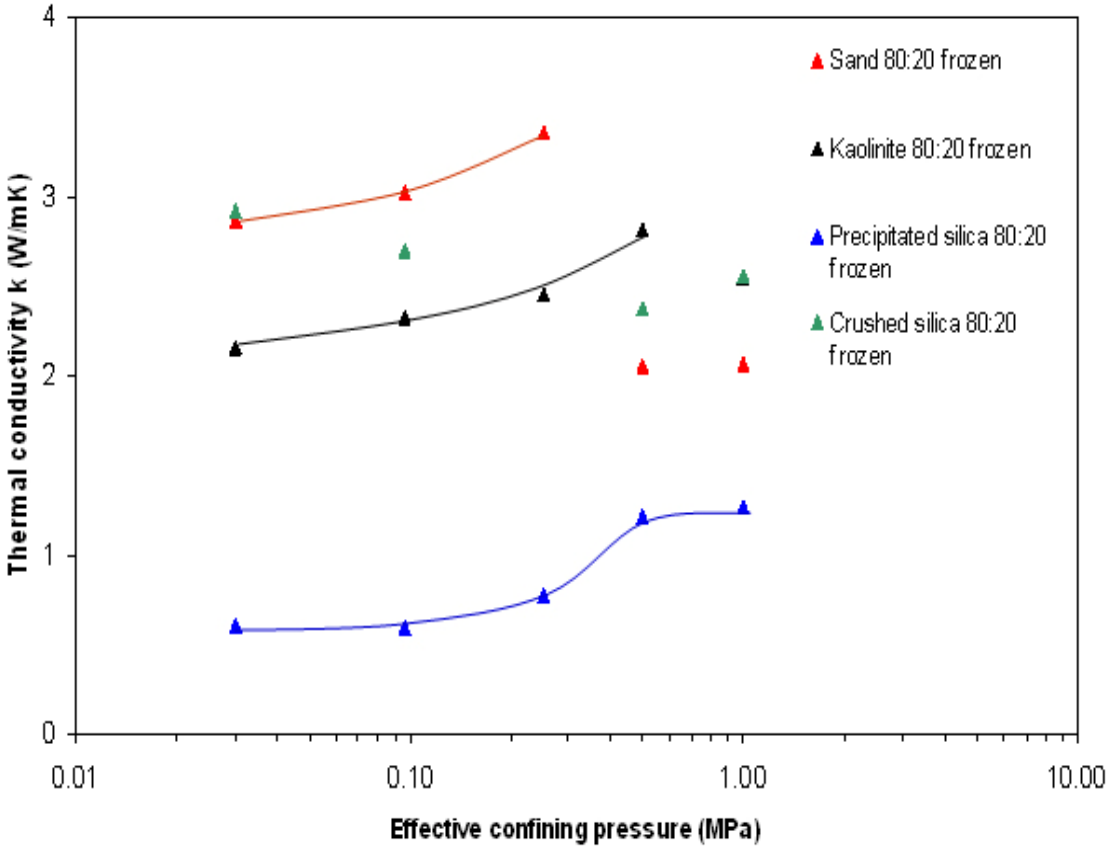

Figure 5.3 Sand, kaolinite, precipitated silica flour and crushed silica flour Thermal conductivity versus effective confining pressure at 80:20 frozen

5.4 Conclusions

The following conclusions are extracted from this study:

- The overall trend is determined by porosity (Figure 5.4).
- The thermal conductivity of soil-fluid mixtures increases as porosity decreases (all soils and fluids).
- Reduction in porosity implies an increase in inter-particle coordination which favors heat conduction.
- The higher the amount of hydrates in pores, the higher the measured thermal conductivity because hydrates facilitate heat conduction.
- Unfrozen THF in the voids reduces the thermal conductivity of the system. The thermal conductivity of 80:20 frozen specimens is higher than the thermal conductivity of 50:50 frozen specimens.
- A higher quartz content (observed in sand and crushed silt (as compared to clay) results in higher thermal conductivity.
- Ther thermal conductivity depends on contacts per unit volume, as well as on effective transfer of heat across the contacts, which increases with effective stress.
- Hydrate formation is possible in sediments with high specific surface area and small pores (clay and precipitated silt).

5.5 Recommendations for Future Research

- Improve future experiments to gain better control of the amount of fluid squeezed out during consolidation and the amount of fluid that remains to form hydrates.
- Test the same soil specimen with ice and hydrates at the same porosity, temperature and pressure.
- Involve advanced techniques (such as nuclear magnetic resonance) to monitor hydrate formation in pores while collecting thermal conductivity data. This will permit clarifying hydrate growth habits in the soil matrix according with the sediment type, and its effect on thermal response.
- Extend this study to include soil mixtures similar to natural sediments.

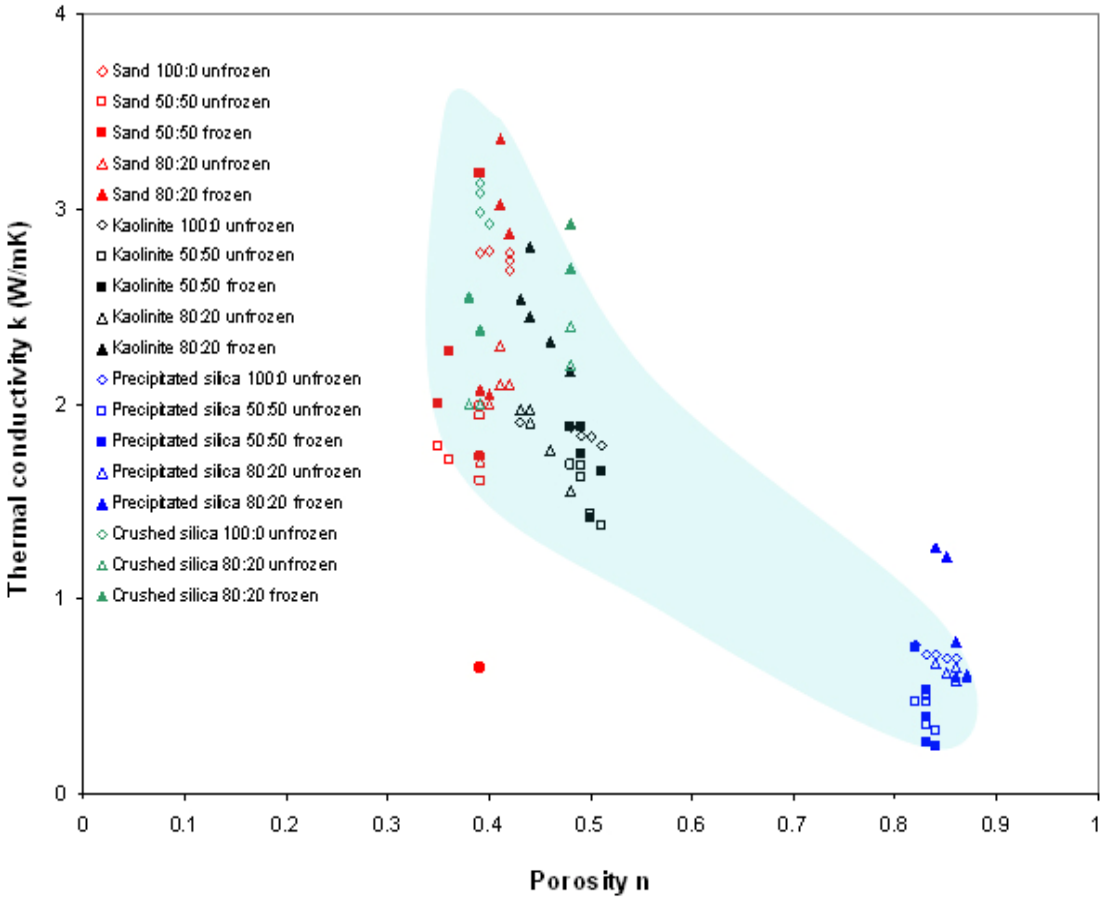

Figure 5.4 Thermal conductivity versus porosity for all the soils tested at: 100:0, 50:50 and 80:20-frozen and unfrozen stages

APPENDIX A
FROZEN SOIL

Frozen soil is a four-component system consisting of soil particles, ice, water and air. Soils experience significant changes in its structural, mechanical and thermal properties during freezing.

A.1 Formation of Ice in Soils

The freezing of soils is related to heterogeneous nucleation, where freezing is induced by the presence of particules (Andersland and Anderson, 1978). The pore water does not start to freeze until the temperature drops to the supercooled temperature T_{sc} (Figure A.1). The supercooled water is in a metastable equilibrium state, and the abrupt transformation of free water into ice is triggered at nucleation centers (nuclei can be aggregations of water molecules or soil particles). Then, ice crystals begin to grow within the pore space, and do not seem attached to the mineral grains (Andersland and Anderson, 1978). The temperature at which this process occurs is the freezing-point depression T_f. The cause of rise in temperature from T_{sc} to T_f is the formation of ice and the release of latent heat. For sands and gravels with small specific surface, T_f is close of 0 ºC. For fine-grained silts and clays, the temperature depression ΔT can be as much as 5 ºC (Andersland and Anderson, 1978). Free water in the soil pores gradually freezes at temperature T_f. As free water changes to ice, the release of latent heat slows the rate of cooling. When most of the water is frozen, the rate of cooling picks up again until the equilibrium temperature T_e is reached. All the free water and most of the bound water (i.e., unfrozen water film on the soil particles) are frozen at T_e about -70 ºC. A significant amount of unfrozen water can exist at higher temperatures for fine-grained soils with high-specific-surface areas (Andersland and Anderson, 1978).

The freezing-point-depression can be predicted from basic thermodynamic arguments (Andersland and Anderson, 1978). In agreement with Hobbs' homogeneous-nucleition theory in 1974, the temperature of spontaneous nucleation is nearly always

lower than the temperature at which the unfrozen soil water is in equilibrium with ice (Andersland and Anderson, 1978).

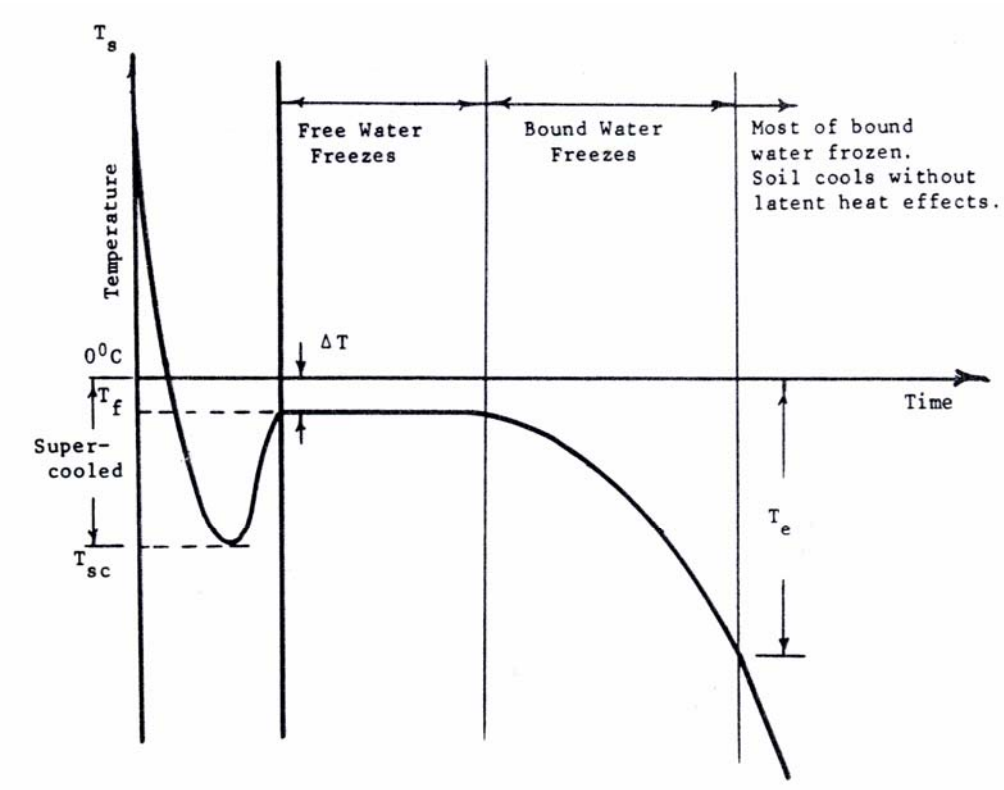

Figure A.1 Cooling curve for soil water and ice

Source: Andersland and Ladanyi, 1994

Once nucleation occurs, ice crystals grow until they interfere with each other. They then may intermingle, but eventually grain boundaries form and begin re-adjusting toward the configuration of minimum surface energy (Andersland and Ladanyi, 1994). When ice does not fill all the soil pores, frozen ground is said to be unsaturated, if the pore space is filled, it is said to be saturated, and when there is still more ice present, the ground is said to be supersaturated with ice. Ice approaches 100 % (by mass), it is referred to as massive ice. The terms ice gneiss and disseminated or intersticial ice distinguish lensed or well-foliated ground ice, from ice lacking a clearly defined structure (Andersland and Ladanyi, 1994).

In general, the ice contained in frozen ground has several forms, ranging from coating on individual soil particles and small lenses to large inclusions and massive deposits. All forms of ice segregation can occur in the same material, including granular soils. The supply of water and ease of movement will often determine the ice lens size and thickness. These lenses are composed of nearly pure transparent ice interlayered with soil. Ice lenses develop only in fine grained silty soils by the addition of water during stationary or slow movement of the freezing front (Andersland and Ladanyi, 1994). The formation of these masses of clear ice requires that water migrates through the soil voids toward the freezing front. In clay specimens, the low permeability limits the rate of water migration toward the freezing front, resulting in reduced ice lens formation. Under field conditions, ice layers formed in silty soils located adjacent to a frozen wall or in the active layer can grow to several centimeters or more in thickness. In perennially frozen silt, these ice lenses can grow to several meters in thickness (Andersland and Ladanyi, 1994).

A.2 Frozen Soils as Complex Systems

The complexity of frozen soils reflects the appearance of the new solid phase, the formation of new interfaces, and the random appearance of air bubbles and brine pockets. All the water in soil and other porous systems does not freeze at the same temperature and the ice content gradually increases as the temperature is lowered. The relation

between temperature below freezing and the amount of ice and water is peculiar to each soil (Penner, 1970).

The main factors thought to control the amount of water in frozen soils are specific surface area, mineral type, kind of exchangeable ions, soluble salt content of the pore water and pore size distribution (Penner, 1970). In general and for an originally saturated system, fine textured soils contain more unfrozen water at a given temperature below freezing than do coarse textured soils (Penner, 1970). Freezing is associated with volume expansion of the water by approximately 9 %. This expansion does not necessarily lead to a 9 % increase in the voids of a saturated sand or gravel because part of the water may be expelled during freezing (Andersland and Anderson, 1978)

A.3 Effect of Unfrozen Water in Frozen Soils

It appears that unfrozen water separates ice from the mineral grains in frozen soil (Andersland and Anderson, 1978). Ionic diffusion is observed in frozen soils; the path seems to be the unfrozen interface separating the particle surfaces from the neighboring ice grains. The magnitude of the chemical diffusion coefficients in frozen soil remains high and it is 10^{-11} m^2/s (Andersland and Anderson, 1978).

In general, the presence of unfrozen water in frozen soils produces a decrease in the effective thermal conductivity at every degree of saturation. Yet, at very low saturation, the bridge of unfrozen water increases the effective thermal conductivity of the soil because k_w is greater than k_{air}. Near the saturation limit the same bridge of unfrozen water decreases the effective thermal conductivity of the soil because the thermal conductivity of water k_w is smaller than the thermal conductivity of ice k_i (Gori, 1983).

A.4 Effect of Solutes in Frozen Soils

The presence of solutes in the pore water alters the ice content and the frozen soil behavior. Water within the soils pores may contain dissolved salts which increase the freezing-point depression and will increase the unfrozen water content (Andersland and

Anderson, 1978). The crystal lattice for ice is very selective; no substitutes for hydrogen or oxygen atoms are accepted. If an aqueous salt solution is frozen slowly, the foreign ions remain in the melt and pure ice is formed. During freezing, impurities will be rejected and concentrated at grain boundaries, which reduces the adhesion between ice grains (Andersland and Anderson, 1978).

A.5 Effect of Pressure

The application or removal of pressure on a frozen soil changes the free energy of the ice. This alters the thermodynamic equilibrium of the ice-water system and restoration of equilibrium requires an equal change in the free energy of the unfrozen water. In a frozen soil, the unfrozen water that is relatively far from the soil particle surface can be considered as capillary water or bulk water. This type of water is not affected significantly by the surface activity of the soil particles (Konrad and Morgenstern, 1982).

A change in external pressure on a frozen soil is also associated with a small increase in the amount of unfrozen water, since the radius of the ice-water interface increases with increasing pressures (Konrad and Morgenstern, 1982). This increase, in turn, produces changes in the local permeability of the frozen soil. Experimental studies demonstrate that the application of pressure also influences the freezing point depression. However, once nucleation has occurred in a freezing soil the pore ice penetrates into the saturated soil as a continuous medium (Konrad and Morgenstern, 1982).

A.6 Effect of Pore-Size in Frozen Soils

The melting or freezing temperature in porous media depends on pore size. The specific surface energy of ice crystallizing in a small pore, and its internal capillary pressure can be very large, meaning that the liquid phase is thermodynamically favored down to lower temperatures than under bulk conditions. This result can be quantified using the Gibbs-Thomson equation, which relates the curvature of the solid surface to the thermodynamic energy required to form the solid-liquid interface (Clennell et al., 2000).

$$\Delta T_{i,pore} = \frac{2\gamma_{iw} T_{bulk} \cos\theta_{iw}}{\rho_i \Delta H_f r_e} \tag{30}$$

where $\Delta T_{i,\ pore}$ is the freezing-melting temperature depression below the bulk melting temperature T_{bulk}, ρ_i is the density of ice, and ΔH_f is the latent heat per unit mass. Thus, in a fine grain soil or sediment that has a range of pore sizes, water freezes progressively over a range of temperatures, penetrating large pores first, followed by smaller pore throats as the temperature is lowered. When the temperature is raised again, the liquid water content profile follows a different path (hysteresis), because the effective pore size now relates to the distribution of larger pore sizes rather than throat apertures (Clennell et al., 2000).

REFERENCES

Abu-Hamdeh, N.H., Reeder, R.C., Khdair, A.I. and Al-Jalil, H.F. (2000), "Thermal conductivity of disturbed soils under laboratory conditions", *Transactions of the ASAE*, 43(4), 855-860.

Abu-Hambeh, N.H. and Reeder, R.C. (2000), "Soil thermal conductivity: effects of density, moisture, salt concentration and organic matter",*Soil Sci. Soc. Am. J.,* 64, 1285-1290.

Andersland, O. B and Anderson, D.M. (1978), Geotechnical engineering for cold regions, McGraw-Hill Inc., New York, N.Y., 1-103.

Andersland, O.B. and Ladanyi, B. (1994), "Physical and thermal properties", An introduction to frozen ground engineering, Chapman and Hall, New York, N.Y., 1-62.

Anderson, O and Suga, H. (1996), "Thermal conductivity of normal and deuterated tetrahydrofuran clathrate hydrates", *Journal Phys. Chem. Solids*., 57(1), 125-132.

Ashworth, T., Johnson, L.R., Lai, L-P. (1985), "Thermal conductivity of pure ice and tetrahydrofuran clathrate hydrates", *High temperatures – high pressures*, 17, 413 – 419.

Ashok, K.S. and Chaudhary, D.R. (1995), "Evaluation of heat and moisture transfer properties in a frozen-unfrozen water-soil system", *Int. J. Heat and Mass Transfer*, 38(12), 2297-2303.

Bagirov, E. and Lerche, I. (1997), "Hydrates represent gas source, drilling hazard", *Oil and Gas Journal*, 95(48), 99-104.

Becker, B.R., Misra, A., and Fricke, B.A. (1992), "Development of correlations for soil thermal conductivity", *Int. Comm. Heat Mass Transfer*, 19 (1), 59-68.

Bollavaram, P., Devarakonda, S., and Sloan, E.D., Jr. (2000), " Growth kinetics of single crystals sII hydrates. Elimination of mass and heat transfer effects", Annals of the New York Academy of Sciences, Edts., G.D. Holder and P.R. Bishnoi, The New York Academy of Sciences, New York, New York, 912, 533-543.

Chaouch, A. and Briaud, J.L. (1997), "Post melting behavior of gas hydrate in soft ocean sediments", *Offshore Technology Conference 1(OTC 8298)*, 217-224.

Cho, G.C. (2002), Unsaturated soil stiffness and post liquefaction shear strength, Ph. D. thesis, Civil and Environmental Engineering, Georgia Institute of Technology, Atlanta, GA.

Cicerone, R.G. and Oremland, R.S. (1988), "Biogeochemical aspects of atmospheric methane", *Global Biochemical Cycles*, 2 (4), 299-327.

Clennell, M.B., Hovland, M., Booth, J. S., Henry, P., and Wimters, W. J. (1999), "Formation of natural gas hydrates in marine sediments. 1- Conceptual model of gas hydrate growth conditioned by host sediment properties", *Journal of Geophysical Research*, 104 (B10), 22985-23003.

Clennell, M.B., Henry, P., Hovland, M., Booth, J.M., Winters, W.J., Thomas, M. (2000), "Formation of natural gas hydrates in marine sediments. Gas hydrate growth and stability conditioned by host sediments properties", Annals of the New York Academy of Sciences, Edts., G.D. Holder and P.R. Bishnoi, The New York Academy of Sciences, New York, New York, 912, 887-896.

Cook, J.G., and Leaist, D.G. (1983), "An exploratory study of the thermal conductivity of methane hydrate", *Geophysical Research Letters*, 10 (5), 397-399.

Cosby, B.J., Hornberger, R.B., Clapp, R.B. and Ginn, T.R. (1984), "A statistical exploration of the relationship of moisture characteristics to the physical properties of soils", *Water Resour. Res*., 20, 682-690.

Cosenza, P. Guerin, R. and Tabbagh, A. (2003), "Relationship between thermal conductivity and water content of soils using numerical modeling", *European Journal of Soil Science*, 54, 81-587.

Devarakonda, S., Groysman, A. and Myerson, A.S. (1999), "THF-water hydrate crystallization: an experimental investigation", *Journal of Crystal Growth*, 204, 525-538.

de Martin, B.J. (2001), Laboratory measurements of the thermal conductivity and thermal diffusivity of methane hydrates at simulated in-situ conditions, Master thesis, Georgia Institute of Technology, Atlanta, Ga.

de Vries, D.A., Borghorst, A. J. W., Businger, J.A., Derksen, W. J., Schmidt, F.H., Scholte Ubing, D.W., Van Wijk, W. R. (1963), "Thermal properties of soils". Physics of Plant Environment, ed. W.R. van Wijk. North-Holland Publishing Company-Amsterdam, Interscience Publishers, a division of John Wiley and Sons, Inc., N.Y., 210-235.

Dvorkin, J and Nur, A. 1993, "Rock physics for characterization of gas hydrates, the future of energy gases", USGS professional paper 1570, 293-298.

Ewen, J. and Thomas, H.R. (1987), "The thermal probe- a new method and its use on an unsaturated sand", *Geotechnique*, 37 (1), 91-105.

Farouki, O.T. (1986), "Thermal properties of Soils", *Series on Rock and Soil Mechanics*, 11, Transactions Tech., 1-136.

Fletcher, L.S. (1988), "Recent developments in contact conductance heat transfer", *Journal of Heat Transfer*, Transactions ASME 110 4 (B), 1059-1070.

Frondel, C. (1962), "Silica minerals", The System of Mineralogy, Edts. John Wiley and Inc., New York, N.Y, 3, 1-34.

Gavril'ev, R.I. (1989), "Thermal conductivity of permafrost soils in relation to natural moisture content", *Journal of Engineering Physics*, 56 (6), 701-706.

Goodrich, L.E. (1985), "Field measurements of soil thermal conductivity". *Canadian Geotechnical Journal*, 23, 51-59.

Gori, F. (1983), "Theoretical model for predicting the effective thermal conductivity of unsaturated frozen soils", *Natl. Acad. Press*., 363-368.

Henry, P., Thomas, M, Clennell, M.B. (1999), "Formation of natural gas hydrates in marine sediments. 2- Thermodynamic calculations of stability conditions in porous sediments", *Journal of Geophysical Research*, 104 (B10), 23005-23002.

Klauda, J.B. and Sandler, S.I. (2001), "Modeling gas hydrate phase equilibria in laboratory and natural porous media", *Industrial Engineering Chemical Research*, 40, 4197-4208.

Konrad, J. M. and Morgenstern, N.R. (1982), " Effects of applied pressure on freezing soils", *Canadian Geotechnical Journal*, 19, 494-505.

Kumar, P., Turner, D. and Sloan, E.D. (2004), "Thermal diffusivity measurements of porous methane hydrate and hydrate-sediment mixtures", *Journal of Geophysical Research*, 109 (B01207), 1-8.

Kuznetsov, F.A. (2000), "Gas hydrates of Siberia", Annals of the New York Academy of Sciences, Edts., G.D. Holder and P.R. Bishnoi, The New York Academy of Sciences, New York, New York, 912,101-111.

Kvamme, B. (2000), "A unified nucleation theory for the kinetics of hydrate formation", Kuznetsov, F.A., (2000), Annals of the New York Academy of Sciences, Ed., G.D. Holder and P.R. Bishnoi, The New York Academy of Sciences, New York, New York, 912, 496- 501.

Kvenvolden, K.A. (1993). "Gas hydrates-geological perspective and global change", *Review Geophysics*, 31,173-187.

Kvenvolden, K.A.(1999), "Potential effects of gas hydrates on human welfare", *Proceedings of the National Academy of Science, U.S.A*, 96, 3420-3426.

Lorenson, T. D. (2000), "Microscopic character of marine sediments containing disseminated gas hydrate", Annals of the New York Academy of Sciences, Ed., G.D. Holder and P.R. Bishnoi, The New York Academy of Sciences, New York, New York, 912, 189-194.

MacDonald, G.T. (1990). "Role of methane clathrates in past and future climates", *Climatic Change*, 16, 247-281.

Mahajan, D., Koetzle, T.F., Klooster, W.T., Brammer, L., McMullan, R.K., and Goland, A.N. (2000), "Crystal growth, structure characterization, and schemes for economic transport: an integrated approach to the study of natural gas hydrates", Annals of the New York Academy of Sciences, Edts., G.D. Holder and P.R. Bishnoi, The New York Academy of Sciences, New York, New York, 912, 940-949.

Matsubayashi, O. and Edwards, R.N. (2000), " Relationship between electrical and thermal conductivities for evaluating thermal regime of gas hydrate bearing sedimentary layers", Annals of the New York Academy of Sciences, Edts., G.D. Holder and P.R. Bishnoi, The New York Academy of Sciences, New York, New York, 912, 167-172.

Mork, M., Schei, G., and Larsen, R. (2000), "NMR imaging study of hydrate in sediments", Annals of the New York Academy of Sciences, Edts., G.D. Holder and P.R. Bishnoi, The New York Academy of Sciences, New York, New York, 912, 897- 905.

Pande, R. N. and Gori, F. (1986), "Effective media formation and conduction through unsaturated granular materials", *International Journal Heat Mass Transfer*, 30(5), 993- 1000.

Penner, E. (1970), " Thermal conductivity of frozen soils". *Canadian Journal of Earth Sciences*, 7, 982- 987.

Peters-Lidard, C. D., Blackburn, E., Liang, X., and Wood, E.F. (1998), "The effect of soil thermal conductivity parametrization on surface energy fluxes and temperatures", *Journal of the Atmospheric Sciences*, 55, 1209-1224.

Qun-Fang, L., Rui-Sen, L., and Dan-Yan, N. (1997), "Thermal conductivities of some organic solvents and their binary mixtures", *J. Chem. Eng. Data*, 42, 971- 974.

Rawls, W. J., Brakensiek, D.L. and Saxton, K.E. (1982), "Estimation of soil water properties". *Transactions American Society Agricultural Engineers*, 25, 1316-1320.

Reece, C. F. (1996), "Evaluation of a line heat dissipation sensor for measuring soil matric potential", Soil Science Society of America Journal, 60, 1022-1028.

Riestenberg, D., West, O., Sangyong, L., McCallum, S. and Phelps, T. J. (2003), "Sediment surface effects on methane hydrate formation and dissociation", *International Journal of Marine Geology, Geochemistry and Geophysics*, 198, 181-190.

Rodger, P. M. (2000), "Methane hydrate: melting and memory", Annals of the New York Academy of Sciences, Ed., G.D. Holder and P.R. Bishnoi, The New York Academy of Sciences, New York, New York, 912, 474-482.

Ross, R.G., Andersson, P. and Backstrom G. (1978), "Effects of H and D order on the thermal conductivity of ice phases", *Journal Chemistry Physics*, 68 (9), 3967-3972.

Sloan, E.D. (1998-a), "Gas hydrates: Review of Physical/ Chemical properties", *Energy and Fuels*, 12, 191- 196.

Sloan, E.D. (1998-b), Clathrate Hydrates of Natural Gas, 2nd Edition, Marcel Dekker, New York.

Sloan, E.D. and Rueff, R.M. (1985), "Effect of granular sediments on some thermal properties of tetrahydrofuran hydrate", *Ind. Eng. Chem. Process Des. Dev*., 24(3), 882-885.

Slusarchuk, W.A. and Watson, G.H. (1975), "Thermal conductivity of some ice-rich permafrost soils", *Canadian Geotechical Journal*, 12, 413-418.

Talley, L.D., Mitchell, G.F. and Oelfke, R.H. (2000), "Comparison of laboratory results on hydrate induction rates in a THF rig, high-pressure rocking cell, miniloop, and large flowloop", Annals of the New York Academy of Sciences, Ed., G.D. Holder and P.R. Bishnoi, The New York Academy of Sciences, New York, New York, 912, 314-321.

Thalmann, R. E. (1950), Thermal conductivity of dry soils, M.S. Thesis dissertation, University of Kansas.

Tarnawski, V.R. and Wagner, B. (1993), "Modeling the thermal conductivity of frozen soils", *Cold Regions Science and Technology*, 22, 19-31.

Tarnawski,V.R., Leong, W.H., Gori, F., Buchan, G.D., and Sundberg, J. (2002), "Inter-particle contact heat transfer in soil systems at moderate temperatures", *International Journal of Energy Research*, 26, 1345-1358.

Tse, J. S. and White, M. A. (1988), "Origin of glassy crystalline behavior in the thermal properties of clathrate hydrates: a thermal conductivity study of tetrahydrofuran hydrate", *Journal Physic Chemistry*, 92, 5006-5011.

Waite, W.F., deMartin, B.J., Kirby, S.H., Pinkston, J. and Ruppel, C.D. (2002), "Thermal conductivity measurements in porous mixtures of methane hydrate and quartz sand", *Geophysical Research Letters*, 29 (24), 82,1-82,4.

Willoughby, E. C., Latichev, K., Edwards, R.N. and Mihajlovic, G. (2000), "Resource evaluation of marine gas hydrate deposits using seafloor compliance methods". Annals of the New York Academy of Sciences, Ed., G.D. Holder and P.R. Bishnoi, The New York Academy of Sciences, New York, New York, 912,146-151.

Winters, W. J., Dallimore, S. R., Collett, T. S., Jenner, K.A., Katsube, J. T., Cranston, R. E., Wright, J.F., Nixon, F.M., and Uchida, T. (2000), "Relation between gas hydrate and physical properties at the Mallik 2L-38 research well in the Mackenzie delta". Annals of the New York Academy of Sciences, Ed., G.D. Holder and P.R. Bishnoi, The New York Academy of Sciences, New York, New York, 912, 94-100.

Yakushev, V.S. and Collett, T.S. (1992), "Gas hydrates in Artic regions: risk to drilling and production". *Proceedings 2nd International Offshore and Polar Engineering Conference*,1, 669-673.

Yasuoka, K. and Murakoshi, S. (2000), "Molecular dynamics simulations of dissociation process for methane hydrate", Annals of the New York Academy of Sciences, Ed., G.D. Holder and P.R. Bishnoi, The New York Academy of Sciences, New York, New York, 912,678-684.

Young, H.D. and Freedman, R.A. (2000), "Temperature and heat", University Physics, tenth edition, Ed. Addison-Wesley, Inc., 15, 460-487.